AN ABSTRACT OF THE DISSERTATION OF

Saran Salakij for the degree of Doctor of Philosophy in Mechanical Engineering
presented on March 18, 2013.

Title: Modeling In-Situ Vapor Extraction During Flow Boiling in Microscale Channel.

Abstract approved:

_____

James A. Liburdy

In-situ vapor extraction is performed by applying a pressure differential across a hydrophobic porous membrane that forms a wall of the channel as a means of reducing the local quality of flow boiling within the channel. As the local quality is reduced, the heat transfer capability can be improve while large pressure drops and flow instability can be mitigated. The present study investigates the potential of vapor extraction, by examining the characteristics and mechanisms of extraction. The physics based models for transition among extraction regimes are developed which can be used as a basis for a regime-based vapor extraction rate model. The effects of vapor extraction on flow boiling in a microscale fractal-like branching network and diverging channels are studied by using a one-dimensional numerical model based on conservation of mass and energy, along with heat transfer and pressure drop correlations. The results show the improvement in reduced pressure drop and enhanced flow stability, and show the potential of heat transfer enhancement.

Modeling In-Situ Vapor Extraction During Flow Boiling in Microscale Channel

by
Saran Salakij

A DISSERTATION

submitted to

Oregon State University

in partial fulfillment of
the requirements for the
degree of

Doctor of Philosophy

Presented March 18, 2013

Commencement June 2013

Doctor of Philosophy dissertation of Saran Salakij presented on March 18, 2013.

APPROVED:

Major Professor, representing Mechanical Engineering

Head of the School of Mechanical, Industrial and Manufacturing Engineering

---

Dean of the Graduate School

I understand that my dissertation will become part of the permanent collection of Oregon State University libraries. My signature below authorizes release of my dissertation to any reader upon request.

_____

Saran Salakij, Author

ACKNOWLEDGEMENTS

I would like to express my sincere gratitude to Dr. James A. Liburdy, my advisor, and Dr. Deborah V. Pence, my committee member, for the research opportunity, and their helpful and insightful guidance in scientific perspective. I would like to thank Dr. Sourabh V. Apte, and Dr. Vinod Narayanan, who are my committee members, for their useful advice and knowledge. I would also like to thank Dr. Rakesh Gupta for their kindness to serve as my graduate representative. I appreciate the helpful assistance from my colleagues: Douglas Heymann, Christopher Stull, Mike Sabo, Randall Fox, Nick Cappello, Xiaoliang He, and Adam Damiano. I gratefully acknowledge the financial support from Office of Naval Research under Grant no. N00014-09-1-1079 for the research studies presented herein. Finally, I would like to express my greatest gratitude to my family, Sommai, Supawan and Rasa Salakij, for their love, encouragement and support throughout my Ph.D. study, and last but not least, to my love, Siwaporn Boonyasuppayakorn, for being there.

CONTRIBUTION OF AUTHORS

Dr. James A. Liburdy and Dr. Deborah V. Pence were involved with the analysis and writing of Chapters 2, 3 and 4. Mario Apreotesi developed a preliminary numerical model and performed an experiment used to validate the results in Chapter 3.

TABLE OF CONTENTS

Page

TABLE OF CONTENTS (Continued)

Page

TABLE OF CONTENTS (Continued)

Page

LIST OF FIGURES

LIST OF FIGURES (Continued)

LIST OF FIGURES (Continued)

Figure Page

LIST OF FIGURES (Continued)

LIST OF FIGURES (Continued)

LIST OF TABLES

MODELING IN-SITU VAPOR EXTRACTION DURING FLOW BOILING IN MICROSCALE CHANNEL

1 GENERAL INTRODUCTION

The benefits of two-phase microscale heat sinks are a minimization of the mass flow rate while still maintaining low surface temperature and low temperature gradients across the heat sinks, see reviews [1-2]. However, two-phase microscale heat sinks also come with drawbacks such as large pressure drops and flow instabilities associated with two-phase microscale flow [3-4]. It is hypothesized that in-situ vapor extraction in a microscale flow boiling heat sink can help mitigate pressure drop and flow instabilities, and enhance the heat transfer capabilities. The main concept of in-situ vapor extraction is to reduce the vapor fraction inside the channel where it forms. It is accomplished by locally extracting vapor through a hydrophobic porous membrane that is used as a wall of the channel. As vapor available within the channel is reduced, flow instability is suppressed and the required pressure to drive the flow through the channel is also reduced. Along with these benefits, in-situ vapor extraction may also have the potential to tune boiling heat transfer characteristics by regulating the local quality in the channel.

While extraction mechanisms and characteristics of extraction depend on flow boiling and channel conditions, vapor extraction also affects the flow boiling. It is important to understand the synergistic effects of vapor extraction with flow boiling. The topic of the present study is to evaluate the potential of in-situ vapor extraction during flow boiling in microscale channels. Similar to two-phase flow regimes, extraction in flow boiling can be characterized by its mechanisms and characteristics in term of extraction regimes. The criteria for extraction regime transition, based on physics based models, are discussed in Chapter 2. This chapter is a manuscript in preparation to be submitted to the Journal of Heat Transfer.

The effects of vapor extraction on flow boiling are studied by using conservation of mass and energy, and heat transfer and membrane transport models to develop a one-

dimensional model. The results of flow boiling with vapor extraction in microscale fractal-like branching network and in single diverging microchannel geometries are presented and discussed in Chapters 3 and 4, respectively. Chapters 3 is a manuscript published in the International Journal of Heat and Mass Transfer and chapter 4 is a manuscript submitted to the Journal of Heat Transfer.

2 MODELING CRITERIA FOR EXTRACTION REGIME TRANSITIONS FOR MICROSCALE IN-SITU VAPOR EXTRACTION APPLICATION

Saran Salakij, Deborah V. Pence, James A. Liburdy

Journal of Heat Transfer

American Society of Mechanical Engineers, Two Park Avenue, New York, NY

In process of preparation to be submitted

2.1 ABSTRACT

A major detriment of two-phase microscale flow systems is a high pressure drop. For flow boiling the potential for flow instabilities is also a major concern. Both disadvantages may be suppressed by extracting vapor through a hydrophobic porous wall in the channel as a means to reduce vapor content as well as vapor expansion. The vapor extraction may occur either as evaporation, bubble extraction or a mix of both. For the design of vapor extraction systems, it is important to accurately predict extraction regimes, extraction rates and the effect of extraction on the heat transfer and flow conditions. This study focuses on two parts: the development of physic-based models for the transition criteria among (i) the extraction mechanism regimes, and (ii) the extraction flow regimes for microscale flow boiling. The identification and conditions for the various extraction regimes are discussed and criteria for transition are developed based on physical concepts. Six potential extraction mechanism regimes are identified: (a) no extraction, (b) pure evaporation, (c) pure bubble extraction, (d) bubble extraction with partial liquid blockage, (e) bubble extraction with evaporation, and (f) liquid breakthrough. Based on the criteria for the extraction mechanism regimes, the rate of vapor extraction is modeled and used to analyze the effects of vapor extraction on the dynamics of two-phase flow boiling. The results show six extraction flow regimes for two-phase flow boiling: (i) single-phase evaporation, (ii) two-phase evaporation – bubble collapse, (iii) full extraction - stable, (iv) full extraction - unstable, (v) partial extraction – stable and (iv) partial extraction – unstable.

2.2 INTRODUCTION

Due to the wide development of performance and miniaturization of electronic devices in the last few decades, the large increase in heat dissipation per unit volume of the devices has become a major concerned as most applications are required to operate at a relatively uniform and stable temperature. A two-phase microscale heat sink has been proposed because of its high surface to volume ratio and large heat transfer coefficient.

Especially for two-phase flow boiling, the additional advantage is the relatively small streamwise temperature variation compared to single-phase applications as the saturation temperature of the fluid only varies with pressure. However, the major undesired issues of flow boiling in microchannels are a large pressure drop and flow instabilities [3-4]. A large pressure drop can lead to large temperature variation along the flow in the two-phase regime. Also, the large pressure drop and thermal oscillations due to flow instability may lead to severe mechanical vibration and dry-out [3].

As flow instability is a severe issue of flow boiling in microchannel, numerous investigators [4-12] have performed channel modification as a means to suppress it. These stabilizing methods may be categorized into three main groups: (i) using an inlet restrictor, (ii) application of engineering nucleation sites, and (iii) using a expanding channel. The first group [4-6] stabilizes flow boiling by placing a flow restrictor at the inlet to decrease the vapor reverse flow. However, the drawback of this method is a large increase in the pressure drop of the system [7]. The second group [7-9] fabricates artificial nucleation sites on the channel walls. This reduces the required superheat surface temperatures and thereby reduces the rapid expansion of the bubble. The third group [7, 10-12] evaluates flow boiling inside channels with increasing cross-sectional area. As the cross-sectional area increases along the flow, the bubbles tend to expand downstream rather than upstream, leading to less vapor reverse flow.

In addition to the channel modification methods mentions above, Salakij et al. [13] proposed that in-situ vapor extraction might be used as an alternative method to stabilize the flow boiling. The main concept of in-situ vapor extraction is to locally extract the generated vapor out of the channel through a hydrophobic porous wall as a means to reduce or control the vapor fraction inside the channel, where the vapor is driven by pressure difference across the porous wall. Salakij et al. [14-15] developed a one dimensional predictive model for flow boiling in microscale diverging channel coupling with in-situ vapor extraction. The results showed significant improvement to the allowable stable heat flux when compared to flow boiling in a straight channel without in-situ vapor extraction.

Apart from the ability to stabilize the flow, several studies [16-21] suggest that in-situ vapor extraction also has the potential to reduce the system pressure drop while maintaining the benefit of enhanced heat transfer. Apreotesi et al. [16-17] investigated diabatic boiling water flowing through a fractal-like branching microchannel network with in-situ vapor extraction. The experimental results show a decrease in the system pressure drop with increasing extraction pressure differential. A later work by Salakij et al. [21], which developed a one dimensional predictive model and validated it by using the experimental results obtain in [16-17], shows up to a 70% decrease in the overall pressure drop. Moreover, the bulk fluid temperature within the channel decreases which shows the potential of in-situ vapor extraction to decrease overall operating temperature of the device. David et al. [19] investigates two-phase flow in parallel microchannels coupled with venting microchannel, where the flow and venting channels are separated by hydrophobic porous membrane, and shows a significant decrease in pressure drop. The computational model of the vapor-venting process studied by Fang et al. [20] also confirmed this result showing that vapor-venting process helps suppress local dry-out in microchannels.

In order to fully utilize the potential of in-situ vapor extraction for two-phase flow, it is necessary to understand the effects of vapor extraction on heat transfer and flow conditions. Basically, effects of vapor extraction are directly related to the vapor extraction mass flow rate. Many studies [14-22] have predicted the vapor/gas transport across the membrane rate based on Darcy's law as:

$$V_{extr} = \frac{\kappa}{\mu_v} \nabla P_{extr} \tag{1}$$

where κ is the specific membrane permeability and ∇P_{extr} is the pressure gradient across the membrane. The model may indeed require added complexities to be accurate for this application. For example, Salakij et al. [14, 21] related vacuum membrane distillation to vapor extraction and included evaporation effects on the vapor extraction where the evaporation rate is based on the local vapor pressure gradient across the membrane. Cappello et al. [23] used the dusty gas model, which is a general form of Darcy's law,

with membrane compaction to successfully predict gas and superheated vapor transport through the membrane.

Several studies suggested that two-phase hydrodynamics and other conditions also affect the vapor extraction. Alexander and Wang [24] studied vapor separating from a two-phase microscale flow through a hydrophobic porous plate, called a breather. The correlation was developed based on the assumption that the extraction rate is also related to flow velocity as a function of the ratio of the pressure differential across the porous plate to the pressure drop associated with drag on the bubble. Xu et al. [22] studied gas bubble removal in microscale channel and proposed criteria for completely removal of gas bubble from the microchannel by considering film formation, bubble size, and liquid breakthrough conditions. Cappello et al. [23] studied gas and vapor transport through a porous membrane. These results show the deviation of extracted mass flow rate from single-phase transport studies, when saturated vapor is extracted from saturated liquid-vapor. They proposed that these results may be caused by effects of two-phase hydrodynamics and condensation within the membrane. Based on these, it is important to identify the extraction mechanism regime. As an analogy to two-phase flow regimes, the extraction mechanism regimes should represent the variation in the physical conditions of the extraction process.

An ability to predict two-phase flow regime is important to the development of flow regime-based pressure drop and heat transfer models [25]. Two-phase flow regime maps are used as a tool to easily identify the transition of flow patterns based on different operating conditions. The methods to develop a two-phase flow regime map may be categorized into two main methods: empirical and physics-based. There are many studies that generate a regime map for microchannel flow using empirical methods, (e.g. [25-26]). For flow boiling with vapor extraction, David et al. [27] observed two-phase flow regimes in a vapor-venting microchannel. Based on flow visualization, stratified flow, which is rarely observed in other microscale geometries, was said to be a dominated flow regime for low liquid velocities. With increasing liquid velocities, this changes to annular flow. In contrast to empirical methods, there are only a few studies that have developed a

regime map based on physics-based relationships such as the pioneering work by Taitel and Dukler [28], and the later work by Barnea et al. [29]. This approach generally uses a dimensionless form of basic relationships to predict the conditions for flow regime transition. Each regime transition criterion is normally developed individually resulting in a relation of different dimensionless parameters.

Similar to the identification of two-phase flow regimes, the extraction is expected to also have characteristics which can be classified as different extraction regimes. The goal of this study is to investigate the potential of vapor extraction by developing physic-based models for the transition criteria among specific identified regimes. The developed models for extraction are expected to help the development of regime-based extraction mass flow rate predictions in two-phase flow, as well as being useful design tools for enhanced performance of liquid-vapor systems.

2.3 PHYSICS-BASED REGIME MAP

2.3.1 General Approach

Basically, the methodology to develop a physics-based regime map can be divided to four main steps: (i) identify possible regimes and physical conditions for each regime, (ii) develop theoretical models for transition between physical conditions, (iii) nondimensionalize the transition criteria, and (iv) plot transition criteria on an appropriate map on a graph to show as a map. The additional step to make a regime map more practical for a specific application is converting the nondimensional map into a dimensional map for a specific set of conditions, such as a working fluid and flow geometry. This step is necessary because the nondimensional map that identifies all considered regimes may be excessively complicated to be used as design tool. This is because regime maps usually consists of several transition criteria to separate regions on the map which may result in a chart with more than four different coordinates which is not easily presented on a two-dimensional chart. For example, Taitel and Dukler [28] developed four transition criteria to separate five flow regimes resulting in the two-phase flow regime map based on four different dimensionless parameters. This nondimensional

map is then converted to the commonly known dimensional flow regime map based on liquid and vapor superficial velocity coordinates for specific geometries and working fluids.

2.3.2 Extraction Map

The extraction map is used to identify different physical conditions related to vapor extraction. The main goal of the extraction map is to help understand the potential of vapor extraction and to be used as design tool. In this study, two main types of extraction maps are proposed: (i) extraction mechanism map, which characterizes how vapor being extracted, and (ii) extraction flow map, which characterizes the results of flow boiling on vapor extraction. Instead of develop a single extraction regime map that includes all considered extraction regimes, this study will focus on the development of each individual regime transition and the corresponding individual map for each specific regime transition which can be further combined to the extraction regime map.

2.4 EXTRACTION MECHANISM REGIMES

To develop the extraction mechanism map, the first step is to identify the extraction mechanism regimes. It is important to understand the membrane transport mechanism such that the developed extraction mechanism regimes capture all of possible different behaviors of extraction.

Membrane transport is usually initiated by applying a pressure differential across the membrane. For hydrophobic porous membrane, the liquid phase is suppressed from leaking into the membrane pores by surface tension forces. If the pressure difference across the membrane is sufficient to overcome the surface tension forces, there will be a liquid leakage through the membrane which is normally an undesirable situation. This maximum possible pressure differential across the membrane without liquid leakage is defined as the breakthrough pressure. By applying Young-Laplace equation for a straight capillary pore, the breakthrough pressure is estimated as:

$$\Delta P_{break} = -\frac{4\sigma_{lv}\cos\theta_{c,mem}}{d_p} \quad (2)$$

where σ_{lv} is the liquid-vapor surface tension, $\theta_{c,mem}$ is membrane contact angle and d_p is equivalent pore size of the membrane. It should be noted that although this breakthrough pressure can be theoretically estimated as shown, many researchers [19, 22, 24, 27] experience breakthrough at much lower pressure differential. This may be because of inconsistencies of membrane pore manufacture and also the more complex nature of porous membranes having a range of pore sizes and shapes. It is recommended to evaluate this breakthrough pressure experimentally.

Table 1. Mechanism and conditions of membrane transport.

Transport mode	Mechanism	Phase transport	Conditions
Evaporation	Thermodynamic transport	Vapor	• Liquid in contact with hydrophobic membrane • Saturation pressure of liquid at membrane interface is higher than extraction pressure
Bubble extraction	Hydrodynamic transport	Vapor	• Bubble in contact with hydrophobic membrane • Bubble pressure is higher than extraction pressure
Breakthrough	Hydrodynamic transport	Liquid	Pressure differential across the membrane is greater than breakthrough pressure

The membrane transport mechanism which is the main objective of in-situ vapor extraction application is vapor extraction. Vapor extraction can occur in two modes: bubble extraction and evaporation. Bubble extraction is a result of hydrodynamic transport, i.e. the vapor phase is extracted through a membrane directly by a pressure differential across the membrane. The evaporation is a result of thermodynamic transport where the liquid phase at the membrane evaporates and transports across the membrane via thermal and pressure forces. The evaporation occurs when the vapor pressure of the liquid in contact with membrane is greater than the extraction pressure on the opposite side of the membrane. More detail explanation of evaporative transport mechanism can

generally be found in discussions of vacuum membrane distillation application, e.g. [30-33]. It should be noted that both modes of vapor evaporation can coexist depending on extraction condition and whether liquid, vapor or both phases are in contact with membrane. The physical conditions of vapor extraction and breakthrough are summarized in Table 1.

Table 2. Phenomenological conditions of extraction mechanism regimes.

Regimes	Phenomenological conditions	
	Membrane contact phase	Transport mechanism
(a) No extraction	Liquid or vapor	None
(b) Pure evaporation	Liquid	Evaporation
(c) Pure bubble extraction	Vapor	Bubble extraction
(d) Bubble extraction with partial liquid blockage	Both	Bubble extraction
(e) Bubble extraction with evaporation	Both	Bubble extraction and evaporation
(f) Liquid breakthrough	Liquid or partial vapor	Breakthrough

Extraction mechanism regimes are classified by using membrane transport mechanisms together with membrane contact conditions as criteria, there are six potential extraction mechanism regimes identified as: (a) no extraction, (b) pure evaporation, (c) pure bubble extraction, (d) bubble extraction with partial liquid blockage, (e) bubble extraction with evaporation, and (f) liquid breakthrough. The physical conditions of each regime are summarized in Table 2 where the characteristic of each regime are described as below:

a) *No extraction* is when the pressure differential across the membrane is not sufficient to initiate either bubble extraction or evaporation resulting in no extraction across the membrane.

b) *Pure evaporation* is when the considered extraction area is in contact with liquid which evaporates and vapor flows through the membrane.

c) *Pure bubble extraction* is when the vapor phase inside the channel is extracted through the membrane. This occurs when the only vapor phase is in contact with the membrane.

d) *Bubble extraction with partial liquid blockage* is when the vapor phase is extracted where a fraction of the extraction area is blocked by liquid, leading to a decrease in the effective bubble extraction area.

e) *Bubble extraction with evaporation* is similar to bubble extraction with partial liquid blockage. However, the liquid that blocks the vapor also evaporates, i.e. both modes of vapor extraction occur.

f) *Liquid breakthrough* is when the liquid phase leaks into the membrane pores and flows through the membrane. This occurs when the pressure difference across the membrane is greater than the breakthrough pressure.

For microscale flow boiling applications, bubble extraction with partial liquid blockage regime may not exist. This is because liquid coexisting with vapor is usually in the saturated condition. Therefore, instead of only partial blocking of the vapor phase, liquid in contact with membrane also evaporates. This regime may only occur in two-phase liquid-gas flow application.

It should be noted that by extracting vapor from the flow, flow conditions change which can result in the change in phenomenological conditions of the extraction mechanism regime along the flow. As a result, extraction mechanism regimes can be seen as a local condition along the flow. For example, a high temperature single-phase flow enters a channel. Liquid in contact with membrane may evaporate, which is the pure evaporation regime. As evaporation takes place, the liquid temperature near the membrane decreases along the flow. It may suppress the evaporation if temperature of the fluid near the membrane is low enough, resulting in a change of regime from pure evaporation to no extraction.

2.5 EXTRACTION MECHANISM REGIME TRANSITION CRITERIA

As previously mentioned, the extraction mechanism regime depends on membrane contact phase and membrane transport mechanism. The development of extraction mechanism regime transition criteria is achieved by modeling the transition of the membrane contact phase and membrane transport mechanism. Then, the transition criteria can be used together with the extraction mechanism regime conditions, summarized in Table 2, to identify the regime. Each condition transition criterion is discussed in detail below.

2.5.1 Membrane Contact Phase

Although the hydrophobic nature of the membrane generally repels the liquid phase, the membrane is not always totally dry unless the contact angle is perfectly 180^{o}. For a non-completely dried membrane, there are three possible situations for fluid to be in contact with membrane, which are (i) vapor only, (ii) liquid only and (iii) a mixture of both phases. Two criteria are used to separate these three membrane in contact situations: liquid film formation, and stratification to an intermittent flow regime. For liquid to be the only phase in contact with the membrane, there must be a liquid film formation on the membrane. If a liquid film formation condition is not satisfied, the membrane can be in contact with either vapor only or mixed phases. To separate between vapor only and mixed phases in contact with the membrane, the contact characteristics are assumed to be related to the two-phase flow regime of the fluid inside the channel. In other words, the vapor phase is likely to be the only phase in contact with membrane for stratified flow, where liquid and vapor are completely separated. On the other hand, mixed of both phases tend to in contact with membrane for an intermittent flow. It should be noted that although stratified flow is rarely found in most microscale flow boiling applications, stratified flow may likely be found in the flow boiling with in-situ vapor extraction applications. This is because at least one wall of the channel is formed by a hydrophobic porous membrane, which lacks surface tension forces to pull the liquid to the wall, causing the extended region of stratified flow. The experiment observations by David et al. [27] support this hypothesis that the stratified flow is reported to be a dominated flow

in low velocity situations. The conditions for liquid film formation and transition from stratified to intermittent flows are discussed in detail below.

2.5.1.1 Liquid film formation

The liquid film formation condition is evaluated based on the fact that the dynamic contact angle decreases with increasing bubble velocity. As the dynamic contact angle approaches zero, the bubble critical velocities corresponding to the liquid film formation is estimated based on criteria by de Gennes et al. [34]:

$$u_{crit} = \frac{1}{9\sqrt{3}} \frac{\sigma/\mu_l}{a} \theta_{c,mem}^3 \tag{3}$$

where $\theta_{c,mem}$ is membrane contact angle and a = 15-20. The liquid film forms when the bubble travels faster than this critical velocity ($u_{bub} > u_{crit}$). For simplicity, the bubble velocity may be estimated as the vapor superficial velocity, j_v . In dimensionless form, film formation criterion is expressed as:

$$Ca_v > \frac{1}{9\sqrt{3}} \frac{\theta_{c,E}^3}{a} \tag{4}$$

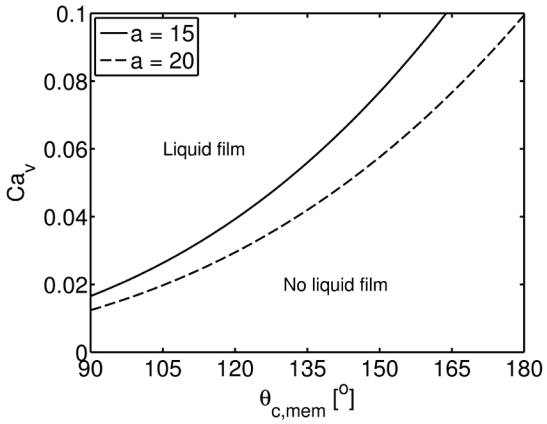

Figure 1. Liquid film formation map

where $Ca_v = \frac{\mu_l j_v}{\sigma}$. A liquid film formation map for a range of values of *a* equal to 15 and 20, based on Eq. (4) is shown in Figure 1 where the region on the left hand side of the line indicates the existent of liquid film on the membrane.

Once a film is formed, it may rupture when the liquid cannot maintain a film. Assuming that the film starts to rupture when its thickness is on the same order as the surface roughness, the criterion for film rupture may be roughly estimated in terms of flow void fraction as:

$$\alpha > \left(1 - \delta_c / A_c^{1/2}\right)^2 \tag{5}$$

where δ_c is the channel surface roughness. The void fraction correlation developed for annular flow by Zivi [35] can be used as:

$$\alpha = \left[1 + \left(\frac{1-x}{x}\right)\left(\frac{\rho_v}{\rho_l}\right)^{2/3}\right]^{-1} \tag{6}$$

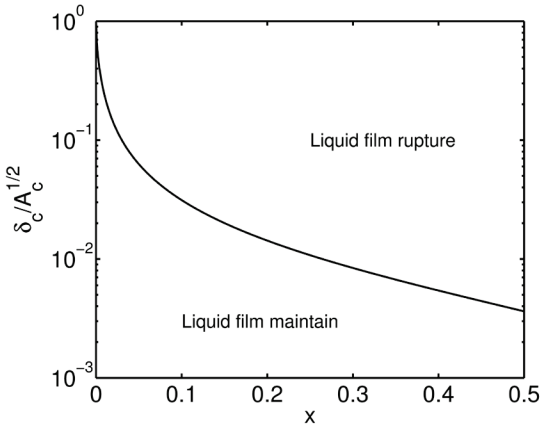

Figure 2. Film rupture map

By combining Eqs. (5) and (6), the film rupture map, shown in Figure 2, shows the film rupture region on the upper right hand side of the line. Both film formation and rupture maps can be used to estimate the existent of liquid film on the membrane. For example,

for flow boiling with constant mass flux, a film may form with increasing quality due to flow acceleration resulting from phase change. As quality further increases the liquid phase may be insufficient to form a film.

2.5.1.2 Stratified to intermittent flow regime transition

The criterion for two-phase flow regime transition from stratified to intermittent flows can be used to identify the transition from vapor only to a mixture of two phases in contact with membrane. To illustrate the transition, the criterion developed by Taitel and Dukler [28] is used in this study. This criterion is developed based on the assumption that the lift, caused by vapor acceleration over a liquid-vapor wave interface, disturbs the liquid-vapor interface of stratified flow leading to the rapid grow of interfacial waves to block the vapor flow path. There are two conditions to satisfy for the transition from stratified to intermittent flows to occur. First, the lift, due to the decreasing of pressure in accelerating vapor over the wave interface owing to the Bernoulli effect, overcomes the gravitation force, which tends to suppress the growing wave. Second, that liquid phase in the equilibrium stratified flow must be sufficient to maintain slug or else annular flow would take place instead. It should be noted that although Taitel and Dukler [28] developed the transition criteria in dimensionless form, it is modeled specifically for two-phase flow in a circular tube. To use those criteria for other channel geometries such as rectangular channel, which is common for microscale application, modification of those models are required.

By considering a finite solitary wave, the condition for rapid wave growth inside the channel is evaluated as [28]:

$$u_v > C_w \left(\frac{\left(\rho_l - \rho_v\right) g \cos\beta}{\rho_v} \frac{A_{c,v}}{dA_{c,l}/dH_l} \right)^{1/2} \tag{7}$$

where β is the channel inclination angle and $C_w = A'_{c,v}/A_{c,v}$ depends on the size of the wave ranging between 0 and 1. $A_{c,v}$ and $A'_{c,v}$ represent a cross-sectional area of vapor flow in the equilibrium stratified flow and over the finite wave peak, respectively. The

rapid wave growth condition can be rewritten as a function of modified Froude number, Fr^*, for a general channel geometry as:

$$Fr^* > \sqrt{C_w^2 \left(\frac{A_{c,v}}{A_c} \right)^3 \frac{A_c / H}{dA_l / dH_l}} \tag{8}$$

where Fr^* is defined as:

$$Fr^* = \sqrt{\frac{\rho_v}{\rho_l - \rho_v}} \frac{j_v}{\sqrt{gH \cos\beta}} \tag{9}$$

For rectangular channel, Eq. (8) is rewritten as:

$$Fr^* > C_w \left(1 - H_l / H\right)^{3/2} \tag{9}$$

For simplicity, C_w is estimated by Taitel and Dukler [28] as:

$$C_w \approx 1 - H_l / H \tag{10}$$

where H_l / H is a normalized liquid height for an equilibrium stratified flow. Substituting the estimated value of C_w from Eq. (10), the criterion for rapid wave growth in rectangular channel becomes:

$$Fr^* > \left(1 - H_l / H\right)^{5/2} \tag{11}$$

For a circular tube, Fr^* can be evaluated as a function of H_l / D. Based on the equilibrium stratified flow condition, provided by Taitel and Dukler [28], H_l / D is a unique function of X^2 and Y, where the Lockhart-Martinelli parameter, X^2, is denoted as:

$$X^2 = \frac{\left(dP/dz\right)\big|_l}{\left(dP/dz\right)\big|_v} \tag{12}$$

and the dimensionless parameter that represents the ratio of gravitational force in flow direction to pressure drop of vapor phase, Y, is denoted as:

$$Y = \frac{\left(\rho_l - \rho_v\right) g \sin\beta}{\left(dP/dz\right)\big|_v} \tag{13}$$

Note that for horizontal flow, $Y = 0$. The condition for an equilibrium stratified flow was developed by considering the momentum equation of each phase for an equilibrium stratified flow and then equating the pressure drop terms of both equations. Using this condition, the criterion for rapid wave growth in circular tube was written as a function of Fr^*, X^2 and Y. By following this approach, the condition for rapid wave growth in other channel geometries can be determined.

The condition for equilibrium stratified flow as modified for any channel geometry is:

$$\begin{aligned} &\mathrm{X}^2\left[\left(\frac{S_l}{S}\right)^{n+1}\left(\frac{A_c}{A_{c,l}}\right)^3\right] - Y \\ &-\left[\left(\frac{S_v + S_i}{S}\right)^m\left(\frac{A_c}{A_{c,v}}\right)^2\left\{\left(\frac{S_v + S_i}{S}\right)\left(\frac{A_c}{A_{c,v}}\right) + \left(\frac{S_i}{S}\right)\left(\frac{A_c}{A_{c,l}}\right)\right\}\right] = 0 \end{aligned} \tag{14}$$

where the exponents m and n are the exponents of the Reynolds number in the Blasius equation for vapor and liquid phases, respectively, which are equal to 1.0 for laminar flow and 0.2 for turbulent flow. Note that for laminar-laminar or turbulent-turbulent flow boiling ($n = m$), X^2 can be rewritten as a function of quality, x, as:

$$\mathrm{X}^2 = \left(\frac{\mu_l}{\mu_v}\right)^n\left(\frac{1-x}{x}\right)^{2-n}\left(\frac{\nu_l}{\nu_v}\right) \tag{15}$$

The cross-sectional area, A_c, and the contact surface area per unit length, S, are different for each channel geometry, as shown in Figure 3. For a rectangular channel, the ratios of S and A_c, in Eq. (14), are evaluated as a function of H_l/H and channel aspect ratio, α_c, as:

$$\frac{A}{A_l} = \left(H_l/H\right)^{-1} \tag{16}$$

$$\frac{A}{A_v} = \left(1 - H_l/H\right)^{-1} \tag{17}$$

$$\frac{S_l}{S} = \frac{2H_l/H + \alpha_c}{2\left(1+\alpha_c\right)} \tag{18}$$

$$\frac{S_v + S_i}{S} = 1 - \frac{H_l/H}{1+\alpha_c} \tag{19}$$

$$\frac{S_i}{S} = \frac{\alpha_c}{2\left(1+\alpha_c\right)} \tag{20}$$

where α_c is channel aspect ratio, denoted as:

$$\alpha_c = W/H \tag{21}$$

Based on this equilibrium stratified flow condition, it is shown that the equilibrium stratified flow condition for rectangular channel can be written as a function of X^2, Y and α_c . The condition for rapid wave growth in a rectangular channel is evaluated as a function of Fr^*, α_c, X^2 and Y by combining Eqs. (9), (14), and (16)-(20).

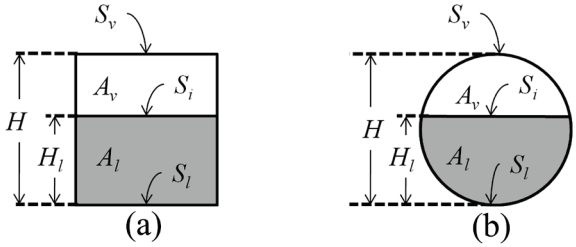

Figure 3. Cross-section of equilibrium stratified flow in (a) rectangular channel and (b) circular tube.

As previously mentioned, in addition to rapid wave growth, the liquid level must be sufficient to form a liquid slug. Taitel and Dukler [28] suggested that the transition between intermittent and annular flow takes place at:

$$H_l/H > 0.5 \tag{22}$$

while in the later work by Barnea et al. [36] it is recommended that the criterion for the transition is:

$$H_l / H > 0.35 \tag{23}$$

This criterion can be used together with the condition for equilibrium stratified flow, Eqs. (14), and (16)-(20), to form a relationship among α_c, X^2 and Y.

It should be noted that the following work by Barnea et al. [29] suggests that the rapid wave growth and sufficient liquid level conditions, developed by Taitel and Dukler [28], is not sufficient to be applied to small channels. An additional criterion is required to account for surface tension forces that pull liquid to the channel walls. However, the additional criterion is not used in this study because the membrane used in vapor extraction application is usually hydrophobic. Thereby, surface tension forces that pull liquid upward to a membrane will be minimal if at all.

Based on rapid wave growth and liquid level conditions, the membrane contact phase can be determined. Figure 4 shows the membrane contact phase for horizontal two-phase laminar-laminar flow in a rectangular channel without a liquid film formation using liquid level criterion from Barnea et al. [36]. The region on the right of the line represents intermittent flow regime which corresponds to mixed phases in contact with the membrane. The sudden change in slope near $X^2 = 1$ is due to the change from rapid wave growth condition to sufficient liquid level condition. It shows that for low value of X^2, i.e. high quality, the condition is independent of Fr^*. This is because the liquid phase is not sufficient to form on the membrane. It also shows that the vapor only region extends with increasing channel aspect ratio. This is due to the fact that as the aspect ratio increases, the channel is wider, and thereby results in a larger contact area for the vapor phase. Therefore, the required quality to match the pressure drop of both phases in channel is less, i.e. higher value of X^2.

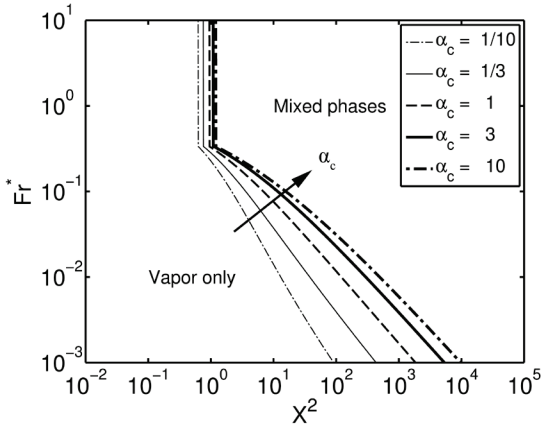

Figure 4. Membrane contact phase for horizontal two-phase laminar-laminar flow in rectangular channel without liquid film formation.

A dimensional membrane contact phase map is developed by combining conditions for liquid film formation with stratified to intermittent flow transition. The two examples of the dimensional membrane contact phase map are shown in Figure 5. Lines A, B, C and D are based on film formation, Eq. (4), film rupture criteria, Eq. (5), rapid wave growth, Eq. (11), and sufficient liquid level, Eq. (23), respectively. It is implied by observing Figure 5(a) that full extraction is hard to achieve since near zero quality there is a "mixed phases" region which has the potential to reduce the effective bubble extraction area. As extracting vapor decreases the available quality, the membrane contact phase may change from "vapor only" to "mixed phases" at around $x = 0.015$. This supports the observation by several studies [22-23] that vapor extraction from two-phase flow is less effective compared with single-phase membrane transport in some flow conditions. This membrane contact phase map can be used as a basis to develop models for vapor extraction from two-phase flow since the vapor extraction from two-phase flow should be related to the area of each phase in contact with the membrane.

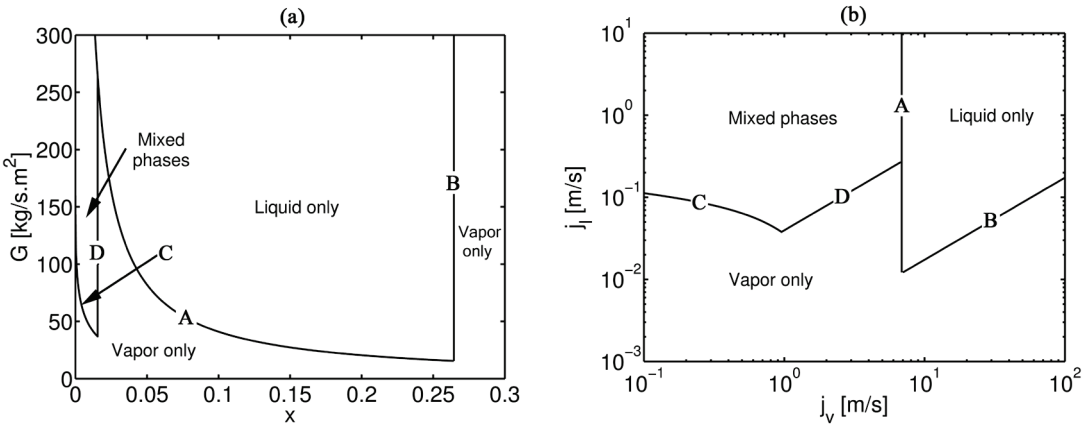

Figure 5. Examples of dimensional membrane contact phase map for water at 100°C and membrane contact angle of 124° in a 500 μm × 500 μm channel with surface roughness of 5 μm in terms of (a) x vs. G, and (b) j_v vs. j_l; Note that the lines A, B, C and D represent transition criteria based on film formation, film rupture, rapid wave growth, and sufficient liquid level conditions, respectively.

2.5.2 Membrane Transport Mechanism

As previously discussed and summarized in Table 1, the conditions to initiate bubble extraction and evaporation are:

$$P_{bub} > P_{extr} \tag{24}$$

and

$$P_{sat}\big|_{T_{mem}} > P_{extr} \tag{25}$$

respectively, while the condition for liquid breakthrough is:

$$P_{chan} - P_{extr} > \Delta P_{break} \tag{26}$$

The bubble pressure, P_{bub}, in Eq. (24) is slightly higher than P_{chan} due to the curvature of the bubble. For simplicity, the difference in pressure is assumed negligible. Therefore, the condition for bubble extraction becomes:

$$P_{chan} > P_{extr} \tag{27}$$

It should be noted that as previously suggested, this breakthrough pressure is more accurate when acquired from experiments than estimated from Eq. (2). It is expected that

the breakthrough pressure may be varied with temperature as it relies on the surface tension force. To account for the variations due to temperature change, the breakthrough pressure may be rewritten in term of the surface tension ratio and experimental breakthrough pressure at a specific temperature. Based on this, the condition for breakthrough can be written as a function of a specific temperature, T_a, as:

$$P_{extr} > P_{chan} - \frac{\sigma|_{T_{mem}}}{\sigma|_{T_a}} \Delta P_{break}|_{T_a} \tag{28}$$

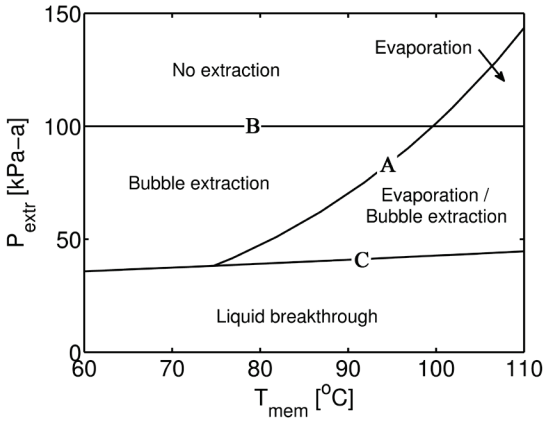

Figure 6. Membrane transport mechanism map for water at 100 kPa-a and membrane breakthrough pressure at 25°C of 70 kPa; Lines A, B and C represent transition criteria for evaporation, bubble extraction and liquid breakthrough, respectively.

Using the conditions for evaporation, bubble extraction, and breakthrough, Eqs. (25), and (27)-(28), the membrane transport mechanism can be determined based on channel pressure, membrane temperature and extraction pressure. For example, a membrane transport mechanism map for water at 100 kPa-a and membrane breakthrough pressure at 25°C of 70 kPa is shown in Figure 6 as a function of extraction pressure and membrane temperature. Lines A, B and C are based on evaporation, Eq. (25), bubble extraction, and breakthrough conditions, respectively. Note that the membrane transport mechanisms shown here are possible transport modes. It may be needed to also consider the membrane contact phase to get the exact transport mechanism. For example, although the region at 75°C with 50 kPa-a extraction pressure in Figure 6 is shown as

"Evaporation/Bubble extraction", only evaporation would occurs if a liquid film is formed on the membrane.

2.6 EXTRACTION FLOW REGIMES

In the previous section, the extraction regime is characterized based on the condition of the fluid near the membrane which can be seen as the local condition for extraction. Globally, as vapor extraction affects the flow boiling, flow conditions change and thereby so does the vapor extraction conditions. In other words, vapor extraction and flow boiling conditions are coupled. In this section, vapor extraction affected by flow boiling is characterized as the extraction flow regime. It should be noted that the extraction flow regimes are considered only when there is a vapor mass extraction without liquid breakthrough, i.e. the extraction mechanism regimes (b) to (e) shown in Table 2.

The following six potential extraction flow regimes are characterized by the amount of vapor leaving the outlet of the channel, the boiling condition, and flow stability as: (i) single-phase evaporation, (ii) two-phase evaporation – bubble collapse, (iii) full extraction - stable, (iv) full extraction - unstable, (v) partial extraction – stable and (iv) partial extraction – unstable. The phenomenological conditions of each regime are summarized in Table 3 where the characteristics of each regime are described as below:

i. *Single-phase evaporation* represents no vapor generation within the channel, but evaporation through the membrane results in vapor extraction.

ii. *Two-phase evaporation - bubble collapse* represents bubbles generated during subcooled boiling, but the generated bubbles are condensed in the main stream flow rather than being extracted.

iii. *Full extraction - stable* represents all generated bubbles extracted and the flow is stable.

iv. *Full extraction - unstable* is similar to regime (iii), however, although all generated vapor is extracted, the vapor extraction is not sufficient to stabilize the flow causing unstable flow.

v. *Partial extraction - stable* represents some generated vapor extracted, leaving excess vapor exiting through the channel outlet while the vapor extraction is sufficient to suppress the flow instability.

vi. *Partial extraction - unstable* is similar to regime (v) but bubbles generation exceeds the rate of vapor extraction such that flow is unstable.

Table 3. Phenomenological conditions of extraction flow regimes.

Regime	Phenomenological Conditions		
	Outlet quality	Boiling condition	Flow stability
i. Single-phase evaporation	$x_{out} < 0$	No boiling	Stable
ii. Two-phase evaporation (bubble collapse)	$x_{out} < 0$	Subcooled boiling	Stable
iii. Full extraction (stable)	$x_{out} = 0$	Saturated boiling	Stable
iv. Full extraction (unstable)	$x_{out} = 0$	Saturated boiling	Unstable
v. Partial extraction (stable)	$x_{out} > 0$	Saturated boiling	Stable
vi. Partial extraction (unstable)	$x_{out} > 0$	Saturated boiling	Unstable

2.7 EXTRACTION FLOW REGIME TRANSITION CRITERIA

Similar to the method used to identify the extraction mechanism regime transition discussed previously, the transition criteria of flow dynamics are not developed directly. Instead, the physical conditions related to extraction flow regime, which are outlet quality, boiling condition and flow stability, are analyzed below. Extraction flow regime is then identified by matching the physical conditions with the phenomenological conditions of extraction flow regime, summarized in Table 3.

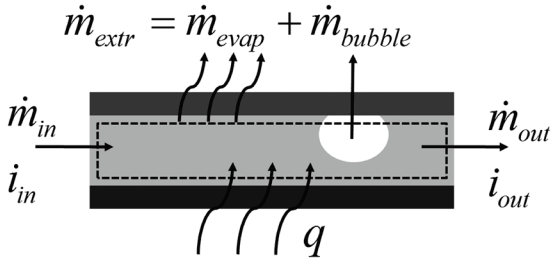

Figure 7. Schematic of the channel control volume.

2.7.1 Outlet Quality

The quality at the channel outlet can be evaluated by considering conservation relationships applied to the entire channel as shown in Figure 7. Combining conservation of mass and energy and neglecting kinetic energy terms results in:

$$q + \dot{m}_{in}\left(i_{in} - i_{out}\right) = \dot{m}_{extr}\left(i_{extr} - i_{out}\right) \tag{29}$$

To arrive at a reasonable approximation, $c_{p,l}$, i_l and i_v are assumed to be constant for the entire channel and the enthalpy of the extracted vapor is estimated as the enthalpy of superheated vapor inside the extraction chamber, i.e. $i_{extr} \approx i_v$. The conservation equation for inlet subcooled liquid becomes:

$$\dot{m}_{in}\left(i_{out} - i_l\right) = q - \dot{m}_{in} c_{p,l} \Delta T_{sub,in} - \dot{m}_{extr}\left[i_{lv} - \left(i_{out} - i_l\right)\right] \tag{30}$$

or

$$\frac{\left(i_{out} - i_l\right)}{i_{lv}} = \frac{\frac{q}{\dot{m}_{in}} - c_{p,l}\Delta T_{sub,in}}{i_{lv}} - \frac{\dot{m}_{extr}}{\dot{m}_{in}}\left[1 - \frac{\left(i_{out} - i_l\right)}{i_{lv}}\right] \tag{31}$$

Based on the definition of thermodynamic equilibrium quality where:

$$x_{out} = \frac{\left(i_{out} - i_l\right)}{i_{lv}} \tag{32}$$

the quality at the channel outlet becomes:

$$x_{out} = \frac{\dfrac{q}{\dot{m}_{in}} - c_{p,l}\Delta T_{sub,in}}{i_{lv}} - \frac{\dot{m}_{extr}}{\dot{m}_{in}} \Bigg/ \left(1 - \frac{\dot{m}_{extr}}{\dot{m}_{in}}\right) \tag{33}$$

or

$$x_{out} = \frac{x_{out}^{*} - N_{extr}}{1 - N_{extr}} \tag{34}$$

where the extraction number, N_{extr}, represents the ratio between the extraction and inlet mass flow rates and x_{out}^{*} represent the quality at the channel outlet that would occur without vapor extraction $\left(\dot{m}_{extr} = 0\right)$, defined as:

$$x_{out}^{*} = \frac{\dfrac{q}{\dot{m}_{in}} - c_{p,l}\Delta T_{sub,in}}{i_{lv}} \tag{35}$$

It should be noted that x_{out}^{*} can be rewritten in term of the modified Boiling number, $Bo_{in}^{*} = \dfrac{q}{\dot{m}_{in} i_{lv}}$, and Jacob number, $Ja_{in} = \dfrac{\rho_l}{\rho_v}\dfrac{c_{p,l}\Delta T_{sub,in}}{i_{lv}}$, as:

$$x_{out}^{*} = Bo_{in}^{*} - \left(\frac{\rho_v}{\rho_l}\right) Ja_{in} \tag{36}$$

The relationship among the variables in Eq. (34) is shown in Figure 8. The quality at the channel outlet decreases with increasing N_{extr}. This trend can be explained by the fact that both energy and mass are extracted through the membrane. Note that vapor extraction can decrease the quality at the outlet to be negative, i.e. the outlet is subcooled liquid, when the extraction mass flow rate is greater than generated vapor $\left(N_{extr} > x_{out}^{*}\right)$ due to excessive evaporation.

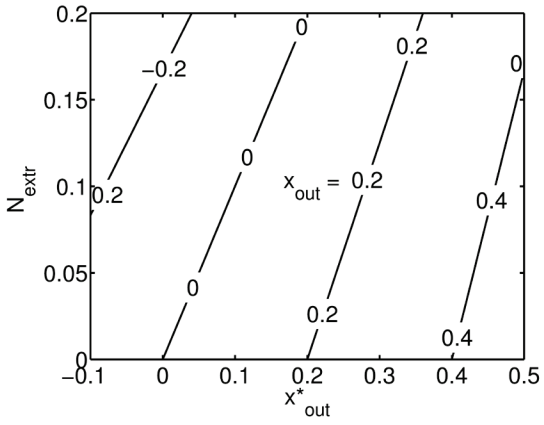

Figure 8. Outlet quality related to N_{extr} and x^*_{out}.

2.7.2 Boiling Condition

Incipience of boiling occurs when the wall superheat, $\Delta T_{sat} = T_w - T_{sat}$, is sufficient such that the local saturation pressure exceeds the combined static and surface tension induced pressures. Many studies have found that this wall superheat requirement depends on the size of active nucleation sites. For example, the nucleation criterion developed by Hsu [37] shows a range of active nucleation size as a function of wall superheat as:

$$\left\{r_{c,\min}, r_{c,\max}\right\} = \frac{\delta_t \sin\theta_{c,w}}{2\left(1+\cos\theta_{c,w}\right)}\left(\frac{\Delta T_{sat,ONB}}{\Delta T_{sat,ONB}+\Delta T_{sub,ONB}}\right)\left[1 \pm \sqrt{1-\frac{8\sigma T_{sat}\left(1+\cos\theta_{c,w}\right)\left(\Delta T_{sat,ONB}+\Delta T_{sub,ONB}\right)}{\rho_v i_{lv}\delta_t\left(\Delta T_{sat,ONB}\right)^2}}\right] \tag{37}$$

where $\theta_{c,w}$ is a wall contact angle and δ_t is estimated as k_l/h. Generally, for a system with sufficient active nucleation site, the minimum required wall superheat for the incipience of boiling can be simplified as:

$$\Delta T_{sat,ONB} = \sqrt{\frac{8C_b\sigma T_{sat} q''_w}{\rho_v i_{lv} k_l}} \tag{38}$$

where C_b was initially proposed by Hsu [37] for pool boiling as:

$$C_b = 1 + \cos\theta_{c,w} \tag{39}$$

Several investigators modified this minimum required wall superheat of boiling incipience model by modifying variable C_b. A few examples of variable C_b for the boiling incipience models are shown in Table 4.

Table 4. Variable C_b for boiling incipience models

Author	Model	Eq.
Sato and Matsumura [38] (Pool boiling)	$C_b = 1$	(40)
Ghiaasiaan and Chedester [39] (Microchannel)	$C_b = 22\xi^{0.765}$ where $\xi = \dfrac{\sigma_l\big\vert_{T_{sat}} - \sigma_l\big\vert_{T_w}}{\rho_l u_{in}^2 R^*}$ and $R^* = \left[\dfrac{2\sigma T_{sat} v_{lv} k_l}{q''_w i_{lv}}\right]^{1/2}$	(41)
Kandlikar [40] (Microchannel)	$C_b = 1.1$	(42)

To determine whether boiling occurs within the channel, the incipience of boiling criterion may be written in term of quality which can be easily compared with the quality at the channel outlet, given in the previous section as Eq. (34). Using definitions of the wall superheat and subcooling, $\Delta T_{sub} = T_{sat} - T_b$, then:

$$\Delta T_{sub} = \frac{q''}{h} - \Delta T_{sat} \tag{43}$$

Assuming that the fluid is entirely liquid from inlet to the point of the onset of nucleate boiling, the heat transfer coefficient is estimated as all-liquid heat transfer coefficient, h_{lo}, where:

$$h_{lo} = \frac{Nu_{lo} k_l}{D_h} \tag{44}$$

At the location where boiling starts, Eq. (43) is rewritten as:

$$\Delta T_{sub,ONB} = \frac{q''}{h_{lo}} - \Delta T_{sat,ONB} \tag{45}$$

Multiplying this by $\frac{c_{p,l}}{i_{lv}}$, and introducing the quality in the liquid region as:

$$x = \frac{i - i_l}{i_{lv}} = -\left(\frac{c_{p,l} \Delta T_{sub}}{i_{lv}} \right)$$

then

$$x_{ONB} = \frac{c_{p,l}}{i_{lv}} \left(\Delta T_{sat,ONB} - \frac{q''}{h_{lo}} \right) \tag{46}$$

For boiling to occurs within the channel, the quality at the channel outlet must be greater than the quality for the onset of nucleate boiling, i.e. $x_{out} \geq x_{ONB}$. Using the relationship among x_{out}, x_{out}^* and N_{extr}, presented in Eq. (34), the boiling condition can be determined in term of x_{out}^* and N_{extr}. The criterions of each boiling condition are summarized in Table 5. An example of the boiling map is generated by using the minimum wall superheat correlation by Hsu [37] and is shown in Figure 9.

Table 5. Boiling condition criteria

Boiling condition	Criterion	Eq.
No boiling	$\left(\frac{x_{out}^* - N_{extr}}{1 - N_{extr}} \right) < x_{ONB}$	(47)
Subcooled boiling	$x_{ONB} \leq \left(\frac{x_{out}^* - N_{extr}}{1 - N_{extr}} \right) < 0$	(48)
Saturated boiling without excess vapor	$x_{ONB} \leq \left(\frac{x_{out}^* - N_{extr}}{1 - N_{extr}} \right) = 0$	(49)
Saturated boiling with excess vapor	$\left(\frac{x_{out}^* - N_{extr}}{1 - N_{extr}} \right) > \begin{cases} x_{ONB}, & x_{ONB} \geq 0 \\ 0, & x_{ONB} < 0 \end{cases}$	(50)

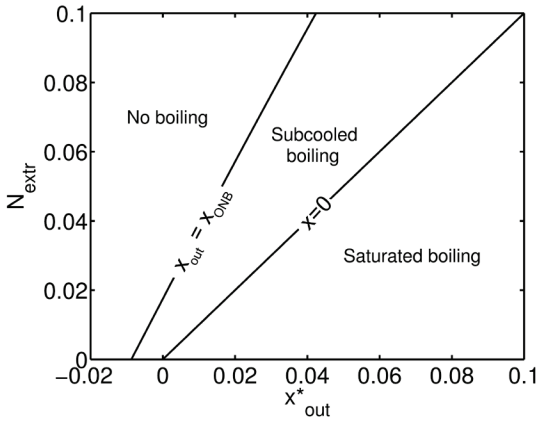

Figure 9. Example of a boiling map for flow in 500 μm × 500 μm channel with length of 50 mm and contact angle of 53° where inlet mass flux and subcooling are 400 kg/m^2·s and 10°C respectively.

2.7.3 Stability

The stability criterion applied to this study is based on whether vapor experiences reverse back flow into the inlet chamber. The criterion based on the model proposed by Salakij et al. [14-15], which was developed for flow boiling in a diverging channel with vapor extraction, is used in this study. The stability parameter, *St*, that represents the ratio of backward to forward forces acting on the upstream side of the liquid-vapor interface of the expanding bubble, is expressed as:

$$St = \sqrt{\frac{\rho_v \left(\dfrac{q''_w A_{heat,bub} - \dot{m}''_{extr} i_v A_{extr,bub}}{\rho_v i_{lv}} \dfrac{1}{A_{c,1} + A_{c,2}} \right)^2 A_{c,1}}{\dfrac{G_{in}^2 A_{c,1}}{\rho_l} + \sigma \wp_{w,1} \cos\theta_d}} \tag{51}$$

where subscript 1 and 2 represent the location of upstream and downstream sides of an expanding bubble, respectively. The transition from stable to unstable flow occurs when $S_t = 1$ at the extreme case where expanding bubble fills the channel and barely reverses into the inlet chamber such that $A_{heat,bub} = A_{heat,chan}$, $A_{extr,bub} = A_{extr,chan}$, $A_{c,1} = A_{c,in}$ and $A_{c,2} = A_{c,out}$. It should be noted that this model does not account for the instability due to

insufficient nucleation sites. Since the half-diverging angle of the channel, θ_d, is usually relatively small on the order of 1°-3°, the term cos θ_d may be approximated as 1. In this study, the criterion for stable flow ($St < 1$) is rearranged and is expressed in dimensionless form as:

$$Bo_{in}^{*} < \left(1+\frac{A_{c,out}}{A_{c,in}}\right)\left[\frac{\rho_v}{\rho_l}\left(1+\frac{4}{We_{in}}\right)\right]^{1/2} + N_{extr}\frac{i_v}{i_{lv}} \tag{52}$$

where Weber number is defined as $We_{in} = \dfrac{G_{in}^2 D_{h,in}}{\rho_l \sigma}$.

The stability map for water at 100°C is shown in Figure 10 where the left hand side of the line is stable region. Figure 10(a) shows that the stability region for a uniform cross-sectional channel is the smallest when We_{in} approaches infinity which represents negligible surface tension effects that suppress the instability compared with the inertia forces. This case is chosen to show the effect of varying cross-sectional area ratio, as shown in Figure 10(b). In general, the stability region can be extended by increasing the cross-sectional area ratio $\left(A_{c,out}/A_{c,in}\right)$ and N_{extr}, and decreasing We_{in}. This supports the results from several investigators [7, 10-12] that expanding the channel improves flow stability.

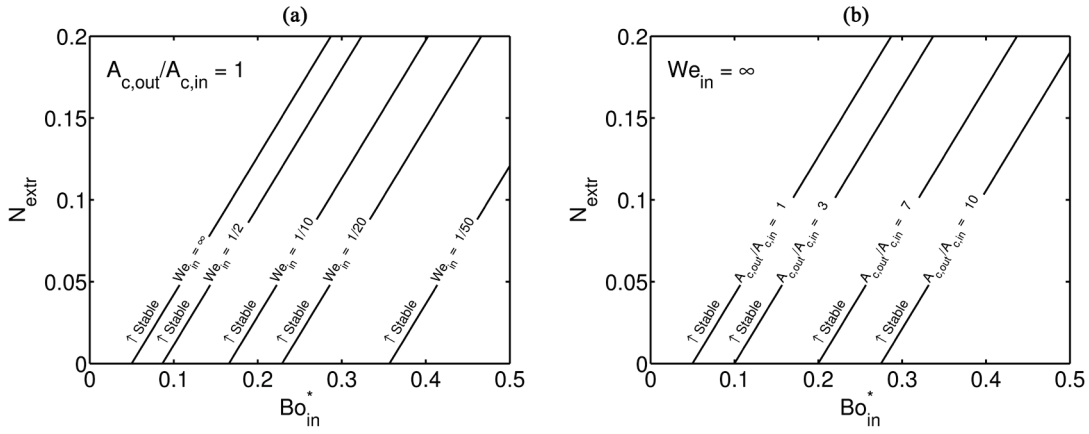

Figure 10. Stability map for water at 100°C.

2.8 DISCUSSIONS

Ideally the completed extraction mechanism and extraction flow regime maps should be developed in form of an independent single map. However, it may not be practical to combine all individual criterion together in this case because there are so many independent variables to be included on a two-dimensional map. For example, to get the complete single dimensional extraction mechanism map for a specific fluid flow in a specific channel geometry still needs four independent variables: either (P_{extr} , T_{mem} , G and x) or (P_{extr} , T_{mem} , j_l and j_v). As previously suggested, it would be more practical to use individual maps to identify physical conditions of the regime, and then combine the known predicted conditions to identify the regime.

The regime transition criteria developed in this study are fully predictive based on physical concepts. The important assumptions used in the development are listed below:

- Film rupture when film thickness is in the same order as surface roughness.
- Membrane contact phase is strongly dependent on hydrodynamics of the flow where stratified flow and intermittent flows are related to vapor only and mixed phases contact, respectively.
- Transition from stratified to intermittent flow is caused by rapid wave growth due to the decreasing in pressure of vapor flow, and liquid phase must be sufficient to form a slugs. (Taitel and Dukler [28])
- Membrane hydrophobicity prevents the surface tension force from pulling liquid to the wall to form slugs.
- Negligible pressure differences occur between pressure inside the bubble and surrounding liquid.
- For extraction flow analysis, fluid properties are assumed to be constant along the flow.

- Enthalpy of the extracted vapor is estimated as the enthalpy of superheated vapor inside the extraction chamber.

Most of the assumptions and models used in this study have been validated and shown to be reliable for specific conditions in other types of applications. It is expected that to apply these models with reasonable adaptation to in-situ vapor extraction application, further modification is required. The models for regime transition criteria in this work are developed such that they can be adjusted easily. For example, dimensionless coefficients C_w and C_b for rapid wave growth, and onset of nucleate boiling criteria, respectively, can be modified to capture other effects.

To validate the assumptions and models for extraction mechanism regime transition, flow visualization on both sides of the membrane is required such that the membrane contact phase and breakthrough can be observed. Because an extraction mechanism regime depends on the local condition, the test section should be small and short such that quality of flow boiling does not vary significantly within the observed section. The membrane surface temperature has to be measureable or, even better, controllable. For extraction flow regime transition, precise measurements of mass flow rate, fluid temperature, pressure and quality at inlet, outlet and extraction chamber are required as well as flow visualization to identify boiling mechanism and flow instability.

2.9 CONCLUSIONS

A systematic development of transition criteria for extraction mechanism and extraction flow regimes has been presented. All of the transition criteria are developed on a basis which can be easily modified to account for additional effects. Although the validation of the extraction mechanism and extraction flow regime transition criteria was not performed here, most models and assumptions have been validated in part in other applications. The methodology to validate transition models has been proposed and recommended for the following works. Examples of membrane contact phase, possibly

extraction mechanism and stability maps, and effect of extraction on outlet quality are shown as tools to identify regimes.

2.10 ACKNOWLEDGEMENTS

The authors acknowledge the financial support of this work from Office of Naval Research (N00014-09-1-1079, Dr. Mark Spector, program manager).

2.11 NOMEMCLATURE

A	Area
Bo^*	Modified Boiling number, $Bo^* = \frac{q}{\dot{m} i_{lv}}$
Ca_v	Capillary number, $Ca_v = \frac{\mu_l j_v}{\sigma}$
C_b	Dimensionless parameter for minimum wall superheat requirement
C_w	Rapid wave growth factor
c_p	Specific heat
d_p	Equivalent membrane pore size
D_h	Hydraulic diameter
Fr^*	Modified Froude number, $Fr^* = \sqrt{\frac{\rho_v}{\rho_l - \rho_v}} \frac{j_v}{\sqrt{gH\cos\alpha}}$
g	Acceleration due to gravity
G	Mass flux
H	Channel depth
H_l	Liquid level height
h	Heat transfer coefficient
i	Enthalpy
i_{lv}	Heat of vaporization
Ja	Jacob number, $Ja = \frac{\rho_l}{\rho_v} \frac{c_{p,l} \Delta T_{sub}}{i_{lv}}$
j	Superficial velocity

k	Thermal conductivity
$\dot{m}$	Mass flow rate
N_{extr}	Extraction number, $N_{extr} = \dot{m}_{extr} / \dot{m}_{in}$
Nu	Nusselt number
P_{extr}	Extraction absolute pressure
$\wp_w$	Wetted perimeter
q	Heat input rate
q''	Heat flux
S	Contact surface per unit length
St	Stability parameter
T	Temperature
u	Velocity
v	Specific volume
W	Channel width
We	Weber number, $We = \dfrac{G^2 D_h}{\rho_l \sigma}$
X^2	Lockhart-Martinelli parameter
x	Thermodynamic equivalent quality
x^*_{out}	Ideal exit quality without vapor extraction, $x^*_{out} = \dfrac{\dfrac{q}{\dot{m}_{in}} - c_{p,l}\Delta T_{sub,in}}{i_{lv}}$
Y	Dimensionless parameter presented in [28], $Y = \dfrac{(\rho_l - \rho_v) g \sin\beta}{\left(dP/dz\right)\Big\vert_v}$

Greek

α	Void fraction
α_c	Channel aspect ratio, $\alpha_c = W/H$
β	Channel inclination angle
δ_c	Surface roughness

δ_t	Thermal boundary thickness, $\delta_t = k_l / h_{lo}$
ΔP_{extr}	Extraction pressure differential
ΔT_{sat}	Wall superheat, $\Delta T_{sat} = T_w - T_{sat}$
ΔT_{sub}	Subcooling, $\Delta T_{sub} = T_{sat} - T_b$
θ_c	Contact angle
θ_d	Half-diverging angle
κ	Specific permeability
μ	Dynamic viscosity
ν	Kinematic viscosity
ρ	Density
σ	Surface tension

Subscripts

b	Bulk
bub	Bubble
c	Cross-sectional
extr	Extraction
heat	Heated
i	Liquid-vapor interface
in	Inlet
l	Liquid phase
lo	All-liquid
mem	Membrane
ONB	Onset of nucleate boiling
out	Outlet
sat	Saturation
v	Vapor phase
w	Wall

3 MODELING IN-SITU VAPOR EXTRACTION DURING CONVECTIVE BOILING IN FRACTAL-LIKE BRANCHING MICROCHANNEL NETWORKS

Saran Salakij, James A. Liburdy, Deborah V. Pence, Mario Apreotesi

International Journal of Heat and Mass Transfer

Elsevier B.V., Radarweg 29, Amsterdam 1043 NX, Netherlands

Volume 60, Pages 700-712

3.1 ABSTRACT

The pressure drop penalty of convective boiling flow in microchannels may be exceedingly large. A proposed method of reducing this penalty is to extract vapor locally along the channel. A potential consequence of this extraction is that the local void fraction reduction positively influences the local heat transfer coefficient. In this study, a one dimensional model was developed to simulate convective boiling flow through a fractal-like branching microchannel network with vapor extraction through a channel wall formed using a hydrophobic porous membrane. The goal of the model is to provide a design tool that can assess the effects of vapor extraction on flow boiling heat transfer performance. Heat was applied through all walls of the channel. Vapor extraction was obtained by applying a pressure difference across the membrane. Membrane transport models of the extraction process based on local channel pressure and local saturation pressure are discussed. Predicted local conditions and global results are presented for two ranges of conditions: (i) relatively low inlet flow rate with low heat flux and (ii) relatively high inlet flow rate with high heat flux. Results shows that as the vapor extraction rate increases, there is a significant reduction in pressure drop through the channel, a reduction of the bulk fluid temperature, and a reduction in exit vapor quality.

Keywords: Vapor extraction, Vapor separation, Fractal, Two-phase flow, One-dimensional model, Heat sink

3.2 INTRODUCTION

An effective heat sink should achieve a high heat removal rate, maintain a low and relatively uniform and stable temperature and minimize the overall pressure loss and/or flow power requirements. The advantages of using microchannels are higher surface area per unit volume, larger heat transfer coefficients, low flow rate requirements and minimal coolant volume. Flow boiling heat sinks can operate at much higher heat flux and more uniform temperature than single-phase heat sinks, see reviews [1-2, 41]. However, these advantages come with consequences such as large pressure drops and flow instabilities associated with two-phase microscale flow [42-43]. A large pressure

drop can also contribute to non-uniform operating temperature when flow is in the two-phase regime.

To help reduce pressure drop, Pence [44] studied the use of a fractal-like branching network which mimics flow distribution patterns found in nature. As fluid flows downstream, the flow cross-sectional area bifurcates and results in an increase in total cross-sectional area. For fixed convective areas (wall area), exit channel dimensions and identical flow rates, the pressure drop and temperature gradient along the branching network are smaller than those of parallel microchannels in both single-phase and two-phase flows; several studies [44-49] have confirmed this both numerically and experimentally. Also, the optimization of the design of the fractal-like branching network was studied by Heymann et al. [50-51].

Studies suggest that the pressure drop across microscale heat sinks can also be improved by locally extracting vapor from two-phase flow through a hydrophobic, porous membrane forming one wall of the channel [16-17, 19]. Apreotesi et al. [16-17] provided experimental results of diabatic boiling water flowing through a fractal-like microchannel heat sink with local vapor extraction that show a decrease in overall channel pressure drop as the extraction pressure difference increases. A study by David et al. [19] with flow boiling in a microchannel heat sink used one wall fabricated from a hydrophobic porous membrane to allow venting of the vapor. Their experimental results with vapor venting show a significantly reduced pressure drop when compared to the non-venting results. Also, David et al. [27] discuss various flow regions with both adiabatic and diabatic flow with venting.

To model pressure drop, separated flow models have been used for two-phase flow in minichannels and microchannels. Most separated flow models are based on the Lockhart and Martinelli [52] relationship, such as the models presented by Mishima and Hibiki [53], Lee and Lee [54], Qu and Mudawar [4], Lee and Mudawar [55], and Hwang and Kim [56]. All of these predictive models do show good agreement with specific experimental data.

The present study has the added complexity of vapor extraction along the channel across a porous membrane. The process can be related to vacuum membrane distillation, which has been described in a number of studies [30-33]. Basically, distillation uses thermally induced transport of vapor through a porous hydrophobic membrane. A heated, aqueous feed solution is brought into contact with the feed side of the membrane. Vapor flow through the membrane has been successfully modeled based on Darcy's law, using the local vapor pressure difference across a membrane of a given permeability.

In order to predict the pressure differential across the membrane, it may be necessary to predict the local wall temperature, using a local heat transfer coefficient. As discussed later, this is to determine a film temperature based vapor pressure. For two-phase boiling flow, flow boiling heat transfer can be divided into nucleate boiling and convective boiling components. The boiling heat transfer coefficient of the nucleate boiling is a function of wall heat flux only whereas convective boiling is a function of quality and mass velocity. Some studies [57-58]suggest that the nucleate boiling mechanism is dominant. Others [10, 59-64] show that the boiling heat transfer coefficient is affected by quality and mass velocity as well as wall heat flux. Bertsch et al. [2] and Ribatski et al. [41] analyzed the experimental results for microscale two-phase flow from various investigators and conclude that the existing flow boiling heat transfer correlations poorly predicts the experimental database. For this study, the model from Lee and Mudawar [64] is used.

In this paper, a predictive one-dimensional model for flow boiling in a microscale fractal-like branching network with local vapor extraction for a range of heat flux and mass flow rate are presented and discussed. Several options of the local extraction driving pressure which drives flow across the membrane are presented. Pressure drop, temperature distribution and extracted vapor mass flow rate are presented. The results are compared with the experimental data of Apreotesi et al. [16-17] for relatively low flow rates and low heat flux conditions; experimental high flow rates and high heat flux data are not available in the literature.

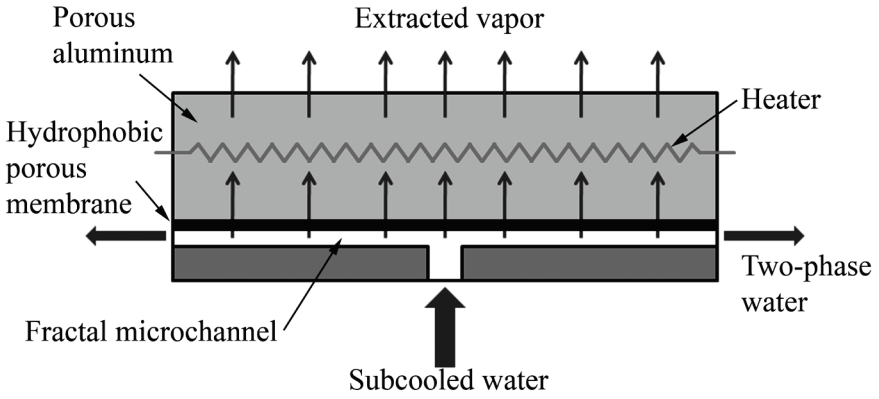

Figure 11. Schematic cross-sectional of assembled heat sink (adapted from [16])

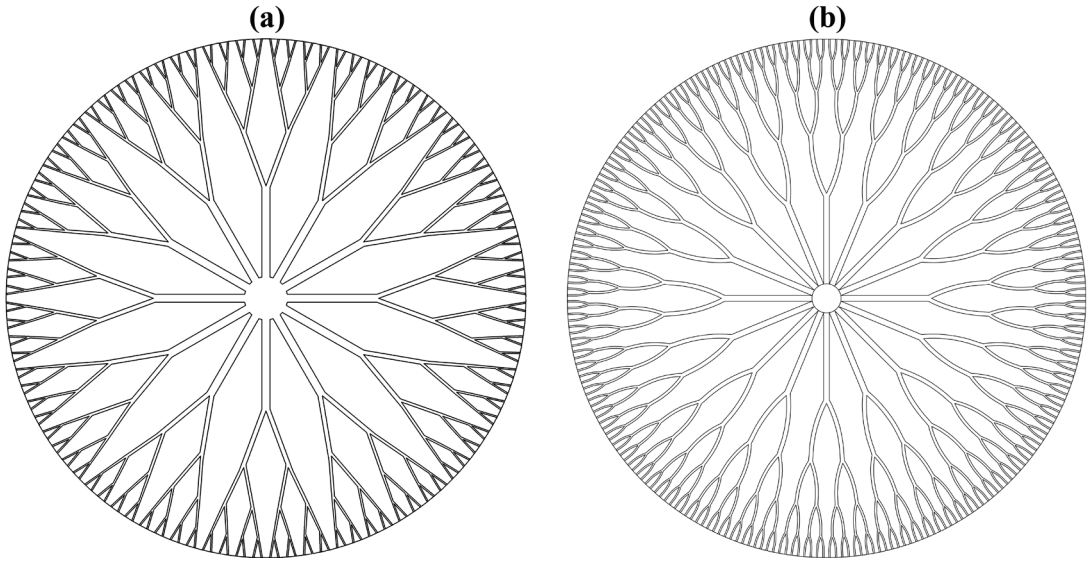

Figure 12. Schematic of two fractal-like channel networks in a circular heat sink described in Table 1 with channel length ratio, γ, of 0.7071 and (a) hydraulic diameter ratio, β_{D_h}, of 0.7937 (geometry F1), and (b) width ratio, β_w, of 0.7071 (geometry F2)

3.3 FLOW GEOMETRY

In this study, a generalized model for vapor extraction is developed and applied to a fractal-like branching microchannel heat sink. A cross-section schematic of the flow

channel is shown in Figure 11, whereas representative planform views are provided in Figure 12. Flow enters from the center of the disk and flows radially through the branching channels. In the experimental investigation, (Apreotesi et al. [16-17]) a hydrophobic porous membrane with a porous aluminum backing for support serves as the porous top wall of the channels. The porous aluminum block had an embedded resistance heater to assure no vapor condensation within the block. The vapor is drawn through the hydrophobic membrane and porous aluminum by applying a vacuum to a plenum located above the aluminum. These conditions are incorporated into the model.

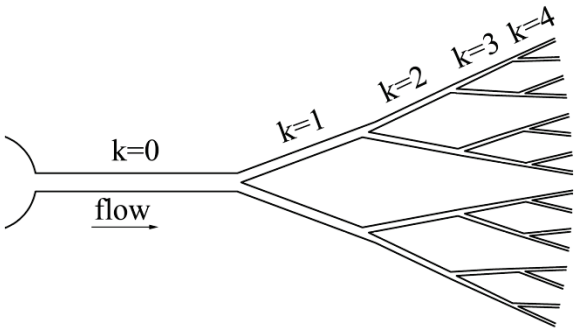

Figure 13. A subset of the fractal flow network showing four bifurcations (M = 4) resulting in a total of five branch levels

A single branch from the experimental test device is shown in Figure 13 where the integer index k indicates the level of the channel with the $k = 0$ level originating at the inlet plenum. There are two types of fractal-like microchannel networks numerically investigated in this study: one with a fixed hydraulic diameter ratio and the other with a fixed width ratio. In all cases, the channel depth, H, remain fixed. The fractal-like network used by Apreotesi et al. [16] has a fixed hydraulic diameter ratio, β_{D_h}, and a fixed length ratio, γ, between the upstream channel level, k, and the downstream channel level, $k+1$, using the following scaling laws:

$$\beta_{D_h} = \frac{D_{h,k+1}}{D_{h,k}} \tag{53}$$

$$\gamma = \frac{L_{k+1}}{L_k} \tag{54}$$

In general, the number of branches into which an upstream channel may split is given by n, in this case, $n = 2$, and N_0 is the number of initial branches emanating radially from the inlet plenum. Consequently, the number of branches at each level k becomes:

$$N_k = N_0 n^k \tag{55}$$

The total length of the channels in the network, L_{tot}, is obtained from the summation:

$$L_{tot} = \sum_{k=0}^{M} L_k \tag{56}$$

where M is the total number of branching level streamwise bifurcations. In Figure 13, $M = 4$ resulting in 5 levels.

The second type of the fractal-like branching network is based on a fixed width ratio. The fractal-like aspects of this geometry are the same as previously described except the width ratio is fixed instead of hydraulic diameter ratio. The width ratio, β_w, is defined by:

$$\beta_w = \frac{w_{k+1}}{w_k} \tag{57}$$

Table 6. Geometry detail of two fractal-like networks, F1 and F2, used in this study

Geometry	F1	F2
Hydraulic diameter ratio, β_{D_h}	0.7937	-
Width ratio, β_w	-	0.7071
Length ratio, γ	0.7071	0.7071
Channel depth, H	250 μm	150 μm
Terminal branch width, w_t	100 μm	100 μm
Total flow length, L_{tot}	18.0 mm	17.5 mm
Disk diameter, D_{disk}	36.6 mm	35.5 mm
Planar area, A_{planar}	10.52 cm^2	9.90 cm^2
Number of initial branches, N_0	12	16
Number of branches per level, n	2	2
Number of branching level, M	4	4

where w is the channel width. This design was first proposed and recommended by Pence and Enfield [65] because a fixed hydraulic diameter ratio with a constant channel depth expects in an infinite channel width for the lower order branching levels for $M > 4$. Details of the geometric variables used in this study are given in Table 6.

3.4 MODEL DESCRIPTION

The predictive model developed here is aimed at predicting global behavior and, once validated, can be used as a design tool for heat sink applications. The model determines the relationship between the vapor extraction rate and the pressure drop through the microchannel network for a given heat flux and inlet mass flow rate. This model is based on conservation laws written for a one-dimensional boiling microchannel flow network. Existing correlations for channel pressure drop and heat transfer coefficients are used and are discussed below. These correlations assume that the onset of boiling occurs at a thermodynamic equilibrium quality of zero, i.e. the fluid remains a single-phase liquid until the local pressure and temperature reach the saturation conditions at which the fluid is converted to a saturated two-phase fluid. For fractal-like branching flow, the hydrodynamic and thermal boundary layers are assumed to redevelop following each bifurcation while the pressure change at each bifurcation is assumed to be

negligible. This was shown to be a realistic assumption by Daniels et al. [47-48]. Although more complex flow physics associated with the boiling process during extraction is not included, it is thought that the overall pressure drop and vapor extraction prediction are still reasonably evaluated. This is because the pressure drop correlations have been validated in microchannel flows in the literature (e.g. [4, 47-48]) and the vapor extraction is based on a Darcy flow through the permeable membrane, which has been validated in membrane distillation applications [32], and other applications.

3.4.1 Model Implementation

The channel pressure drop and the extracted vapor mass flow rate are the desired outputs from the one-dimensional model. The model has been developed using conservation of mass and energy as well as a pressure drop model based on conservation of momentum for discrete elements along the microchannel accounting for local vapor mass and energy extraction. The inputs are the flow geometry, porous membrane and support backing properties, the outlet pressure, the inlet mass flow rate, the heat input, the extraction pressure, and either inlet subcooling or inlet temperature. For the fractal-like branching microchannel network, required geometric inputs are the channel height, the terminal channel width, the total length of the flow path, the number of initial branches, the number of branch levels, the length ratio and either the hydraulic diameter ratio or width ratio. The porous membrane and porous backing require inputs of their specific permeability and the thickness.

A schematic of the model transport is shown in Figure 14. The flow path is divided into non-uniform elements. Nominally, a 5 μm element length is initially specified. Because the two-phase pressure gradient is much larger than the single-phase pressure gradient, the two-phase region nodal spacings are reduced, typically to approximately 1 μm, based on local conservation constraints. Each branching level is divided into an integer number of elements. At the bifurcation node, fluid flow is assumed to be split equally into each channel with the new cross-sectional area. The geometric details of the bifurcation are not included, although the hydraulic and thermal development models are included as mentioned earlier. A grid refinement analysis was

performed. The local pressure and local quality values varied by less than 0.5% and 0.25%, respectively when the grid size was reduced by a factor of one half (2.5 μm in the single phase and 0.5 μm in the two phase region).

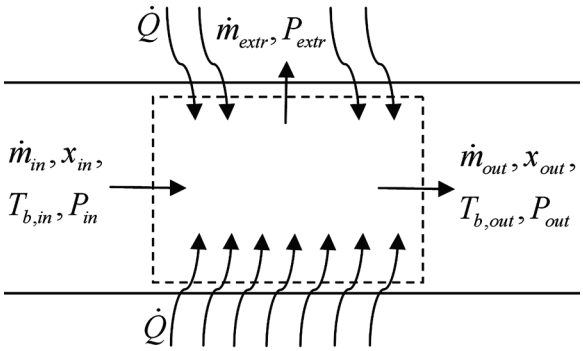

Figure 14. Schematic of discretized control volume used in predictive model

The model is initiated by guessing the inlet pressure for a specified exit pressure and marching in the streamwise direction to calculate the local static pressure, bulk fluid temperature, wall surface temperature and fluid properties. For each element, pressure drop and extracted vapor flow rate, based on the membrane transport model, are evaluated. The governing equations for pressure drop, membrane transport and heat transfer models are discussed in later sections. Using conservation of mass and energy, the pressure drop and the heat transfer models, each element undergoes an internal iteration to satisfy local pressure and temperature values. Upon reaching the exit of the channel, if the calculated exit pressure differs from the specified value by more than 0.05%, the inlet pressure is updated and the pressure along the entire channel length is recalculated.

The internal iteration of elements in the single-phase region includes extracted vapor mass flow rate by evaporation, which is accounted for in the energy and mass flow rates of each element. Both mass flow rate and fluid properties, which are sensitive to temperature variations, are simultaneously updated in the internal iteration. Because the liquid phase properties are not a strong function of pressure, and the pressure variation in

each element in this study is small, the single-phase pressure drop of each element is evaluated after the internal iteration of conservation of mass and energy. In the two-phase region, the pressure drop calculation is included in the internal iteration because the pressure and temperature in equilibrium conditions are related. Besides mass flow rate and fluid properties, the quality in the two-phase flow is updated simultaneously in the internal iteration. This is because quality varies with both pressure and temperature and is an important parameter in two-phase pressure drop model. Further details of the model implementation are given by Salakij [66].

3.4.2 Conservation of Mass and Energy

Conservation of mass and energy is used which accounts for local vapor extraction for the discretized control volume, as shown in Figure 14:

$$\dot{m}_i = \dot{m}_{i-1} - \dot{m}_{extr,i} \tag{58}$$

and

$$\dot{m}_i i_i = \dot{m}_{i-1} i_{i-1} + \dot{Q}_i - \dot{m}_{extr,i} i_{extr,i} \tag{59}$$

The last term in Eqs. (58) and (59) represents the mass flow rate of extracted vapor and its convective energy transfer rate that leaves the control volume with the extracted vapor, respectively. The enthalpy of extracted vapor, $i_{extr,i}$, is evaluated as the enthalpy of saturated vapor based on the average bulk fluid temperature inside the control volume where the extracted mass flow rate, $\dot{m}_{extr,i}$, is determined from the membrane transport model discussed in detail in a later section. In this study, there is a membrane support backing through which heat is supplied to the channel. Consequently, the membrane which forms the channel's top surface, performs as a heated surface. By assuming a constant heat flux applied to the channel's top surface, the heat transfer rate into the element i, $\dot{Q}_i$, is determined based on the element channel's top area fraction as:

$$\dot{Q}_i = \dot{Q} \frac{A_i}{A_{chan,top}} \tag{60}$$

where

$$A_i = w_i \Delta z_i \tag{61}$$

and $$A_{chan,top} = N_0 \sum_i \left(2^n A_i\right) \tag{62}$$

It should be noted that the total top area of the channel network, given in Eq. (62), is different (less) than the disk planar area.

3.4.3 Pressure Drop Model

The pressure drop for each element along the flow path is calculated individually. The pressure drop has two components: friction, ΔP_{fric}, and acceleration, ΔP_{acc}. Therefore, the pressure drop for element i in the flow network is expressed as:

$$-\Delta P_{chan}\Big|_i = -\left(\Delta P_{fric} + \Delta P_{acc}\right)\Big|_i \tag{63}$$

The frictional pressure drop, ΔP_{fric}, can be determined from the product of the two-phase multiplier, ϕ_l^2, and the liquid phase pressure gradient:

$$\left.\frac{dP}{dz}\right|_{fric} = \phi_l^2 \left.\frac{dP}{dz}\right|_{fric,l} = -\phi_l^2 \left(\frac{2 f_{loc,lo} \left(1-x\right)^2 G^2}{\rho_l D_h}\right) \tag{64}$$

where $f_{loc,lo}$ is the local all-liquid Fanning friction factor. Because the local all-liquid Reynolds number never goes beyond 900 for all predicted results, the flow is taken to be laminar. For laminar flow, the local friction factor varies along the flow accounting for hydrodynamic boundary layer development. This local friction factor is based on the apparent friction factor model given by Shah and London [67], which provides an average value up to a specific location z, such that the local value can be evaluated as:

$$f_{loc,lo}\Big|_z = f_{app}\Big|_z + z \left.\frac{df_{app}}{dz}\right|_z \tag{65}$$

where $$f_{app}\,\mathrm{Re}_{lo} = \frac{3.44}{\sqrt{z^+}} + \frac{f_{lo}\,\mathrm{Re}_{lo} + \dfrac{K(\infty)}{4z^+} - \dfrac{3.44}{\sqrt{z^+}}}{1 + \dfrac{C}{\left(z^+\right)^2}}, \tag{66}$$

$$\text{and} \quad \frac{df_{app}}{dz} = \frac{1}{D_h \,\mathrm{Re}_{lo}^2}\left[\frac{-3.44}{2\left(z^+\right)^{3/2}} + \frac{\dfrac{2 f_{lo}\,\mathrm{Re}_{lo}\,C}{\left(z^+\right)^3} - \dfrac{K(\infty)\left(1-\dfrac{C}{\left(z^+\right)^2}\right)}{4\left(z^+\right)^2} + \dfrac{3.44\left(1-\dfrac{3C}{\left(z^+\right)^2}\right)}{2\left(z^+\right)^{3/2}}}{\left(1-\dfrac{C}{\left(z^+\right)^2}\right)^2}\right]. \quad (67)$$

Here the non-dimensional length is given by:

$$z^+ = \frac{z/D_h}{\mathrm{Re}} \quad (68)$$

$K(\infty)$ is the incremental pressure defect and C is a constant dependent on the channel aspect ratio given as tabulated values in Shah and London [67]. Further model details can be found in Salakij [66]. By integrating the frictional pressure gradient, Eq. (64), across element i, the frictional pressure drop across element i is evaluated as:

$$-\Delta P_{fric}\Big|_i = \frac{2}{D_h}\int_{i-1}^{i}\left(\frac{f_{loc,lo}\left(1-x\right)^2 G^2 \phi_l^2}{\rho_l}\right)dz \quad (69)$$

Using a trapezoidal integration approximation, Eq. (69) becomes:

$$-\Delta P_{fric}\Big|_i = \frac{\Delta z_i}{D_h}\left[\left(\frac{f_{loc,lo}\left(1-x\right)^2 G^2 \phi_l^2}{\rho_l}\right)\Bigg|_i + \left(\frac{f_{loc,lo}\left(1-x\right)^2 G^2 \phi_l^2}{\rho_l}\right)\Bigg|_{i-1}\right] \quad (70)$$

It should be noted that the mass flux of fluid in the channel, G, changes along the flow direction due to changes in both cross-sectional area and vapor extraction. For single-phase flow, the two-phase multiplier and quality are equal to 1 and 0, respectively. For two-phase separated flow, Chisholm and Laird [68] and Chisholm [69] present closed form expressions for the two-phase multiplier, ϕ_l^2, as a function of Lockhart-Martinelli parameter, X^2, and the phase interaction parameter, C_{LM}:

$$\phi_l^2 = 1 + \frac{C_{LM}}{\mathrm{X}} + \frac{1}{\mathrm{X}^2} \tag{71}$$

where X^2 is given by Carey [70]:

$$\mathrm{X}^2 = \frac{\left(dP/dz\right)\Big|_l}{\left(dP/dz\right)\Big|_v} = \left(\frac{\mu_l}{\mu_v}\right)^n \left(\frac{1-x}{x}\right)^{2-n} \left(\frac{\nu_l}{\nu_v}\right) \tag{72}$$

and n is the exponent of the Reynolds number in the Blasius equation which is equal to 1 for laminar flow. The phase interaction parameter is dependent on the mass flux as proposed by Qu and Mudawar [4]:

$$C_{LM} = 21\left(1 - e^{-319 D_h}\right)\left(0.00418G + 0.0613\right) \tag{73}$$

The acceleration pressure drop, ΔP_{acc}, in a constant area channel can be determined from the acceleration pressure gradient [70]:

$$-\left.\frac{dP}{dz}\right|_{acc} = \frac{d}{dz}\left(\frac{G^2 x^2 v_v}{\alpha} + \frac{G^2 \left(1-x\right)^2 v_l}{\left(1-\alpha\right)}\right) \tag{74}$$

where α is the void fraction. The void fraction is expressed as a function of local quality, x, as proposed by Zivi [35]:

$$\alpha = \frac{1}{1 + \left(\frac{1-x}{x}\right)\left(\frac{v_l}{v_v}\right)^{2/3}} \tag{75}$$

It should be noted that although this void fraction correlation was not directly developed for microchannel flow, it was developed assuming annular flow which is documented to be the dominated flow pattern in microchannel [71]. By integrating the acceleration pressure gradient across element i, the two-phase acceleration pressure drop across element i is evaluated as:

$$-\Delta P_{acc,i} = \left\{ G^2 \left[\frac{x^2 v_v}{\alpha} + \frac{\left(1-x\right)^2 v_l}{\left(1-\alpha\right)} \right] \right\}_i - \left\{ G^2 \left[\frac{x^2 v_v}{\alpha} + \frac{\left(1-x\right)^2 v_l}{\left(1-\alpha\right)} \right] \right\}_{i-1} \tag{76}$$

For single-phase flow, the quality, *x*, and void fraction, α, are set to 0.

3.4.4 Membrane Transport Model

Transport across the membrane may occur either as evaporation or bubble extraction. Evaporation will occur in the single-phase region and both modes can coexist in the two-phase flow region. The evaporative extraction, similar to membrane distillation, occurs when the liquid phase near the membrane evaporates and is then extracted through the membrane. The bubble extraction occurs when a bubble is directly in contact with the membrane and is extracted through it.

In this study, a hydrophobic membrane, matched in terms of permeability and thickness with that used in experiment. The mass transport of vapor across the membrane is based on Darcy's law [32] and can be expressed as:

$$\dot{m}''_{extr} = \rho_v K \nabla P^0_{vap} = \frac{\kappa}{\nu_v} \nabla P^0_{vap} \tag{77}$$

where $\dot{m}''_{extr}$ is the vapor mass flux flowing through the porous media, κ is the specific permeability, ν_v is the vapor kinematic viscosity and ∇P^0_{vap} is the vapor pressure gradient across the porous media. Because experimental data will be used to validate the model, which includes a porous backing material to support the membrane, the membrane and backing are treated as a series of flow resistors dependent upon the thickness and the specific permeability of each layer. The total pressure drop is then determined based on the membrane and backing material, By assuming a linear pressure distribution in each porous layer, the pressure gradient through each layer of thickness δ_i reduces to $\Delta P / \delta_i$, which is then used to determine the total pressure drop between the channel and extraction plenum chamber based on the total resistance Writing this in terms of the mass flow rate through the membrane, the local extracted vapor mass flow rate of element i is expressed as:

$$\dot{m}_{extr}\Big|_i = \left[\frac{A_{extr}}{\nu_v} \left(\frac{\delta_{mem}}{\kappa_{mem}} + \frac{\delta_{back}}{\kappa_{back}} \right)^{-1} \Delta P_{driv,loc} \right]_i \tag{78}$$

where A_{extr} is the area of extraction and $\Delta P_{driv,loc}$ represents the local value of the total differential pressure across the combined membrane and porous backing.

It should be noted that mass transport across the membrane may occur due to both evaporation and bubble extraction, Eq. (78) is used to account for both transport processes in the two-phase flow region. The model for the extracted vapor mass flux for both evaporative and bubble extraction is a function of the driving pressure differential based on the saturation pressure of the liquid for evaporative extraction and pressure of the vapor at the membrane for bubble extraction. Although these pressures in the two-phase region may be slightly different, say as a result of surface tension effects, this difference is assumed to be negligible in this model.

Three different models were evaluated for the local extraction driving pressure, $\Delta P_{driv,loc}$, which are shown in Table 7, where the local channel pressure is denoted by $P_{chan,loc}$ and P_{extr} is the extraction pressure, both expressed as absolute pressures. The first model, denoted as Eq. (79) in Table 7, is based on a driving pressure differential using the local bulk pressure in the channel. This was used by Apreotesi [17] where vapor was assumed to be only extracted when vapor phase is present, i.e. thermodynamic equilibrium quality is greater than zero. Consequently this model does not account for evaporation in the single-phase liquid region. The other two models, Eqs. (80) and (81), relax this restriction and allow vapor to be extracted from the liquid phase by evaporation in both single-phase and two-phase regions. The driving pressure in the second and third models is based on the saturation pressure on the channel side of the membrane. In the second model, Eq. (80), the saturation pressure is defined using the bulk channel temperature, T_b, as the saturation temperature and in the third model, Eq. (81), the saturation pressure is determined using a film temperature, $(T_w + T_b)/2$ to represent the local saturation temperature. The idea in the latter model is that the driving mechanism for vapor transport based on Darcy flow through the membrane is related to the local saturation pressure adjacent to the membrane. Consequently, the third model requires

determination of the wall temperature which can be determined based on the local heat transfer coefficient.

Table 7. Local extraction driving pressure models and extracted mass flow rate variation from experimental results [16-17]

Pressure differential	$MAE_{\dot{m}_{extr}}$ (%)	Eq.
$\Delta P_{driv,loc} = \begin{cases} P_{chan,loc} - P_{extr} & ,x > 0 \\ 0 & ,x \le 0 \end{cases}$	20.3	(79)
$\Delta P_{driv,loc} = P_{sat}\big\vert_{T_{b,loc}} - P_{extr}$	15.5	(80)
$\Delta P_{driv,loc} = P_{sat}\big\vert_{T_{film,loc}} - P_{extr}$ $T_{film,loc} = \frac{T_{w,loc} + T_{b,loc}}{2}$	13.2	(81)

3.4.5 Heat Transfer Model

The local heat transfer coefficient in the channel is only necessary to determine the local membrane wall temperature, which is used in turn to determine the film temperature for use in the membrane transport model, Eq. (81). It should be noted that in this study the membrane is also a heated wall for the channel flow. In the heat transfer model, thermally developing and hydrodynamically developing flow are assumed after each bifurcation. The single-phase Nusselt number in the simultaneously developing flow region of laminar flow is determined by linear interpolation of data provided by Shah and London [67]. There are a few widely disparate heat transfer coefficient models and correlations for microchannel flow boiling, (e.g. [10, 57-64]). However, none of these have been validated for fractal-like flow geometries. The two-phase heat transfer coefficient correlation proposed by Lee and Mudawar [64] for microchannel flow boiling is used here and is given as Eqs. (82)-(84) in Table 8.

Table 8. Lee and Mudawar [64] boiling heat transfer correlation

x	Correlation	Eq.
0-0.05	$h_{2\varphi} = 3.856\mathrm{X}^{0.267} h_{1\varphi,l}$	(82)
0.05-0.55	$h_{2\varphi} = 436.48 Bo^{0.522} We_{lo}^{0.351} \mathrm{X}^{0.665} h_{1\varphi,l}$	(83)
0.55-1.0	$h_{2\varphi} = \max\left\{\left(108.6\mathrm{X}^{1.665} h_{1\varphi,v}\right), h_{1\varphi,v}\right\}$	(84)

3.5 MODEL VALIDATION

Pressure drop calculations were validated using a fractal-like branching network used to obtain adiabatic experimental data with no vapor extraction by Daniels et al. [48]. The fractal-like flow network is designated as F2 in Table 1 and is represented in Figure 12(b). The accuracy of the predictions was assessed using the mean absolute error, defined as:

$$MAE_{\Delta P_{chan}} = \frac{1}{N}\sum_{i=1}^{N}\left(\frac{\left|\Delta P_{chan,pred} - \Delta P_{chan,\exp}\right|}{\Delta P_{chan,\exp}}\right) \tag{85}$$

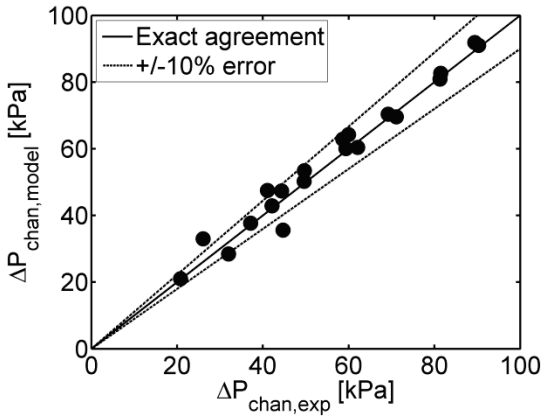

Figure 15. Comparison of experimental and predicted pressure drop for adiabatic flow in fractal network, F2, at inlet mass flow rate ranging from 100 to 225 g/min (or inlet mass flux of 1,736-3,906 kg/m^{2}s) and inlet subcooling ranging from 0.66 to 6.25 K [48]

Figure 15 shows comparison between the model and experimental results. The predicted channel pressure drops yield very good agreement with the experimental data, a mean absolute error of 5.5%.

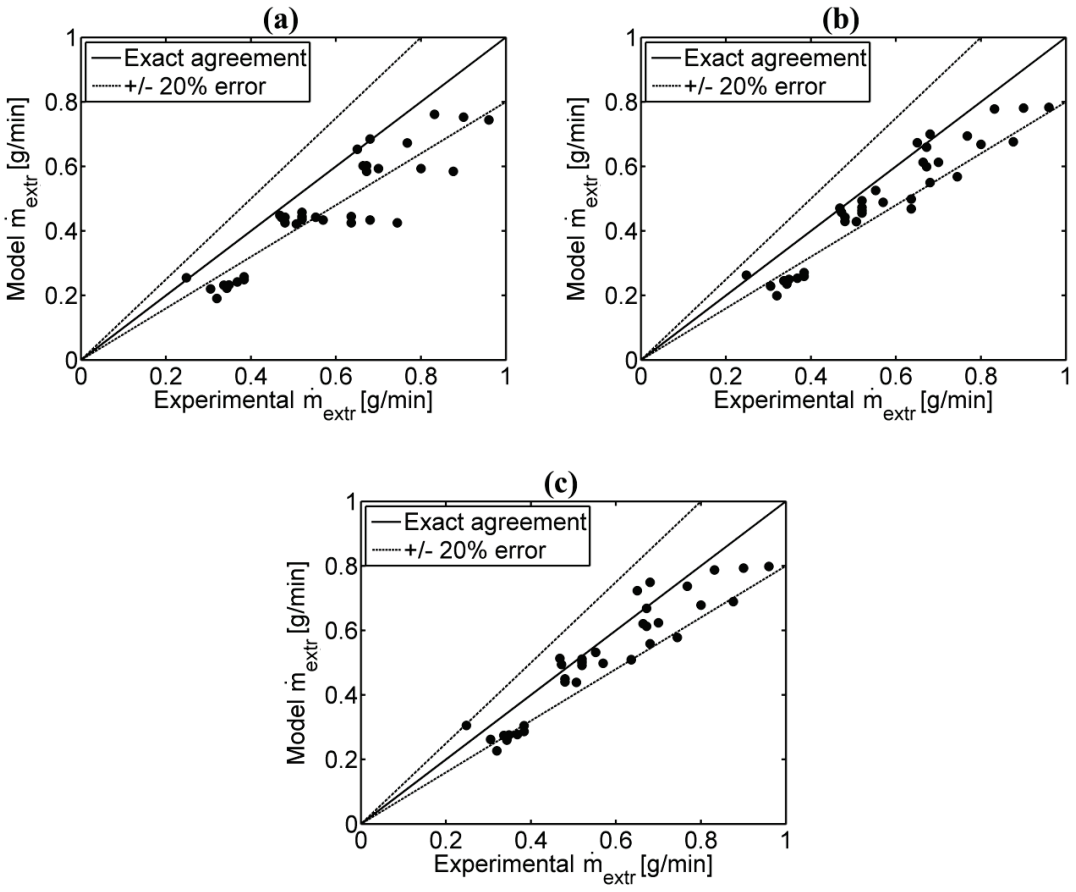

Figure 16. Comparison of experimental [16-17] and predicted extracted vapor flow rates; with extraction pressure differential based on (a) local channel pressure (b) saturation pressure at local bulk temperature, and (c) saturation pressure at local film temperature.

Diabatic vapor extraction predictions are compared with the experimental data of Apreotesi et al. [16-17] based on the fractal-like flow network F1 in Table 1 and represented in Figure 12(a). Vapor extraction mass flow rates based on all three extraction driving pressure models, given in Table 2, are compared with experimental values in Figure 16. The accuracy of the predictions for all models based on the mean absolute error is shown in Table 2. All models are within approximately 10% to 20% of

measured values with predictions using the saturation pressure based on film temperature yielding the best results. These results support the hypothesis that the saturated pressure based on the local average film temperature better represents the local saturated pressure adjacent to the membrane than the others. This may be a consequence of sufficiently large temperature gradients near the wall which influence the local vapor pressure, modeled as the saturation pressure at the film temperature. This results in an increase in mass flux compared to basing the transport on the bulk channel pressure.

Comparisons of the predicted and experimental results of Apreotesi et al. [16-17] for the vapor mass flow rate versus extraction pressure differential are shown in Figure 17 for an inlet flow rate of 8 g/min and heat input of 18W for fractal geometry F1. Results indicate that the predictions from the two models using the saturation pressure rather than bulk pressure more accurately reflect the trend of the experimental data. Because the saturation pressure based on the film temperature model gives the least error, 13.2%, this model was used to generate all further results presented.

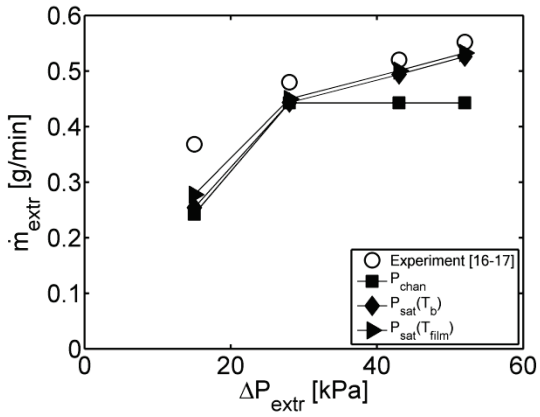

Figure 17. Extracted vapor mass flow rate as a function of extraction pressure differential. Comparison of experimental data [16-17] and three different vapor pressure models for a flow rate of 8 g/min (or inlet mass flux of 86 kg/m^{2}s) and heat input of 18 W (or heat flux of 1.82 W/cm^2 based on planar heated area); the different symbols identify the channel pressure used to determine the pressure differential across the membrane.

3.6 RESULTS AND DISCUSSIONS

Results of model predictions are presented as both local distributions of quality, pressure and bulk temperature, as well as global results of pressure drop, exit quality and vapor extraction rates. Because the pressure and temperature vary along the channel, a global extraction pressure differential is used to characterize the results, which is defined as the difference between the extraction absolute pressure and the channel outlet pressure which represents the lowest channel pressure:

$$\Delta P_{extr} = P_{chan,out} - P_{extr} \tag{86}$$

Results are presented for the fractal-like geometry designated as F2 (given in Table 1). Water was used as the working fluid with an inlet subcooling of 2.5 K to ensure significant vapor formation. The outlet was set to atmospheric pressure, i.e. 101 kPa-a. The range of numerical model conditions is divided into two groups: (i) low inlet flow rate-low heat flux and (ii) high inlet flow rate-high heat flux. The low heat flux cases use three flow rates ranging between 8-12 g/min (or inlet mass flux of 139-208 kg/m^{2}s), three heat inputs ranging from 18 to 30 W (or heat flux of 1.77-2.95 W/cm^2 based on planar heated surface area) and five extraction differential pressures ranging between 0-55 kPa and no extraction. The high heat flux cases use four flow rates ranging between 30-60 g/min (or inlet mass flux of 521-1,042 kg/m^{2}s), four heat inputs ranging from 250 to 1,000 W (or heat flux of 24.56-98.24 W/cm^2 based on planar heated surface area) and four extraction differential pressures ranging between 0-61 kPa and no extraction. It should be noted that zero extraction differential pressure is not the same as no extraction because the local pressure decreases along the channel and upstream there is sufficient pressure differential to drive vapor through the membrane.

3.6.1 Local Conditions

Five cases are presented in this section to provide representative local distributions of pressure, temperature and quality along the channel. To represent the low flow rate, low heat flux case, the following conditions are used: inlet flow rate of 10 g/min, heat input of 18 W and extraction pressure differentials of 14 and 41 kPa and no

extraction. For the high flow rate, high heat flux case, the conditions are: inlet flow rate of 50 g/min, heat input of 750 W and extraction pressure differential of 41 kPa and no extraction. The predicted local quality and bulk fluid temperatures are plotted as a function of streamwise location along the microchannel network in Figures 18 and 19, respectively. The degree of local subcooling is represented by negative qualities in Figure 18(a) where quality is defined by:

$$x = \frac{i - i_l}{i_v - i_l} \tag{87}$$

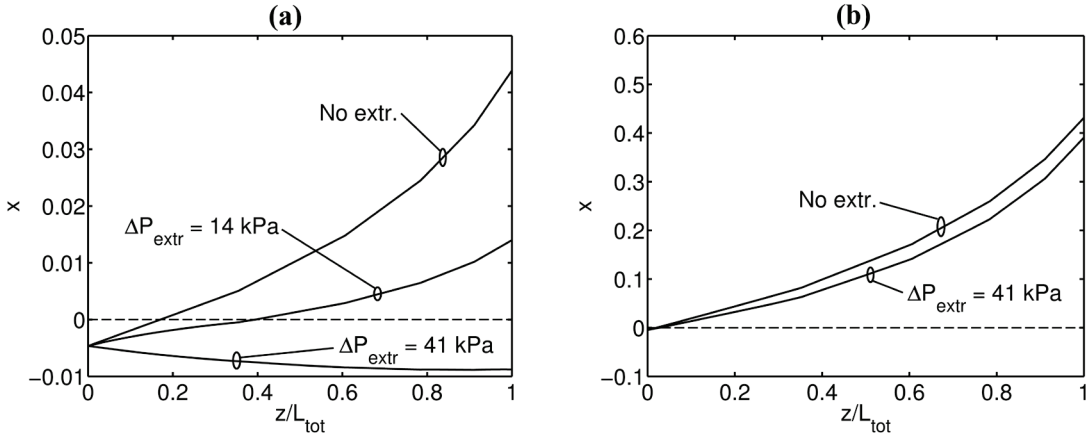

Figure 18. Local thermodynamic equilibrium quality with and without local vapor extraction; (a) inlet flow rate of 10 g/min, heat input of 18 W, and extraction pressure differentials of 14 and 41 kPa, (b) inlet flow rate of 50 g/min, heat input of 750 W, and extraction pressure differential of 41 kPa.

In Figure 18 when the quality is above zero, phase change is implied. For the low flow rate-low heat flux case and the highest extraction pressure differential of 41 kPa, the flow remains single phase. In both the high-high and low-low flow rate-heat flux cases, local vapor extraction delays the streamwise location at which transition to two-phase flow occurs. Evident from Figure 19 is that vapor extraction significantly reduces the local bulk temperature. This implies that the local wall temperature can be reduced by vapor extraction because of the significant energy extraction with the vapor. The saturated temperature for the given conditions coincides with the bulk temperature for the no extraction case once two-phase flow begins, indicated by the arrow in the figure. The

bulk fluid temperature distribution for the 10 g/min flow rate, 18 W heat input and 41 kPa extraction pressure differential case, shown in Figure 19(a), indicates that the bulk fluid temperature remains well below the local saturation temperature as a result of evaporative extraction, which is also shown as negative quality in Figure 18(a). Because the overall bulk fluid temperature with vapor extraction of 41 kPa extraction pressure differential is lower than the inlet temperature, there is potential of using evaporative extraction in a single-phase heat sink to improve the heat removal by evaporative cooling, and thereby improve overall performance.

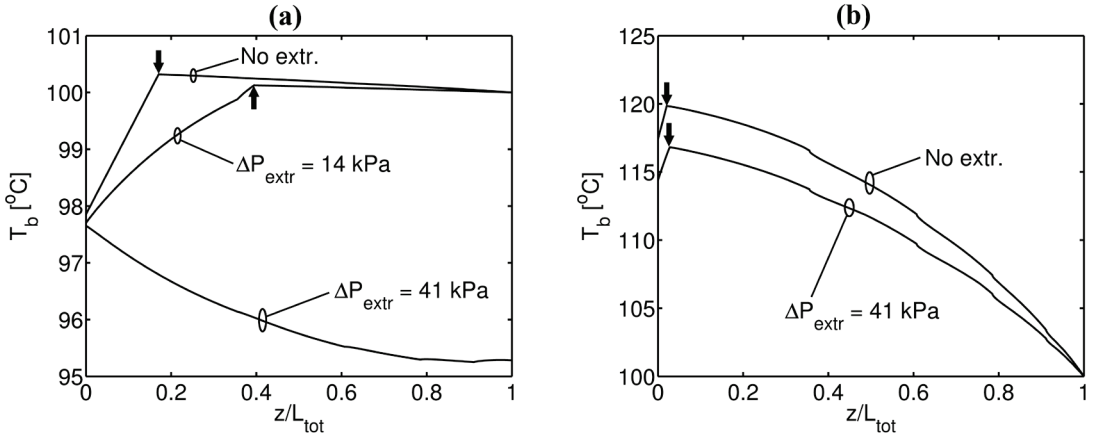

Figure 19. Local bulk fluid temperature with and without local vapor extraction; (a) inlet flow rate of 10 g/min, heat input of 18 W, and extraction pressure differentials of 14 and 41 kPa, (b) inlet flow rate of 50 g/min, heat input of 750 W, and extraction pressure differential of 41 kPa; arrows indicate location of initial phase change, i.e. $x = 0$.

The variation in channel pressure along the flow direction is shown in Figure 20 for the same conditions as Figures 18 and 19. Figure 19(a) shows that the thermodynamic quality significantly decreases as vapor is extracted from the low flow rate-low heat flux case. The pressure distributions for these cases indicate the expected decrease in pressure drop. However, because total pressure drops of these cases are very low, the pressures show little change. For the higher flow rate-higher heat flux cases where much larger pressure drops occur, the two-phase pressure drop is significantly reduced when vapor is extracted. This large decrease in overall pressure drop is because the two-phase pressure

drop is a strong function of quality, and these cases generate significant vapor, shown as high quality in Figure 18(b). This significant drop in pressure occurs despite the fact that all of the vapor is not extracted from the channel.

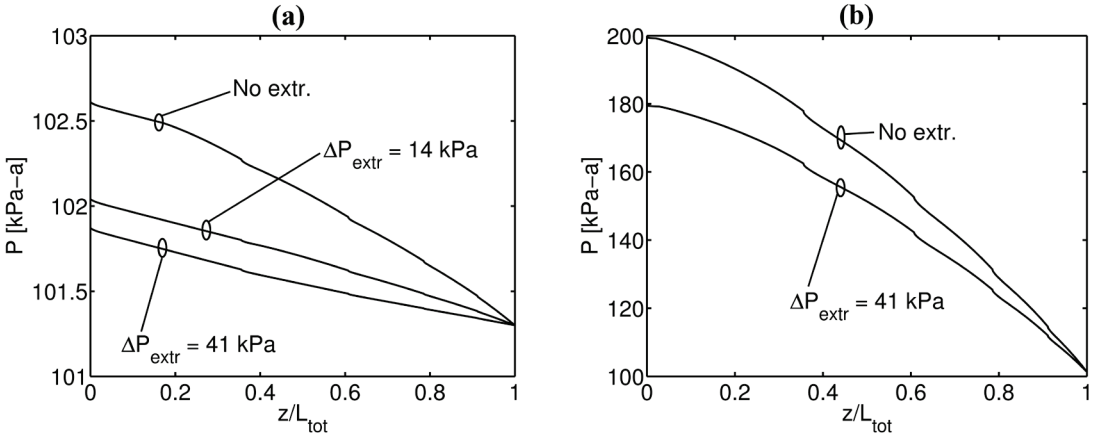

Figure 20. Local pressure with and without local vapor extraction; (a) inlet flow rate of 10 g/min, heat input of 18 W, and extraction pressure differentials of 14 and 41 kPa, (b) inlet flow rate of 50 g/min, heat input of 750 W, and extraction pressure differential of 41 kPa.

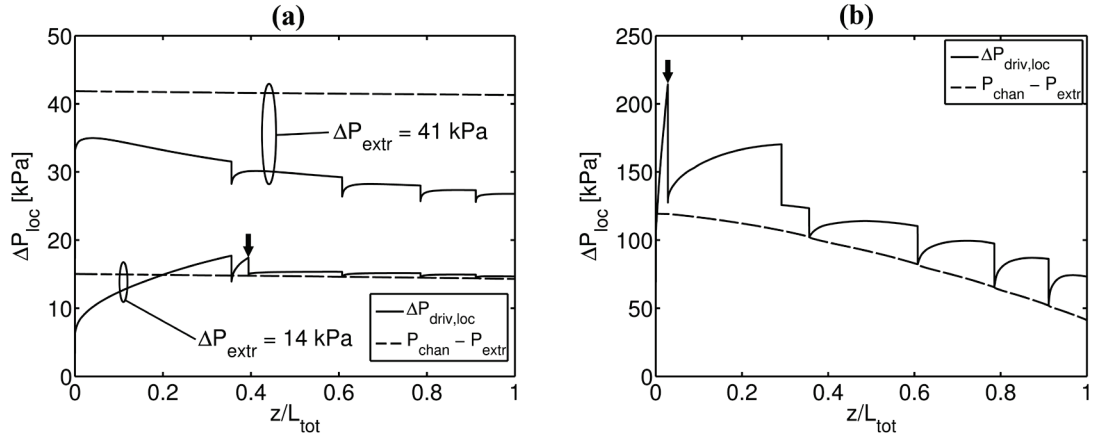

Figure 21. Local extraction driving pressure, $\Delta P_{driv,loc}$, using saturated pressure based on film temperature, $P_{sat}\big|_{T_{film}}$, and local pressure differential between channel pressure and extraction pressure, $P_{chan} - P_{extr}$, as a function of streamwise distance along the microchannel network; (a) inlet flow rate of 10 g/min, heat input of 18 W, and extraction pressure differentials of 14 and 41 kPa, (b) inlet flow rate of 50 g/min, heat input of 750 W, and extraction pressure differential of 41 kPa; arrows indicate location of initial phase change, i.e. $x = 0$.

The local extraction driving pressure that drives vapor through the membrane is shown in Figure 21. The extraction driving pressure depends on the extraction driving pressure model that is used. As stated previously, the model based on the difference between the saturation pressure at the film temperature and the extraction pressure, Eq. (81), is used because it is shown to give the best agreement with experimental data.

The extraction driving pressure distributions along the channels show a significant number of step changes, which are not necessarily realistic and are an artifact of both the pressure drop and surface temperature models. The transition from single-phase to two-phase flow produces a step change in heat transfer coefficient and consequently wall temperature. In addition, the Lee and Mudawar [64] heat transfer model has three regions resulting in step changes based on the local quality, shown in Table 3. Lastly, imposing flow redevelop at each bifurcation also results in a surface temperature step change at the beginning of each bifurcation. Although the step changes noted in these figures of the pressure differential profile are not expected to be realistic, the overall global results are shown to well predict total mass extraction rates, shown in Figures 16 and 17, and pressure drop data, shown in Figure 15. It may be concluded that these local profile singularities are not significant in predicting overall global results.

Figure 21 also indicates the local pressure difference between the channel pressure and the extraction pressure. Results show that, in the single-phase flow region, local values of this pressure difference can be either greater or less than the local extraction driving pressure using Eq. (81). The relative value depends on the wall heat flux, heat transfer coefficient and degree of local subcooling which are used to calculate the film temperature, and in turn used in the extraction driving pressure model. Based on this result, it can be concluded that the average extraction driving pressure does not proportionally increase as the extraction pressure increases. Also, the average value of the difference between channel pressure and the extraction pressure may not well represent the average of the local extraction driving pressure. It should be noted that, unlike for the single-phase flow region, local extraction driving pressure in the two-phase flow region is always greater than the local value of pressure difference between extraction pressure and

channel pressure because, in equilibrium saturated conditions, the channel pressure is equal to the saturated pressure at the bulk fluid temperature and the membrane film temperature is always greater than the bulk temperature. It is therefore suggested that a heated membrane wall improves vapor extraction efficiency especially in the two-phase region because it increases the effective extraction driving pressure due to higher film temperature.

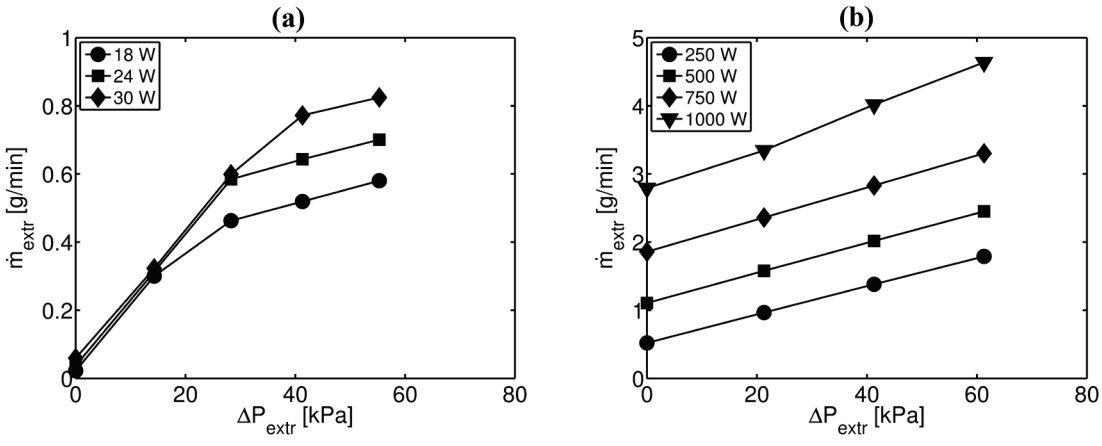

Figure 22. The extracted vapor mass flow rate versus the extraction pressure differential for a range of heat input values for an inlet mass flow of (a) 10 g/min and (b) 50 g/min.

3.6.2 Global Results

Global mass and energy balances were carried out based on inlet and exit conditions, including the flow and energy through the membrane. The global results consist of the total extracted mass flow rate, exit quality and channel pressure drop. The total extracted vapor mass flow rate and the exit quality are plotted as a function of the extraction pressure differential in Figures 22 and 23, respectively. In Figure 23 the horizontal arrows indicate the exit quality for no extraction for the various heating rates. Figure 22 illustrates the increase in extracted vapor mass flow rate with increasing extraction pressure differential. It should be noted that the zero extraction pressure differential condition still results in some mass extraction through the membrane and an exit quality slightly less than the no extraction case. This is due to vapor extraction that

occurs across the membrane because zero differentials are based on the exit conditions and as such vapor can be transported due to a pressure differential near the inlet portions of the channel. At higher pressure differentials, the extracted mass flow rate asymptotically reaches a value dependent on the heat input rate. For the low flow rate-low heat flux case, Figure 22(a), all heating rates result in nearly the same mass extraction at low extraction pressure differentials. As ΔP_{extr} increases, the lower heating cases show a decreasing extraction rate, but eventually all cases show a reduction in the rate of increase of mass extraction versus ΔP_{extr}, that is the slope decreases. The reason for this can be explained by examining Figure 23(a). As expected, the exit quality decreases as the extraction pressure differential increases, shown in Figure 23(a). The exit quality can be decreased to zero or a negative value if sufficient energy is extracted with the vapor. The extraction pressure differential required to obtain zero or negative exit quality depends on the heat input rate. As the heating rates increase, a higher extraction pressure differential is required to remove sufficient vapor, and energy, to maintain an exit quality of zero.

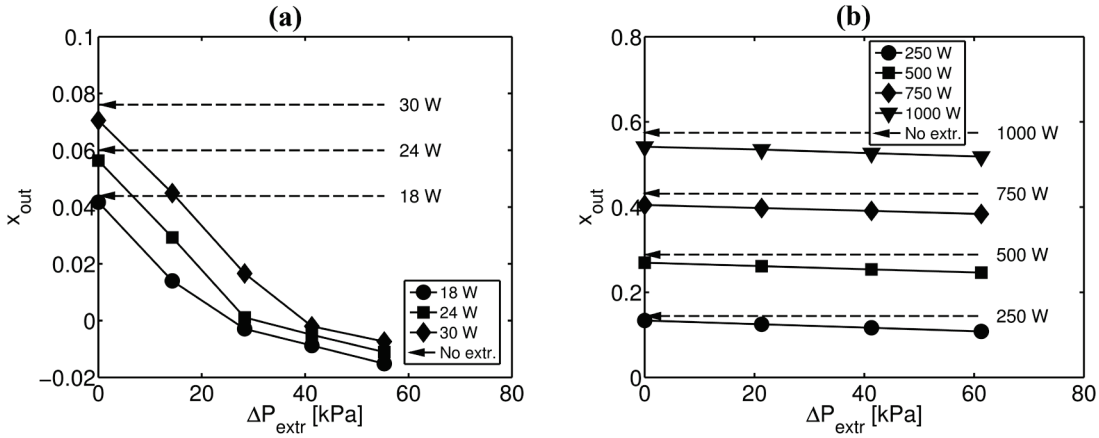

Figure 23. The exit quality versus the extraction pressure differential for a range of heat input values for an inlet mass flow of (a) 10 g/min and (b) 50 g/min.

Comparing Figures 22(a) and 23(a), the no boiling condition (that is x_{out} less than zero) coincides with the high extraction pressure region, which is where there is a distinct

difference in the mass extraction for the different heating rates. Under these circumstances extraction is purely evaporative such that higher heat inputs evaporate more vapor at a given extraction pressure. As the heating rate increases the liquid phase enthalpy increases and less energy is required per mass for vaporization. Results indicate an asymptotic limit to the mass extraction rate that is higher for higher heating rates.

For the high flow rate-high heat flux cases, shown in Figures 22(b) and 23(b), the relative increase of mass extraction and decrease in exit quality with increasing ΔP_{extr} is noticeably smaller than for the lower flow rate cases. Note that for these flow rates and heating rate values the flow is always two-phase prior to the exit of the channel. Also the increase of extraction rate with increasing heating rate is significant. Higher heat flux results in higher channel pressures and higher pressure differentials for vapor extraction. Also, at these higher heating rates, the local membrane wall temperatures are significantly higher. This results in higher film temperature values. Therefore, the saturation pressure near the wall increases which increases the net extraction driving pressure for the same extraction pressure. Between the low and the high flow rate and heating rate extremes shown, clearly different trends emerge. The low flow rate-low heat flux cases allow for significant control over the local quality and thus the flow characteristics and pressure drop, as is shown next. At the higher flow rates and higher heating rates, the variations of both mass extraction and exit quality is much smaller, at least over the range of extraction pressure differential studied.

The predicted overall pressure drop is presented as a function of the extraction pressure differential in Figure 24 for the low and the high flow rate-heat flux conditions. The two-phase pressure drop along the channel initially decreases nearly linearly as the extraction pressure differential increases. The pressure drop is reduced by increasing the extraction pressure differential to the point where single-phase pressure drop occurs, seen in Figure 24(a) when the extraction pressure differential is greater than 40 kPa. Once this occurs, the pressure drop in this region is nearly independent of heating value. In the single-phase flow regime, the pressure drop slightly increases rather than decrease when the extraction differential pressure increases. This is because as the energy is extracted

from the liquid flow, the fluid's temperature decreases, and the viscosity increases. Consequently, excessive extraction can be somewhat detrimental to channel pressure drop. For the high flow rate-high heat flux cases shown in Figure 24(b), for the range of extraction pressures study the flow remains two-phase. There is a modest monotonic decrease in channel pressure drop with extraction pressure differential, with the largest decrease for the highest heat input. However, the relative pressure drops are all comparable (less than 30% change). These results indicate that vapor extractions impact on pressure drop is most effective at relatively low flow rate conditions on a per channel bases. This is because of the higher fraction of vapor extracted, shown in Figure 23. Therefore, using a large channel array would be beneficial for the same total flow rate.

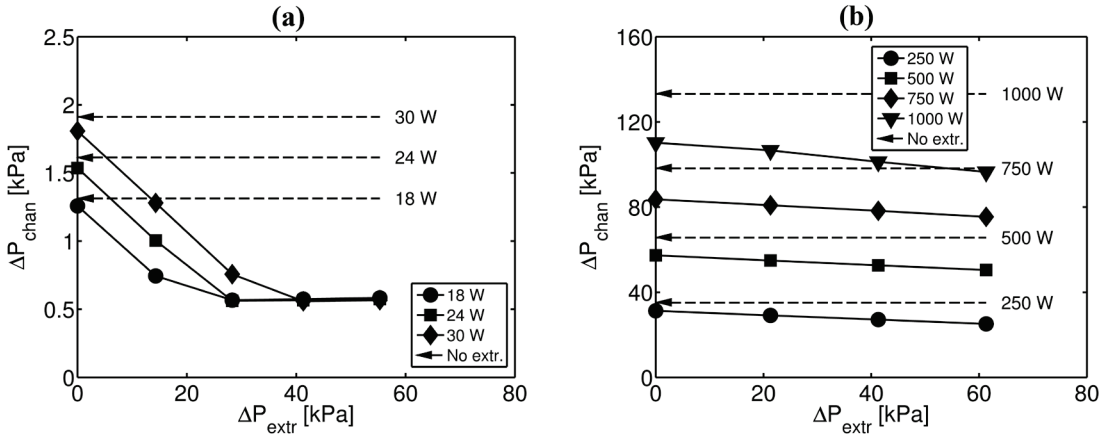

Figure 24. The network pressure drop versus the extraction pressure differential for a range of heat input values for an inlet mass flow of (a) 10 g/min and (b) 50 g/min.

Because the quality is an important parameter in determining the two-phase pressure drop, it is useful to understand the relationship between pressure drop and exit quality. Apreotesi et al. [16] introduced the ideal exit quality that would occur without vapor extraction, denoted as x_{out}^{*}. This quality is obtained from a global energy balance, while neglecting the change of the channel pressure in determining exit conditions. This quality is a function of inlet flow rate, heat input, and degree of subcooling and is expressed as:

$$x_{out}^{*} = \frac{\dfrac{\dot{Q}}{\dot{m}_{in}} - c_{p,in}\left(T_{sat,in} - T_{in}\right)}{i_{lv}} \tag{88}$$

where all symbols are defined in the Nomenclature.

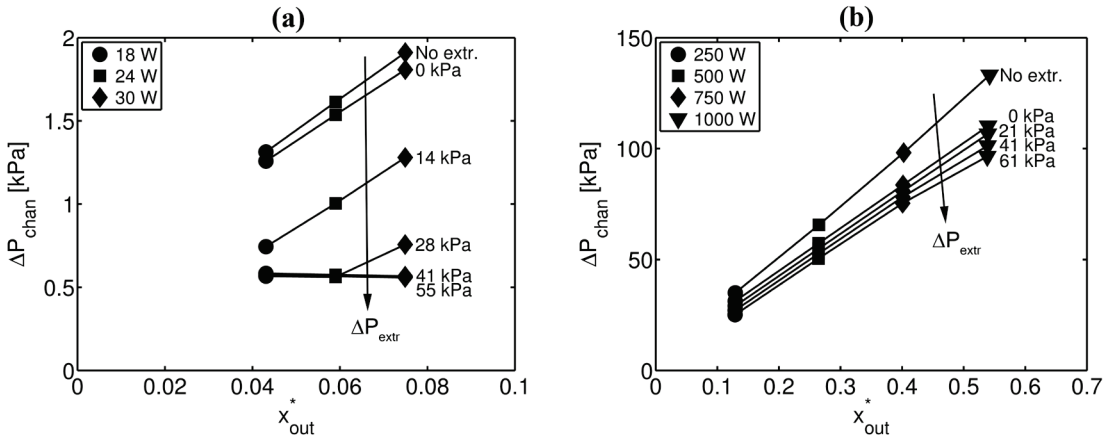

Figure 25. The network pressure drop versus the ideal exit quality without vapor extraction for a range of heat input and extraction pressure differential values for an inlet mass flow of (a) 10 g/min and (b) 50 g/min.

The predicted network pressure drop versus x_{out}^{*} is presented in Figure 25 for the low and the high flow rate-heat flux conditions. The pressure drop increases as the ideal exit quality without vapor extraction, x_{out}^{*}, increases. Results for the low flow rate-low heat flux cases, in Figure 25(a), show the channel pressure drop increases with x_{out}^{*} because more vapor is formed within the channel. However, at higher extraction pressure differential, this trend is reversed because vapor content is totally eliminated. For high heat flux-high inlet flow rate cases, in Figure 25(b), the rate of increase of the pressure drop versus x_{out}^{*} for flow without vapor extraction is larger than the cases with vapor extraction. This indicates that the pressure drop reduction due to vapor extraction is more effective when the ideal vapor quality without vapor extraction is high. Because the two-phase pressure drop varies with vapor quality, at high quality the pressure inside the channel is also high, resulting in a large local extraction driving pressure and

consequently larger vapor extraction. By increasing the extraction differential pressure, the extracted vapor flow rate increases and the exit quality decreases. However, for high vapor content cases, which occur for the high heat flux cases, decreasing the absolute extraction pressure might not be sufficient to obtain zero or negative exit quality.

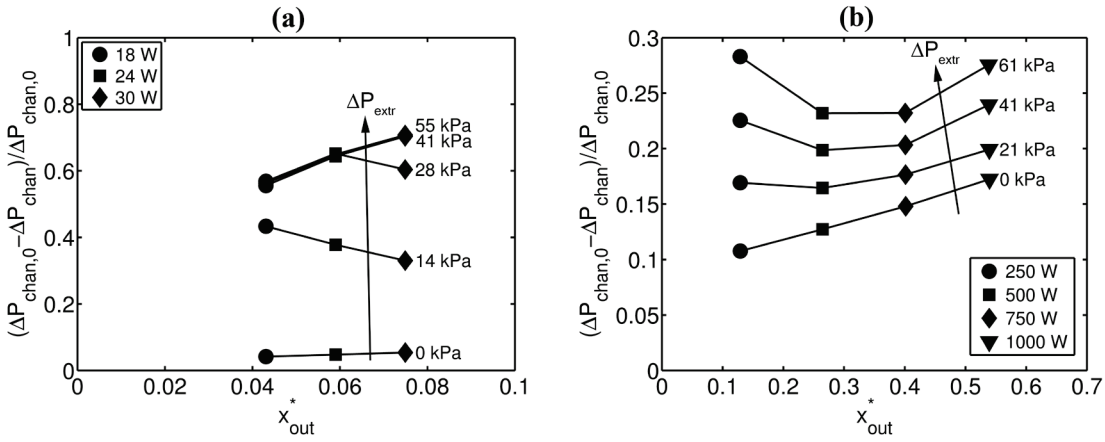

Figure 26. Pressure drop reduction due to vapor extraction per pressure drop without vapor extraction for a range of heat input values for an inlet mass flow of (a) 10 g/min and (b) 50 g/min.

To better illustrate the impact on channel pressure drop, the pressure drop reduction ratio is used to represent the vapor extraction effectiveness. This pressure drop reduction ratio is defined as $\left(\Delta P_{chan,0} - \Delta P_{chan}\right)/\Delta P_{chan,0}$ where $\Delta P_{chan,0}$ is the pressure drop for no extraction. Results are shown versus x_{out}^{*} in Figure 26. As expected, the pressure drop reduction ratio increases as the extraction pressure differential increases. For low flow rate-low heat flux cases, the vapor extraction effectiveness decreases as x_{out}^{*} increases except for the cases where the exit quality is negative indicative of single-phase flow (flow rate of 10 g/min and extraction pressure differential of 41 kPa and greater). The rather large percentage changes of pressure drop are due to the high sensitivity of the two-phase acceleration pressure drop to void fraction.

The vapor extraction process is somewhat less effective in term of pressure drop reduction for the high flow rate-high heat flux cases. However, these cases still show

improvements. This reduction of effectiveness is because vapor void fraction in two-phase flow with a high quality is not reduced as much because void fraction becomes less sensitive to quality when the quality is high. The general trend is that the pressure drop reduction ratio increases as x_{out}^{*} increases for the high flow rate-high heat flux cases where x_{out}^{*} is relatively large. This is the result of quantitatively large channel pressures when the quality is high which leads to large extraction driving pressures with correspondingly high extracted vapor mass flow rates. Although void fraction does not change as much when the quality is large, the reduction in vapor content inside the channel by extracted vapor due to large driving pressures may be more significant in term of reducing the pressure drop.

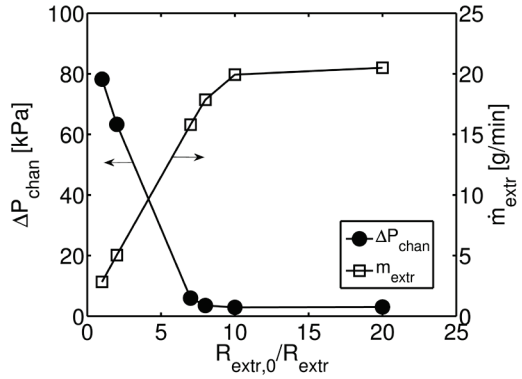

Figure 27. The pressure drop and extracted vapor mass flow rate versus the extraction flow resistance ratio for an inlet mass flow of 50 g/min, heat input of 750 W and extraction pressure differential of 41 kPa where $R_{extr,0} = 3\times10^{10}$ m^{-1}.

The predicted pressure drop and extracted vapor mass flow rate is largely affected by the membrane permeability for a given extraction pressure, as is shown in Figure 27. This plot shows channel pressure drop and extracted mass flow rate versus the extraction flow resistance, R_{extr}, which in this study is defined as:

$$R_{extr} = \left(\frac{\delta_{mem}}{\kappa_{mem}} + \frac{\delta_{back}}{\kappa_{back}} \right) \tag{89}$$

which accounts for both the membrane and porous backing resistances. This result is for a given flow rate, heat flux and extraction pressure differential. However, all conditions follow this same trend. Here the resistance is normalized by the resistance value used in this study denoted as $R_{extr,0}$. It should be noted that increasing the permeability is equivalent to reducing R_{extr} and thereby increasing $R_{extr,0}/R_{extr}$. As shown, the amount of vapor extraction increases with decreasing R_{extr} resulting in reducing exit quality and reduced channel pressure drop. In this example, sufficient extraction occurs near $R_{extr,0}/R_{extr}=10$ to cause the two-phase flow to become single-phase flow for this high flow rate-high heat flux case. Beyond the tenfold increase in permeability, there is no further increase in vapor extraction or a reduction in channel pressure drop.

3.7 CONCLUSIONS

The development of a predictive one dimensional model of flow boiling in a microchannel flow network with local vapor extraction has been presented and discussed with results of the effect of mass extraction on the local and global pressure drop, bulk temperature, and quality. The predictive model is based on conservation of mass and energy, coupled with pressure drop and heat transfer correlations used for microchannel flow with boiling. The extraction rate was modeled with Darcy's law for flow through the porous membrane. Based on the vapor extraction rate validation, the channel pressure adjacent to the membrane that drives the vapor through the membrane is best represented by the saturated pressure based on the local average film temperature rather than the bulk channel pressure. The predictive model, as applied to a fractal-like microchannel flow network, confirms the premise that the vapor extraction helps to reduce two-phase pressure drop. This is shown to be a consequence of decreased local quality resulting in reduced two-phase pressure drop. The percent decrease in pressure drop is much higher for the low channel flow rate cases, but even for large heat transfer conditions where the overall pressure drops are much larger due to larger flow rates, the decrease in pressure drop can be over 25%. The extracted vapor mass flow rate is shown to be dependent on the extraction pressure, the inlet mass flow rate and the applied heating rate. Vapor

extraction is shown to reduce the bulk fluid temperature within the channel. This additional means of energy transfer has the potential to reduce the overall operating temperature of the heat sink.

The ultimate goal of the one dimensional model is its use to optimize operating conditions to minimize channel pressure drop and increase overall heat transfer rates or heat flux conditions. There are several recommendations suggested to improve the predictive model. New heat transfer and pressure drop models need to be developed to eliminate step changes in local pressure and wall temperature. However, it is shown that the current models match well with experimental data globally, but a wider range of operating conditions are needed to further verify the model. Once detailed local data are available, mechanistic models for pressure drop with vapor extraction may be possible so that optimal membrane characteristics could be identified.

3.8 ACKNOWLEDGEMENTS

S. Salakij acknowledges the financial support from Office of Naval Research (N00014-09-1-1079).

3.9 NOMENCLATURE

Bo	Boiling number
c_p	Specific heat
C_{LM}	Phase interaction parameter
D_h	Hydraulic diameter
$f_{loc,l}$	Local liquid phase friction factor
G	Mass flux
h	Heat transfer coefficient
H	Channel depth
i	Enthalpy
i_{lv}	Heat of vaporization
k	Channel branching level

L	Channel branching length
L_{tot}	Total flow length
n	Number of branches
M	Number of branching levels
$MAE_{\Delta P_{chan}}$	Mean absolute error between model and experimental results of ΔP_{chan}
$MAE_{\dot{m}_{extr}}$	Mean absolute error between model and experimental results of $\dot{m}_{extr}$
$\dot{m}_{in}$	Inlet mass flow rate
$\dot{m}_{extr}$	Extracted vapor mass flow rate
N_0	Number of inlet branches
N_k	Number of k^{th} level channels
P_{extr}	Extraction absolute pressure
∇P_{vap}^0	Vapor pressure gradient
$\dot{Q}$	Heat rate
R_{extr}	Extraction flow resistant
Re	Reynolds number
T	Temperature
v	Specific volume
w	Channel width
w_t	Terminal branch width
We	Weber number
x	Thermodynamic equivalent quality
x_{out}^*	Ideal exit quality without vapor extraction
X^2	Lockhart-Martinelli parameter

Greek

α	Void fraction

β_{D_h}	Hydraulic diameter ratio
β_w	Width ratio
γ	Length ratio
ΔP_{chan}	Channel pressure drop
$\Delta P_{driv,loc}$	Local extraction driving pressure
ΔP_{extr}	Extraction pressure differential $\left(\Delta P_{extr} = P_{chan,out} - P_{extr}\right)$
δ	Thickness
κ	Specific permeability
μ	Dynamic viscosity
ν	Kinematic viscosity
ρ	Density
ϕ_l^2	Two-phase multiplier

Subscripts

acc	Acceleration
back	Porous backing
fric	Frictional
in	Inlet
l	Liquid phase
lo	All-Liquid
mem	Porous membrane
out	Outlet
s	Surface
sat	Saturation
v	Vapor phase

4 MODELING CONVECTIVE BOILING IN SINGLE DIVERGING CHANNEL WITH IN-SITU VAPOR EXTRACTION

Saran Salakij, Deborah V. Pence, James A. Liburdy

Journal of Heat Transfer

American Society of Mechanical Engineers, Two Park Avenue, New York, NY

Submitted for review

4.1 ABSTRACT

The present work evaluates the potential of using a diverging channel with in-situ vapor extraction as a means to reduce flow instability in microscale flow boiling. It has been shown that diverging channel helps stabilize convective boiling flow. In-situ vapor extraction is proposed as an additional method that helps further stabilize flow boiling. The main concept of in-situ vapor extraction is to reduce the vapor available inside the channel where it forms by locally extracting vapor through a hydrophobic porous membrane that forms a wall of the channel. This in turn stabilizes the flow. In-situ vapor extraction also has the potential to reduce the required pressure to drive the flow through the channel without losing the benefit of convective boiling heat transfer. In this study, four microchannel geometries are evaluated over a range extraction pressures using a one-dimensional predictive model. Each channel is 50 mm and has a mid-channel width of 500 microns and height of 500 microns. The half angle of divergence of the channels is varied: 0, 0.11, 0.23, and 0.34 degrees. Wall heat flux values range from 13.3 to 133 W/cm^2. Extracted mass flow rates, global pressure drop along the channels, and quality at the channel outlet are presented as a function of heat flux and extraction pressure. Local variations of pressure, quality and bulk fluid temperature are also presented. Stability is predicted by a newly proposed criterion applicable for a diverging channel with in-situ vapor extraction. The results show that in-situ vapor extraction significantly reduces pressure drop for all channel configurations. Although the drop in pressure along the diverging channels is less influenced by vapor extraction than the non-diverging channel, the coupling of diverging channels and vapor extraction considerably improves the predicted stability of the flow.

Keywords: Vapor extraction, Vapor separation, Diverging channel, Flow boiling, Modeling, Flow instability

4.2 INTRODUCTION

An important characteristic of an effective heat sink is its ability to maintain a relatively low uniform and stable surface temperature. A two-phase flow microscale heat

sink should achieve this characteristic while reducing the required flow rate due to its high surface area per unit volume and large heat transfer coefficients, for details see reviews [1-3]. However, the advantages of two-phase microscale heat sinks also come with undesired issues such as large pressure drops and flow instabilities associated with microscale flow boiling [1-2]. A large pressure drop can cause non-uniform operating temperatures even when flow is in the two-phase regime. Flow instabilities cause both pressure drop oscillations, which can result in mechanical vibration, and thermal oscillations, which may lead to burn-out [3].

To suppress the flow instability, numerous investigators [4-12] have performed modifications to microscale channel geometries. These channel modifications are commonly categorized into three main groups: (i) applying inlet restrictors, (ii) engineering artificial nucleation sites, and (iii) using diverging cross-section channel design. The first group [4-6] stabilizes the flow by placing inlet restrictors to increases the inlet pressure, which reduces the tendency for reverse flow of vapor, however this delays the onset of nucleate boiling because of the increase in the system pressure [7]. The second group [7-9] uses fabricated nucleation sites on the channel walls to reduce the wall superheat and thereby achieve a reduction of the rapid expansion of bubbles. The third group [7, 10-12, 72-73] reduces flow reversal during flow boiling by using diverging cross-section channels which suppressing bubble expansion upstream.

In addition to these channel modifications, Salakij et al. [13] proposed that flow instability might also be reduced by using in-situ vapor extraction. This is accomplished by forming a hydrophobic porous membrane as a wall of the channel to allow local vapor extraction that reduces the vapor content inside the channel where it is generated. As the vapor fraction decreases, the flow is stabilized. In-situ vapor extraction may not only help stabilizing the flow, but also improved the pressure drop along the channel, which has been confirmed by several studies [16-19, 21]. Apreotesi et al. [16-17] studied diabatic boiling water flowing through a fractal-like microchannel heat sink with in-situ vapor extraction. The experimental results show a decrease in overall channel pressure drop while increasing the extraction pressure differential. A later work by David et al. [19],

which investigated flow boiling in parallel microchannels in contact with a venting vapor microchannel separated by a hydrophobic membrane, also confirms that the pressure drop of flow boiling in microscale channel can be significantly reduced by venting of the channel.

The ability to extract vapor, without allowing the liquid phase to pass through the membrane is dependent on the membrane hydrophobicity and permeability. Models exist to predict vapor flow rate versus applied pressure differential. Although a few studies related to in-situ vapor extraction exist, the somewhat related process of membrane transport vacuum membrane distillation, is well described in numerous studies [30-33]. The membrane distillation process is performed by thermally driving the vapor across the hydrophobic porous membrane while the membrane prevents the liquid from leaking through it. The vapor flow rate is typically modeled based on Darcy's law where the driving pressure is the local vapor pressure differential across the membrane. Salakij et al. [13] proposed that the vapor transport through the porous wall may be classified into two modes: (i) evaporative extraction, and (ii) bubble extraction. The evaporative extraction, similar to membrane distillation, occurs when liquid in contact with the membrane evaporates and flows across the membrane. Both vapor extraction modes can coexist in a two-phase flow region. By applying the membrane distillation process to the in-situ vapor extraction, Salakij et al. [18, 21] developed a one dimensional predictive model, accounting for both in-situ vapor extraction modes, for flow boiling through a fractal-like microscale heat sink and predicted the extracted vapor mass flow rate which agreed well with experimental results obtain in [16-17]. Their predictive results also confirmed the hypothesis that the total pressure drop can be reduced by applying in-situ vapor extraction and also showed that the extracted vapor mass flow rate is dependent on the extraction pressure differential, the inlet mass flow rate and the heating rate.

To model the entire process it is necessary to have a two-phase pressure drop model. These are generally developed based on either homogeneous flow or separated flow models. The homogenous flow model assumes two phases flow at the same velocity and act as single-phase ideal-fluid with average fluid properties. This model is suitable

for mixed flow such as bubbly and slug flows. On the other hand, the separated flow model considers each phase as separate and is better suited for stratified and annular flows. Generally, the dominate flow pattern in microchannels is annular flow [71]. Several predictive models for pressure drop of two-phase flow through microchannels have been developed based on the classic Lockhart-Martinelli separated flow model [52], for instance models presented by Mishima and Hibiki [53], Lee and Lee [54], Qu and Mudawar [4], Lee and Mudawar [55] and Hwang and Kim [56]. Flow models were also used to investigate nonuniform microscale geometries, such as studies of diverging channel by Hwang et al. [74] and Lee and Pan [10]. All of these predictive models do show reasonably good agreement with specific experimental data.

There are a number of types of flow instabilities that can occur in microchannel flow boiling, see review [3]. Predictions have been proposed by various authors for dynamic instabilities. In most of these studies, flow instability is assumed to occur when vapor experiences reverse flow back towards the inlet. Kandlikar [75] proposed a stability condition based on the force ratio, denoted as K_1, of the forward to backward directional forces, caused by expansion due to phase change and liquid inertia, respectively. In a later work, Kandlikar [40] proposed another model to justify flow instability based on the assumption that a large pressure spike produced by bubble expansion during initial growth may overcome inertia forces and cause the flow to reverse. Flow instability is then assumed to occur when this pressure spike is greater than the inlet pressure. The pressure spike is estimated as the saturated pressure corresponding to the surface temperature at the location of the onset of nucleated boiling. Lee and Pan [10] used this same criteria and explained that diverging channels cause a steep single-phase pressure gradient in the entrance region which improves flow stability. Lee and Yao [12] and Lee et al. [76] developed an instability parameter model for diverging channel with an inlet restriction by modifying the force ratio proposed by Kandlikar [75] to include a net surface tension force acting on a bubble. Salakij et al. [13] proposed a stability map for adiabatic flow boiling inside uniform cross-sectional area channel with in-situ vapor extraction based on a force balance for the bubble similar to the approach by

Kandlikar [75]. Heymann [77] proposed geometry based criteria for flow instability for a fractal-like branching channel network based on the assumption that flow resistance must decrease in the streamwise direction in order to assure flow stability.

In this study, in an attempt to further suppress flow instability, flow boiling through diverging cross-section channels is coupled with in-situ vapor extraction. The potential to suppress flow instability and reduce pressure drop along the channel is studied by using a one-dimensional predictive model for flow with in-situ vapor extraction and a newly developed stability parameter. Although these models may not precisely capture all of the detailed physical phenomenon of the flow, the trend of the results can be use as a design tool to optimize the design and operating condition of flow boiling through diverging cross-sectional channels with in-situ vapor extraction.

Table 9. Geometry of the microscale channels used in this study

Geometry designation	U	D1	D2	D3
Length, L, (mm)	50	50	50	50
Height, H, (μm)	500	500	500	500
Mid-channel width, W_{mid}, (μm)	500	500	500	500
Inlet width, W_{in}, (μm)	500	400	300	200
Outlet width, W_{out}, (μm)	500	600	700	800
Half-diverging angle, θ_d, (^{o})	0	0.11	0.23	0.34
Heated wall area, A_{heat}, (cm^2)	0.75	0.75	0.75	0.75

4.3 TEST PLAN

Flow predictions are made for diverging microchannels with flow boiling for a range of channel geometries and heating conditions. A schematic of the microscale channel is shown in Figure 28. The channel is formed by three heated walls and one hydrophobic porous wall, which allows vapor and energy to flow through it. Four different microscale channels are investigated in order to compare the effects of diverging

channel on the flow. Geometric details of each channel are shown in Table 9. All channels studied are configured such that the cases with the same heat input and inlet mass flow rate also represent an identical average mass flux and wall heat flux. Each channel has an identical length of 50 mm, identical mid-channel width of 500 microns and identical height of 500 microns. Four different half angles of divergence, from 0 to 0.34 degrees, θ_d, are studied. The angle is defined as that between the diverging wall and the centerline of the channel.

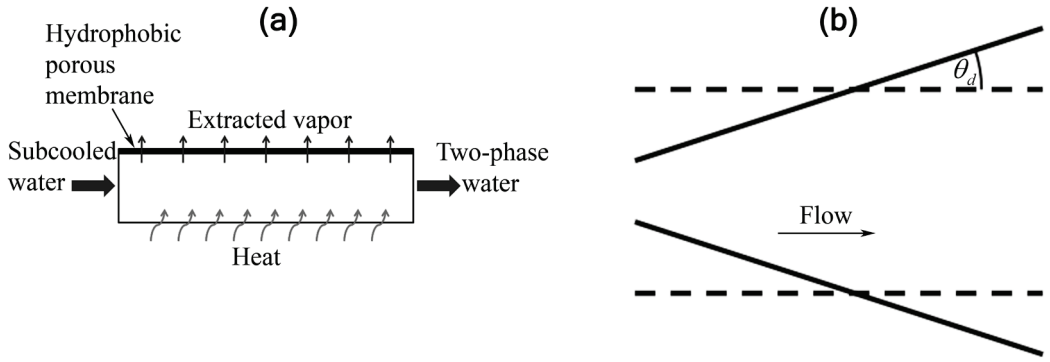

Figure 28. Schematic of diverging microscale channel; (a) cross-sectional view, and (b) planform view.

The operating conditions are summarized in Table 10. In this study, water was used as the working fluid with a fixed inlet mass flow rate of 10 g/min and a fixed inlet subcooling of 5 ^{o}C. The channel outlet was set to atmospheric pressure, i.e. 101 kPa-a. The heat input and extraction pressure where varied using six heat input rates ranging between 10-100 W, or in term of heat fluxes ranging between 13.3-133 W/cm^2, and three extraction pressures ranging between 40-80 kPa-a as well as no extraction for comparison. Results include the local pressure, quality and temperature, along with the local rate of vapor extraction. In addition, overall pressure drop, outlet quality and total mass extracted are presented. The stability prediction for each case is evaluated and is used to illustrate the effect of combined diverging channel with vapor extraction.

Table 10. Summary of operating conditions

Quantity	Value
Inlet subcooling (^{o}C)	5
Inlet mass flow rate (g/min)	10
Exit pressure (kPa-a)	101
Heat input (W)	10, 20, 30, 50, 75, 100
Surface wall heat flux (W/cm2)	13.3, 26.7, 40.0, 66.7, 100, 133.3

4.4 MODEL DESCRIPTION

In this study, a numerical model is developed for flow inside a microscale heat sink with variable cross-sectional flow area with in-situ vapor extraction to predict the total pressure drop and vapor extraction rate for a given inlet mass flow rate and surface heat flux. This model assumes one-dimensional, incompressible, Newtonian fluid flow. The hydrodynamic boundary layer is assumed to start developing at the begin of the channel. Rather than including a subcooled boiling model, the fluid is assumed to remain single-phase liquid until the local thermodynamic equilibrium quality, x, reaches zero (i.e. saturated condition). The thermodynamic equilibrium, x, is defined as:

$$x = \frac{i - i_l}{i_{lv}} \tag{90}$$

At the point where $x \geq 0$, the flow converts to an equilibrium saturate two-phase flow. This condition is also consistent with the pressure drop models discussed below.

To predict the total pressure drop and the rate of vapor extraction, the inputs required in the numerical model are the inlet mass flow rate, input heat rate, either degree of subcooling or inlet temperature, the outlet pressure, the extraction pressure and the flow geometry. The extraction flow resistance is described in a later section. The model is initiated by segmenting the flow path along the channel into discrete uniform length elements. Using a grid refinement analysis, the uniform element length of 10 μm was chosen which showed less than 0.01% variation in total pressure drop when compared with a 5 μm element length. An initial guess of the inlet pressure is made for a specified exit pressure of the channel. The solution then marches along the flow calculating the

local pressure, bulk temperature, quality and mass flux of the fluid in each element. Upon reaching the exit, if the difference between the calculated and the specified exit pressure is greater than 0.05%, the inlet pressure is updated and the local conditions along the entire channel length is recalculated until this convergence criterion is satisfied.

The calculation of local conditions of the fluid in each element is performed by undergoing an internal iterative process to satisfy conservation of mass and energy. In the single-phase region, both flow rate and fluid properties, which are sensitive to temperature variations, were simultaneously updated in the internal iteration of conservation of mass and energy, accounting for the mass and energy transports through the porous wall due to evaporative extraction. After the internal iteration, the single-phase pressure drop of each element is evaluated because the pressure variation across each element is small and only weakly affects the liquid properties. Unlike single-phase flow, the pressure and temperature in equilibrium two-phase flow are related. In the two-phase region, the two-phase pressure drop calculation is also included in the internal iteration because the variation in pressure also affects temperature and thereby the fluid properties. Moreover, an important parameter in the two-phase pressure drop model is quality which varies with temperature and pressure in the two-phase flow region for a specific enthalpy. Therefore, it is also necessary to simultaneous update the quality in the internal iteration in addition to the mass flow rate and fluid properties. Conservation of mass and energy as well as related pressure drop and membrane transport models are discussed below.

4.4.1 Conservation of Mass and Energy

Conservation of mass and energy for element i are shown as:

$$\dot{m}_i = \dot{m}_{i-1} - \dot{m}_{extr,i} \tag{91}$$

and

$$\dot{m}_i i_i = \dot{m}_{i-1} i_{i-1} + q_i - \dot{m}_{extr,i} i_{extr,i} \tag{92}$$

respectively. The heat rate is determined by assuming constant heat flux through three heated walls while the extracted mass flow rate is determined from the membrane transport model, discussed later. By assuming heat loss within the membrane wall is

negligible, the enthalpy of extracted vapor is evaluated as saturated vapor at the local average bulk temperature of fluid in element i.

4.4.2 Pressure Drop Model

The pressure drop for flow in a horizontal channel has two components: frictional, ΔP_{fric}, and acceleration, ΔP_{acc}. The pressure drop in each element is calculated individually with consideration that the mass flux, *G*, may vary due to both vapor extraction and changes of the cross-sectional area along the diverging channel. The frictional pressure drop for element i is evaluated as:

$$-\Delta P_{fric,i} = \frac{\Delta z_i}{D_h}\left[\left(\frac{f_{loc,lo}\left(1-x\right)^2 G^2 \phi_l^2}{\rho_l}\right)_i + \left(\frac{f_{loc,lo}\left(1-x\right)^2 G^2 \phi_l^2}{\rho_l}\right)_{i-1}\right] \tag{93}$$

where $f_{loc,lo}$ is the local single-phase liquid friction factor when fluid is assumed to be all-liquid and ϕ_l^2 is the two-phase multiplier. Because the local Reynolds number in this study, defined based on the local cross-sectional hydraulic diameter, is consistently less than 2,000 for all predicted results, the flow is assumed to be laminar. The local single-phase liquid friction factor, $f_{loc,lo}$, was determined from the apparent friction factor, f_{app}, which is defined as an average of local friction factor up to a specific location, and is given by Shah and London [67] for laminar flow in single-phase region, further details are given in Salakij [66].

An important parameter for modeling two-phase frictional pressure drop is the two-phase multiplier. For homogeneous flows, the two-phase multiplier for laminar flow can be expressed in term of the two-phase viscosity and specific volume as [78]:

$$\phi_{lo}^2 = \frac{\mu_{2\phi}}{\mu_l}\frac{v_{2\phi}}{v_l} \tag{94}$$

The two correlations used in the present study for the two-phase viscosity were proposed by McAdams et al. [79] and Chicchitti et al. [80], respectively, as:

$$\mu_{2\phi} = \left(\frac{x}{\mu_v} + \frac{1-x}{\mu_l} \right)^{-1} \tag{95}$$

$$\mu_{2\phi} = x\mu_v + (1-x)\mu_l \tag{96}$$

For separated flows, the two-phase multiplier is usually expressed as a function of the Lockhart-Martinelli parameter, X^2, which, for laminar flow is given by [78]:

$$X^2 = \frac{(dP/dz)\big|_l}{(dP/dz)\big|_v} = \left(\frac{\mu_l}{\mu_v} \right) \left(\frac{1-x}{x} \right) \left(\frac{\nu_l}{\nu_v} \right) \tag{97}$$

In the present study, three two-phase multiplier relationships developed for separated flows in microchannels, shown in Table 11 as Eqs.(98)-(100), were studied. The correlations proposed by Lee and Lee [54] and Qu and Mudawar [4] were developed for a straight channel while the correlation proposed by Lee and Pan [10] was developed for a diverging channel.

Table 11. Two-phase multiplier correlation developed for microchannel flow

Source	Formula	Eq.
Lee and Lee [54]	$\phi_l^2 = 1 + \frac{C_{LM}}{X} + \frac{1}{X^2}$ $C_{LM} = A\varphi^{C_1}\psi^{C_2}\,\mathrm{Re}_{lo}^{C_3}$ $\varphi = \frac{\mu_l^2}{\rho_l \sigma D_h}; \psi = \frac{\mu_l G}{\rho_l \sigma}$ Laminar-laminar: A=6.833×10^{-8};C_1=-1.317;C_2=0.719;C_3=0.557 Laminar-turbulent: A=6.185×10^{-2};C_1=0;C_2=0;C_3=0.726	(98)
Qu and Mudawar [4]	$\phi_l^2 = 1 + \frac{C_{LM}}{X} + \frac{1}{X^2}$ $C_{LM} = 21\left(1 - e^{-319 D_h}\right)(0.00418G + 0.0613)$	*(99)*
Lee and Pan [10] (Microscale diverging channel)	$\phi_l^2 = 1 + \frac{0.29}{X} + \frac{0.21}{X^2}$	(100)

The acceleration pressure drop, ΔP_{acc}, in element *i*, based on the two-fluid model [78], is evaluated from:

$$-\Delta P_{acc,i} = \left\{ G^2 \left[\frac{x^2 v_v}{\alpha} + \frac{(1-x)^2 v_l}{(1-\alpha)} \right] \right\}_i - \left\{ G^2 \left[\frac{x^2 v_v}{\alpha} + \frac{(1-x)^2 v_l}{(1-\alpha)} \right] \right\}_{i-1} \tag{101}$$

where α is the void fraction. For homogeneous flows, the homogeneous void fraction, which is denoted as β_v, is expressed as a function of quality and specific volume fraction of fluid:

$$\beta_v = \frac{x v_v}{(1-x) v_l + x v_v} \tag{102}$$

For separated flows, the predicted void fraction is less than the homogeneous void fraction. The two void fraction correlations developed for minichannel and microchannel separated flows used in this study were proposed by Armand [81], and Zivi [35], respectively, as:

$$\alpha = 0.833 \beta_v \tag{103}$$

$$\alpha = \frac{1}{1 + \left(\frac{1-x}{x} \right) \left(\frac{v_l}{v_v} \right)^{2/3}} \tag{104}$$

It should be noted that the frictional pressure drop, shown in Eq. (93), and the acceleration pressure drop, shown in Eq. (101), can also be used for single-phase liquid flow when the quality, *x*, and void fraction, α, are set to 0, and the two-phase multiplier, ϕ_l^2, is set to 1.

In this study, the predictive model results based on the combinations of five two-phase multiplier and three void fraction models are compared with experimental data of Qu and Mudawar [4], as shown in Figure 29. The five two-phase multiplier models are the two-phase multiplier for homogeneous flows, Eq. (94), based on the two correlations of the two-phase viscosity, given in Eqs. (95) and (96), and three correlations for

separated flows in microchannels, given in Table 11. The three void fraction models are the homogeneous flow void fraction model, Eq. (102), and the two separated flow void fraction correlations, given in Eqs. (103) and (104). It clearly shows that the predicted results based on all of the model combination, which includes either the homogeneous frictional pressure drop or void fraction model, significantly overpredict experimental results. This is most likely because the dominate flow pattern in microchannels is annular flow which is more compatible with the separated flow model than the homogeneous flow model. Quantitatively, the accuracy of predictions of each combination of two-phase multiplier and void fraction models are shown in Table 12 in term of the mean absolute error, $MAE_{\Delta P_{chan}}$, which is defined as:

$$MAE_{\Delta P_{chan}} = \frac{1}{N}\sum_{i=1}^{N}\left(\frac{\left|\Delta P_{chan,pred} - \Delta P_{chan,\exp}\right|}{\Delta P_{chan,\exp}}\right)\times 100\% \tag{105}$$

Table 12. Mean absolute error of pressure drop models prediction comparing to experimental data from Qu and Mudawar [4]

		Void fraction models		
		Homogeneous	Armand [81]	Zivi [35]
Two-phase multiplier models	Homogeneous per McAdams et al. [79]	269.4	147.8	150.7
	Homogeneous per Chicchitti et al. [80]	435.9	323.3	325.8
	Lee and Lee [54]	118.2	18.8	14.0
	Qu and Mudawar [4]	141.1	15.7	17.2
	Lee and Pan [10]	101.9	35.8	30.5

where $\Delta P_{chan,pred}$ and $\Delta P_{chan,\exp}$ are the predicted and experimental channel pressure drop, respectively. The best combination of models uses the two-phase multiplier correlation by Lee and Lee [54], and void fraction correlation by Zivi [35] where the experimental

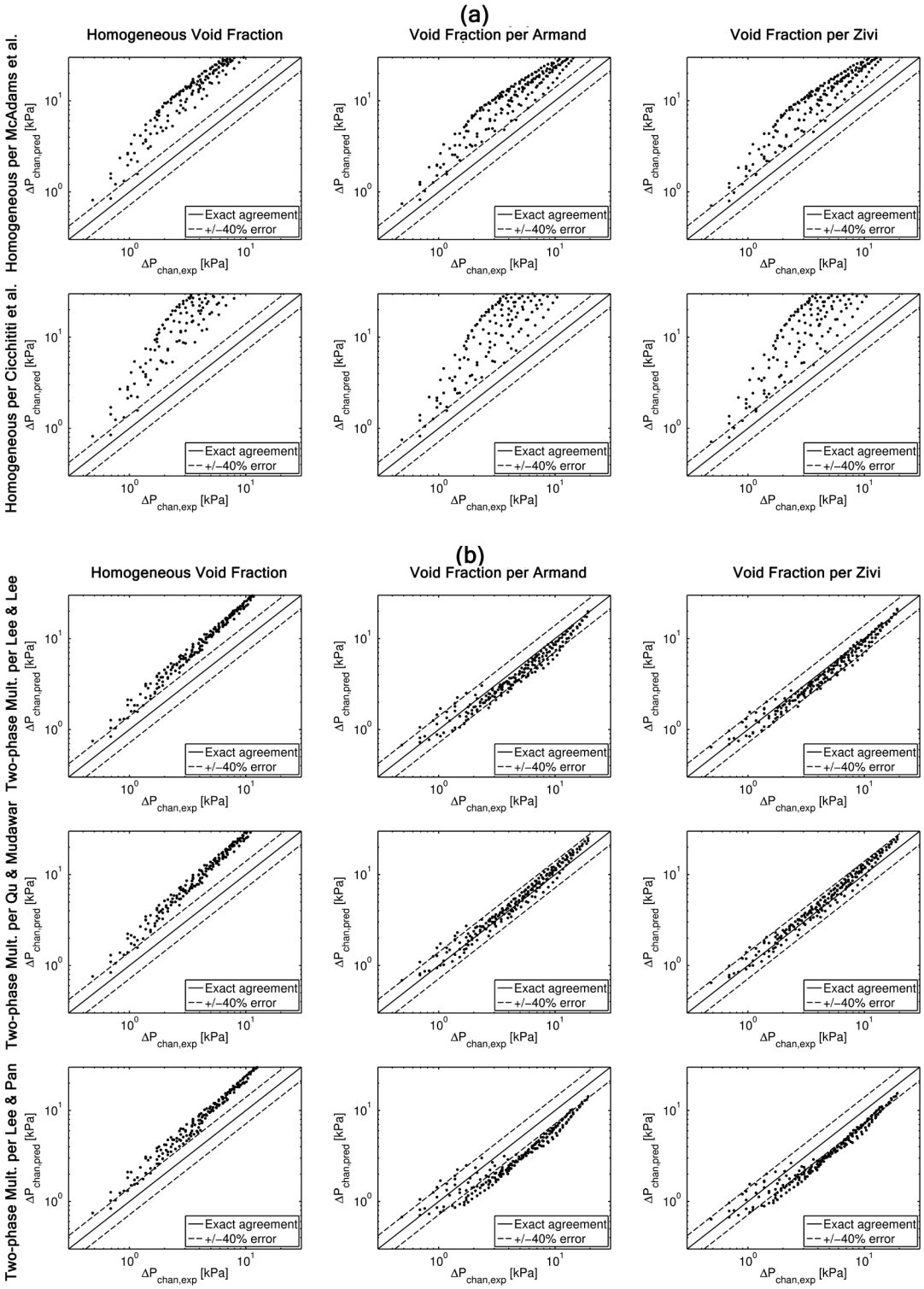

Figure 29. Comparison of experimental [4] and predicted pressure drop using two-phase frictional pressure drop models based on (a) the homogeneous flow models (b) the separated flow models

and predicted pressure drop agree with a mean absolute error less than 14.0%. These models were used to generate all further results presented.

4.4.3 Membrane Transport Model

The rate of mass transport through the hydrophobic membrane was determined based on the application of Darcy's law [32]. The breakthrough pressure of the hydrophobic porous wall in this study is assumed to be sufficiently high to completely prevent leaking of the liquid phase through the membrane. The local extracted vapor mass flow rate across the porous wall of element i is expressed as:

$$\dot{m}_{extr,i} = \left[\frac{A_{extr}}{\nu_v} \frac{\Delta P_{driv,loc}}{(\delta/\kappa)} \right]_i = \left[\frac{A_{extr}}{\nu_v} \frac{\Delta P_{driv,loc}}{R_{extr}} \right]_i \tag{106}$$

where ν_v is the vapor kinematic viscosity, A_{extr} is the area of extraction, δ is the thickness of the porous wall, κ is the specific permeability of the porous membrane, and $\Delta P_{driv,loc}$ is the local extraction driving pressure. By combining the related membrane characteristic, which are the thickness, δ, and the specific permeability, κ, to a single parameter that represents the resistance of the flow through the membrane, the extraction flow resistance, R_{extr}, is defined as:

$$R_{extr} = \delta/\kappa \tag{107}$$

For all channels presented, the extraction flow resistance is 5×10^9 m^{-1}. This is a reasonable value when compared to other general hydrophobic membrane using in membrane transport process such as 220 nm pore, hydrophobic PTFE membrane whose value of R_{extr} reported by David et al. [19] as 8.13×10^9 m^{-1}.

For vapor flowing through the hydrophobic porous wall, the local extraction driving pressure, $\Delta P_{driv,loc}$ in Eq. (106), is defined as a vapor pressure difference between two sides of the porous membrane. The vapor pressure on the outer side of the channel is the absolute value of extraction pressure. The vapor pressure on the inner channel side is

the saturated pressure of the liquid based on the local bulk channel temperature when evaluating the evaporative extraction. For bubble extraction, the bulk pressure of the vapor based on the local channel pressure was used. The difference between the saturated pressure of the liquid and pressure of the vapor in two-phase flow, (which may exist due to surface tension effects), is assumed to be negligible. The local extraction driving pressure, accounting for both evaporative and bubble extractions, can be expressed by a single equation as:

$$\Delta P_{driv,loc} = P_{sat}\big|_{T_{b,loc}} - P_{extr} \tag{108}$$

Extracted vapor mass flow rate predictions were compared with the experimental data of Apreotesi et al. [16-17] based on diabatic flow boiling in a microscale fractal-like flow network with in-situ vapor extraction. The model results match the experimental results very well with mean absolute error of 15.5%. Further details of membrane transport model validation are given in Salakij et al. [18, 21].

4.5 STABILITY PARAMETER MODEL

A stability parameter model for a diverging channel was first proposed by Lee and Yao [12] and Lee et al. [76] which they defined as an "instability parameter, *R*". They used a similar concept to a stability model proposed by Kandlikar [75] by considering a force balance acting on the liquid-vapor interface of the bubble. If the backward force is less than the forward force, the bubble is said to flow upstream towards the channel inlet causing an unstable flow. The parameter R is based on a ratio of the backward vapor expansion force, $F_{exp,back}$, to the combination of the forward inertia force, F_I, the net surface tension, $F_{net\ S}$, and the orifice force, F_{orf}, acting on the bubble. The parameter R is expressed as:

$$R = \sqrt{\frac{F_{exp,back}}{F_I + F_{net\ S} + F_{orf}}} \tag{109}$$

and the flow is said to becomes unstable when R is greater than one.

The backward force $F_{exp,back}$ is equivalent to the momentum change caused by the expansion due to the boiling phase change mechanism expressed as:

$$F_{\exp,back} = \rho_v u_{\exp,back}^2 A_{c,1} \tag{110}$$

where $u_{exp,back}$ is the expanding rate of the liquid-vapor interface of the bubble in the upstream direction and $A_{c,1}$ is the channel cross-sectional area at the back, or upstream side, of the bubble. Figure 30 illustrates the movement of the liquid-vapor interfaces at the ends of the bubble. The interface velocity is estimated from the volumetric expansion rate, $\dot{V}_{exp}$, and the bubble cross-sectional area of the upstream, $A_{c,1}$, and downstream, $A_{c,2}$, as:

$$u_{\exp,back} = \frac{\dot{V}_{\exp}}{A_{c,1} + A_{c,2}} = \frac{\dot{m}_{v,\exp} v_{lv}}{A_{c,1} + A_{c,2}} \approx \frac{\dot{m}_{v,\exp}}{\rho_v \left(A_{c,1} + A_{c,2} \right)} \tag{111}$$

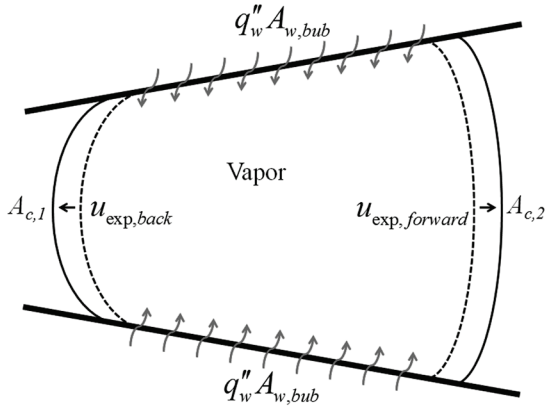

Figure 30. Sketch of expanding confined bubble resulting from liquid film evaporation

Here, the volumetric expansion rate, $\dot{V}_{exp}$, is rewritten in term of the net rate of increase of the vapor, $\dot{m}_{v,\exp}$, which is based on the total heat input rate from the wall to the bubble through the latent heat of vaporization. For a given wall heat flux, $\dot{m}_{v,exp}$ can be evaluated as:

$$\dot{m}_{v,exp} = \frac{q''_w A_{heat,bub}}{i_{lv}} \tag{112}$$

where $A_{heat,bub}$ is the channel heated wall area in contact with the bubble. Combining these, the backward force can be expressed as:

$$F_{\exp,back} = \rho_v \left(\frac{q''_w A_{heat,bub}}{\rho_v i_{lv}} \frac{1}{A_{c,1} + A_{c,2}} \right)^2 A_{c,1} \tag{113}$$

Lee and Yao [12] and Lee et al. [76] proposed that the forward force is the combination of the forward inertia force, F_I, and the net surface tension force, $F_{net\ S}$, that acts on the bubble. These forces are expressed as:

$$F_I = \frac{G_{in}^2 A_{c,1}}{\rho_l} \tag{114}$$

$$F_{net\ S} = \sigma \left(\frac{1}{W_1} - \frac{1}{W_2} \right) A_{c,1} \tag{115}$$

where W_1 and W_2 are the channel widths on the upstream and downstream sides of the bubble, respectively. This expression is based on the assumption that the radii of curvature of the liquid-vapor interface may be approximated, on average, by the height and the width of the channel. Because the surface tension is inversely proportional to the local radius of curvature, the surface tension force on the upstream is greater than the downstream sides for a diverging channel. If there exists an inlet orifice that restrict the flow, Lee and Yao [12] and Lee et al. [76] included a resulting inlet force, F_{orf}, added to the forward force. This additional force is based on the pressure drop of the orifice due to friction, contraction and expansion, and is expressed as:

$$F_{orf} = \frac{1}{2\rho_l} \left(\frac{G_{in} A_{c,1}}{A_{orf}} \right)^2 K_{orf} A_{c,1} \tag{116}$$

where A_{orf} and K_{orf} are the area and the loss coefficient of the orifice, respectively. By substituting Eqs. (113)-(115) into (109), the stability parameter R becomes:

$$R = \sqrt{\frac{\rho_v \left(\frac{q''_w A_{heat,bub}}{\rho_v i_{lv}} \frac{1}{A_{c,1} + A_{c,2}} \right)^2 A_{c,1}}{\frac{G_{in}^2 A_{c,1}}{\rho_l} + \sigma \left(\frac{1}{W_1} - \frac{1}{W_2} \right) A_{c,1} + \frac{1}{2\rho_l} \left(\frac{G_{in} A_{c,1}}{A_{orf}} \right)^2 K_{orf} A_{c,1}}} \tag{117}$$

To apply a similar condition on a diverging channel with in-situ vapor extraction, a newly proposed stability parameter St is developed based on the ratio of the backward to forward forces. However, unlike the instability parameter R, this model more closely follows the model developed by Kandlikar [75] which considers the force balances only on the liquid-vapor interface at the upstream side of the bubble. This is because the criterion used for unstable flow is when the bubble expands toward the inlet chamber which is better represented by the upstream side of the bubble. It should be noted that surface tension force on the liquid-vapor interface at the downstream side of the bubble is not considered in this case because the control volume only includes the liquid-vapor interface at the upstream side of the bubble, (see Figure 31). Moreover, the orifice force is not directly included in this model. This is because the orifice force is not a physical force that is acting on the liquid-vapor interface, and the effects of inlet restrictor can be physically included when the orifice is included in the system as the inlet of the system. To include the effects of the in-situ vapor extraction, a net reduction in the net rate of vapor expansion is accounted for by allowing vapor to leave through the porous wall based on the local extraction driving pressure discussed previously.

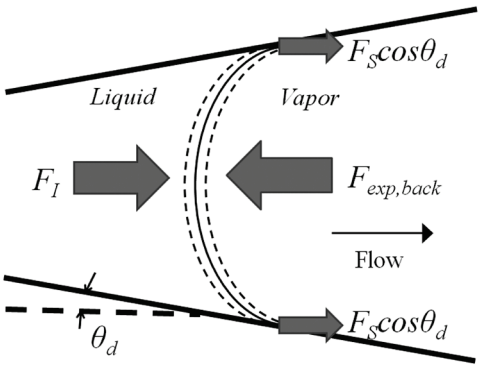

Figure 31. Schematic forces acting on the upstream side of the liquid-vapor interface for the present stability model.

The newly proposed stability parameter St is based on the ratio of backward vapor expansion force, $F_{exp,back}$, to the combination of forward inertia, F_I, and surface tension forces, F_S, aligned along the channel centerline, expressed as:

$$St = \sqrt{\frac{F_{exp,back}}{F_I + F_S \cos\theta_d}} \tag{118}$$

where a schematic of the relevant forces is shown in Figure 31. The forward inertia force is evaluated from Eq. (114) while the forward surface tension force, F_S, is expressed as:

$$F_S = \sigma \wp_{w,1} \tag{119}$$

where $\wp_{w,1}$ is the wetted perimeter of the channel at the upstream side of the bubble.

The vapor mass flow rate that causes bubble expansion, $\dot{m}_{v,\exp}$, is modified for flow with in-situ vapor extraction with the assumption that the net latent energy associated with the rate of increase of vapor mass that causes the expansion is the net energy added to the fluid in the channel. This net energy rate is equal to the rate of heating minus the rate of energy loss due to the extracted vapor. By assuming a uniform wall heat flux and sufficient nucleation sites, the net rate of vapor mass that causes bubble expansion can be evaluated as:

$$\dot{m}_{v,\exp} = \frac{q''_w A_{heat,bub} - \dot{m}''_{extr} i_v A_{extr,bub}}{i_{lv}} \tag{120}$$

where $A_{extr,bub}$ is the porous membrane area in contact with the bubble. It should be noted that Eq. (120) is valid only when the term $q''_w A_{heat,bub} - \dot{m}''_{extr} i_{lv} A_{extr,bub}$, which represents the net energy transfer to cause the expansion of the bubble, is positive. This term can be negative when the rate of energy transfer with extracted vapor is greater than the supplied heat rate. In this case, there is no expansion of the bubble, i.e. $\dot{m}_{v,\exp}$ = 0, resulting in stable flow. Combining Eqs. (110), (111) and (120), the backward expansion force for St can be written as:

$$F_{\exp,back} = \rho_v \left(\frac{q''_w A_{heat,bub} - \dot{m}''_{extr} i_v A_{extr,bub}}{\rho_v i_{lv}} \frac{1}{A_{c,1} + A_{c,2}} \right)^2 A_{c,1} \tag{121}$$

Finally, by substitute Eqs. (114), (119) and (121) into (118), the stability parameter St becomes:

$$St = \sqrt{\frac{\rho_v \left(\frac{q''_w A_{heat,bub} - \dot{m}''_{extr} i_v A_{extr,bub}}{\rho_v i_{lv}} \frac{1}{A_{c,1} + A_{c,2}} \right)^2 A_{c,1}}{\frac{G_{in}^2 A_{c,1}}{\rho_l} + \sigma \wp_{w,1} \cos\theta_d}} \tag{122}$$

It should be noted that both stability parameters (R and St) are based on the cross-sectional area of the liquid-vapor interface of the expanding bubble and may vary with the size of the expanding bubble, which is constrained by the channel size. As maxima we can set $A_{heat,bub} = A_{heat,chan}$, $A_{extr,bub} = A_{extr,chan}$, $A_{c,1} = A_{c,in}$ and $A_{c,2} = A_{c,out}$. Consequently if the stability parameter based on these conditions is less than one, the flow is defined as stable. Because the evaluation is focused on the liquid-vapor interface on the upstream side of the bubble, the fluid properties used to defined St are evaluated at the inlet temperature and pressure. Therefore, the effects of the inlet subcooling are included in these models.

The main drawback of the present stability model is that it lacks the ability to predict the instability due to insufficient nucleation sites. This is because the high degree of superheated liquid may cause instantaneous rapid expansion of bubbles. The rate of vapor expansion in this case would be expected to be higher than the predicted value, with an under prediction in instability. A possible method to include the effect of instability due to insufficient nucleation sites in the present model is by adding a correction factor to the predicted vapor generation rate term in Eq. (120). The development of this nucleation factor is not included in this study. This factor should be a function of boiling surface conditions such as surface roughness and contact angle to account for the potential for rapid expansion of bubbles.

4.6 RESULTS AND DISCUSSIONS

To observe the effects of the diverging channel and in-situ vapor extraction on the flow, results of the model predictions are presented and discussed in two main sections that describe: (i) local conditions and (ii) global results. In the local conditions section, distributions of flow conditions along the channels are discussed in details to help understand the effects of both a diverging channel and in-situ vapor extraction on flow boiling. In the global results, overall pressure drop, outlet quality, vapor extraction rate and the stability parameter are presented and compared. The results of variations in heat rate input, extraction pressure and half-diverging angle of the channels, are discussed.

4.6.1 Local Conditions

To provide representative results of the local distributions of pressure, temperature and quality as well as the local vapor extraction mass flux along the channels, sixteen cases are presented in this section. The results for an extraction pressure of 80 kPa-a and no extraction are compared among four channels with different diverging angles. Heat flux values of 26.7 W/cm^2 and 133.3 W/cm^2 are chosen as representatives of low and high heat flux cases, respectively.

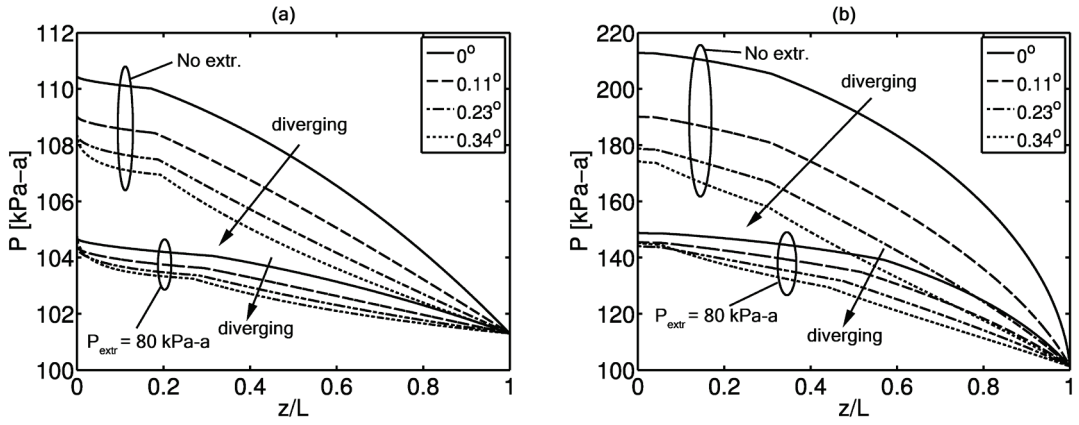

Figure 32. The local channel pressure for four different diverging angles without and with in-situ vapor extraction at an extraction pressure of 80 kPa-a; (a) heat flux of 26.7 W/cm^2, (b) heat flux of 133.3 W/cm^2; note the difference in channel pressure scales.

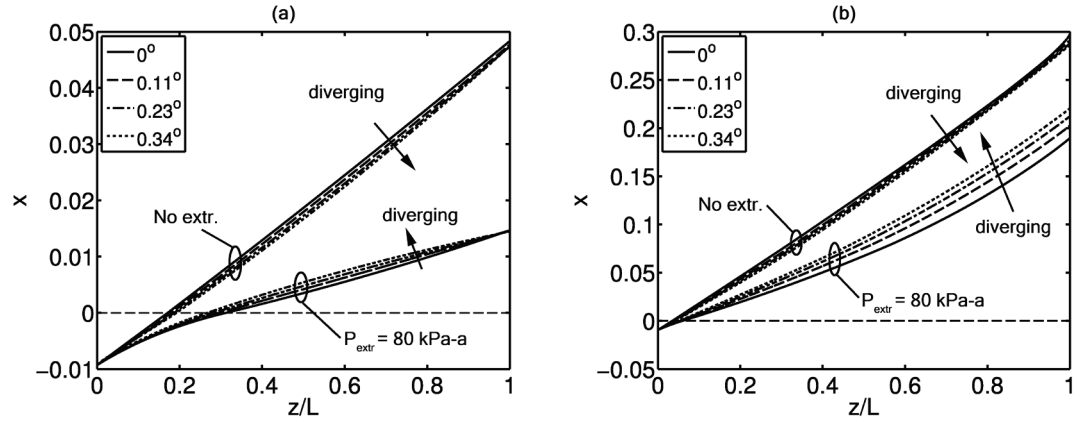

Figure 33. The local quality for four different diverging angles with and without in-situ vapor extraction at an extraction pressure of 80 kPa-a; (a) heat flux of 26.7 W/cm^2, (b) heat flux of 133.3 W/cm^2; note the difference in quality scales.

The predicted local channel pressure and quality, as a function of streamwise location long the channel, is shown in Figures 32 and 33, respectively. The pressure decreases along the flow until it reaches the outlet pressure which is at atmospheric pressure while the pressure of the extraction cases is significantly lower than the no-extraction cases as a result of quality reduction due to the effect of vapor extraction. On the other hand, the local quality increases along the flow and the local quality with

extraction is lower than that without extraction. The slight variation in local quality distribution for no-extraction case among the channel configurations is the result of the differences in streamwise pressure variation while the greater variation for high heat flux with extraction is the result of differences in vapor extraction mass flux. Both variations in local pressure distributions and local extracted mass flux among the channels are discussed below.

It should be noted that the sudden change in slope of pressure distribution, which may not be strictly realistic, are due to the pressure drop model that is used. However, these sudden changes do not cause any discontinuity in pressure along the channel. The slope change occurring near the inlet is caused by the transition from single-phase to two-phase flow which occurs at the point where $x = 0$ in Figure 33. The other sudden change is because the two-phase pressure drop correlation by Lee and Lee [54] has two regions which are for laminar-laminar and for laminar-turbulent flows. This transition occurs only when the vapor generation rate is sufficient to cause vapor phase to become turbulent flow. For conditions in this study, this transition occurs around $x = 0.08$ which corresponds to z/L = 0.3 and 0.5 for the case with a heat flux value of 133.3 W/cm^2, for extraction and non-extraction cases, respectively, as shown in Figure 32(b).

Figure 32(a) supports the results of Lee and Pan [10] that diverging channel provides a steep pressure gradient near the entrance of the diverging channel. This suppresses the upstream flow of any expanding vapor and helps stabilizing the flow. It clearly shows that the pressure gradient at the beginning of the diverging channel, which is the single-phase flow region, is greater than in the straight channel. Moreover, as the diverging angle increases, the pressure gradient near the beginning of the channel increases. This is a result of a larger frictional pressure drop because the mass flux of the diverging channel near the beginning of the channel is greater than in the straight channel due to a smaller cross-sectional area. Although there is a pressure gain due to the expansion of the cross-sectional area of the diverging channel, this effect is small compared to the larger frictional pressure drop near the beginning of the channel. However, this steep pressure drop phenomenon is not as clearly shown in high heat flux

case shown in Figure 32(b). Based on this observation, it can be implied that the stabilizing effect of the larger pressure drop at the inlet may be nonconsequential for high heat flux cases in diverging channels. This explains the results by Lee and Pan [11] that although the flow instability in diverging channel was fully suppressed in low heat flux case, yet failed to suppress flow instability when input heat flux value is high.

Based on results in Figure 32, the local pressure distribution in straight channels is generally higher than in the diverging channels. As previously mention, the diverging channel has a larger pressure gradient near the beginning of the channel than the straight channel. For single-phase flow, as the channel diverges, the flow generally decelerates resulting in a slight pressure gain that reduces the pressure gradient. For two-phase flow, the increase in channel cross-sectional area opposes the acceleration caused by vapor expansion resulting in lower pressure gradient compared to that in the straight channel. In other words, pressure in the diverging channel generally drops steeper than in the straight channel near the beginning while it drops less steep near the outlet. The rate of change of the pressure gradient along the channel increases as the channel divergence increases. In some cases, the two-phase pressure gradient decreases rather than increasing; as seen for flow in the channel with a half-diverging angle of 0.34^{o} without extraction shown in Figure 32(a). The pressure gradient near $z/L = 0.2$, where flow boiling starts, is clearly steeper than the pressure gradient near the outlet. This is because the effects of increasing cross-sectional area along the flow in the diverging channel causing deceleration overcome the effects of increasing flow quality tending to accelerate the flow. This variation in local channel pressure among the different channel geometries affects the differences in the local driving pressure which influences the extracted vapor mass flux which is discussed below.

In order to understand the variation in local extracted vapor mass flux, it is important to observe the local bulk fluid temperature. This is because the local extraction driving pressure, presented in Eq. (108), is modeled based on the saturation pressure evaluated at the local bulk temperature. The local bulk fluid temperature distribution along the flow is presented in Figure 34 for the same conditions as in Figures 32 and 33.

In the single-phase region, the bulk fluid temperature increases in the streamwise direction until it reaches a maximum, which is the location where the transition to two-phase flow occurs (x = 0). Then, the bulk fluid temperature, which is equal to the saturation temperature, decreases in the streamwise direction because of the decrease of pressure along the flow. The location at which the transition to two-phase flow occurs varies with the diverging angle of the channel, and vapor extraction conditions. For the low heat flux and no extraction cases, shown in Figures 33(a) and 34(a), the transition to two-phase flow occurs earliest for the straight channel. The length of the single-phase region increases with increasing channel divergence, since the surface area of the first half of the channel of the channel decreases with increasing channel divergence. Since the diverging channel has a smaller heating area near the inlet to the channel, the total heat input rate per unit length of the channel for the applied uniform heat flux condition is lower, and thereby a longer length is required to reach two-phase flow conditions.

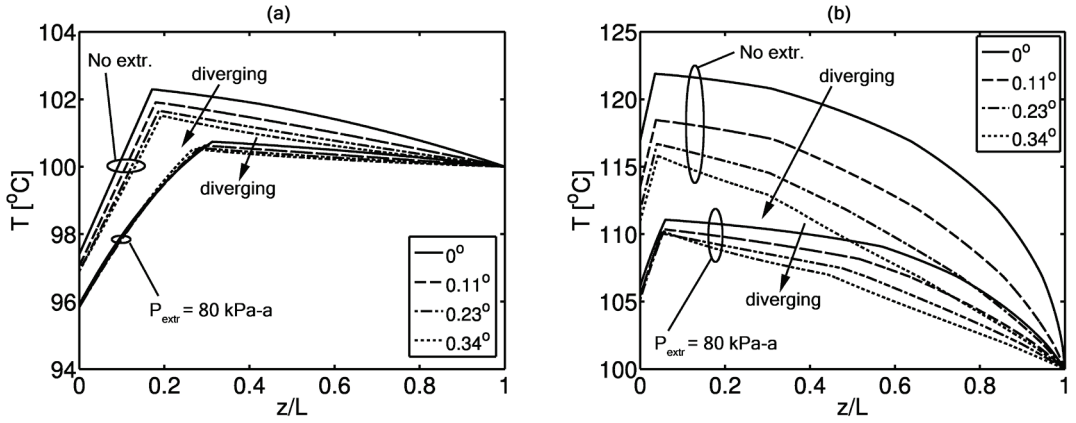

Figure 34. The local bulk temperature for four different diverging angles with and without in-situ vapor extraction at an extraction pressure of 80 kPa-a; (a) heat flux of 26.7 W/cm^2, (b) heat flux of 133.3 W/cm^2; note the difference in temperature scales.

Compared to the no-extraction case, in-situ vapor extraction reduces the temperature gradient, and delays the streamwise location at which transition to two-phase flow occurs, since the energy extracted with the evaporative vapor reduces the net energy retained in the liquid. It should be noted that although the onset of boiling is delayed

because of vapor extraction, the bulk fluid temperature, shown in Figure 34, is more uniform along the channel comparing with the no-extraction cases. With increasing channel divergence, the extended single-phase region decreases. It is shown that vapor extraction extends the single-phase region and reduces the temperature gradient greater in the straight channel. This is because of the larger extraction area per unit length of channel near the beginning of the channel, resulting in more evaporative vapor extraction in the single-phase region. For a heat flux of 26.7 W/cm^2 and extraction pressure of 80 kPa-a, the delay of boiling caused by vapor extraction is sufficient to reverse the trend shown in the no-extraction case, such that the length of the single-phase region in the straight channel is the greatest among the channels studied. This phenomenon is not as clearly seen in the high heat flux cases because the sensible heat required to bring the fluid from subcooled to saturated is significantly less than the applied heat input rate.

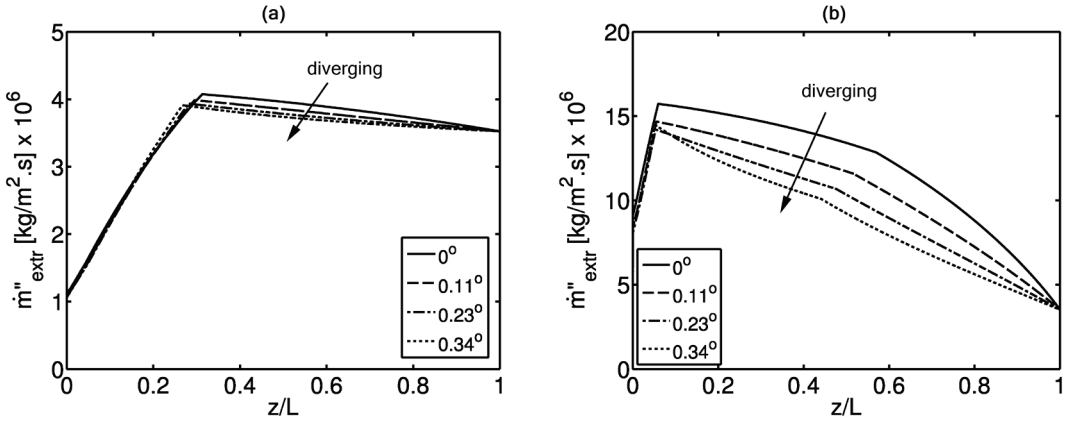

Figure 35. The local vapor extraction mass flux for four different diverging angles with an extraction pressure of 80 kPa-a; (a) heat flux of 26.7 W/cm^2, (b) heat flux of 133.3 W/cm^2; note the difference in mass flux scales.

As previously mentioned, the trend of the local extracted vapor mass flux, shown in Figure 35, matches that of the bulk temperature. In the single-phase region, as the local bulk temperature increases in the streamwise direction, the local extraction driving pressure increases, and thereby increases the local extraction by evaporation. This is explained by the fact that higher temperature subcooled liquid tends to have a higher

evaporation rate because of its higher vapor pressure. It should be noted that although the extracted vapor mass flux in the single-phase region in the diverging channel is somewhat higher than in the straight channel, the rate of energy loss due to evaporative extraction per unit length near the begin of the channel may be less because the extraction area is smaller. For example, for the cases with a heat flux of 26.7 W/cm^2 and extraction pressure of 80 kPa-a, shown in Figures 33(a) and 34(a), the single-phase region is extended by extraction. In the two-phase flow region, the extracted mass flux decreases along the flow because the local extraction driving pressure decreases along the flow, as shown in Figure 35. Consequently, there is a decrease in local extracted vapor mass flux. Comparing the local extracted vapor mass flux in the two-phase flow region, value for the diverging channel is generally less than that of the straight channel. The extraction mass flux in the low heat flux cases, shown in Figure 35(a), does not differ much among the channel configurations, while the extracted mass flux in the high heat flux cases, shown in Figure 35(b), shows large differences. This is because in the two-phase region the absolute pressure and the bulk temperature among the channel geometries for the high heat flux cases are significantly different compared to those of the low heat flux cases. Therefore, the lower local extracted vapor mass flux in the diverging channel is the results of the difference in variation of the pressure gradient along the channel, as discussed previously.

The overall pressure drop in the diverging channel with larger diverging angles can be larger, while the extracted vapor rate in the diverging channel is lower for the same operating conditions. This is because the average channel pressure in the diverging channel is actually lower. This is because of the consequence of the difference in pressure gradient variation along the channel between diverging channels shown in Figure 32(b). Although the inlet pressure in the diverging channel with half-diverging angle of 0.34^o is higher, the pressure gradient near the inlet is larger than in the channel with a half-diverging angle of 0.23^o. Consequently, the local pressure of the diverging channel of 0.34^o drops below that of the diverging channel of 0.23^o near the beginning of channel. Therefore, the pressure in the rest of the diverging channel of 0.34^o is lower. The

result is less extracted vapor mass flux at the same extraction pressure, as shown in Figure 35(b). In addition, this effect is also aided by the fact that the extraction area is changing along the channel. Although the local extracted mass flux near the beginning of the diverging channel of 0.34^{o} is greater than that of the channel of 0.23^{o}, see Figure 35(b), the local extracted mass flux near the end is less. This is caused by a reduction of extraction area in the beginning half of the channel and an increase near the end of the channel. Since the total extracted mass flow rate is mostly affected near the end of the channel with high quality conditions, the total extracted mass flow rate in the diverging channel is less than in the straight channel although the pressure drop is larger. The results of the total extracted mass flow rate is presented in the Global results section.

The variation of the local extracted vapor mass flux among the channels helps to explain the significant variation in local quality in the flow in the high heat flux case shown in Figure 35(b). As the rate of vapor extraction increases, the removal of energy from the flow also increases, and consequently the quality is reduced compared to the no-extraction cases. Figure 35(b) shows that in the high heat flux cases the local extracted vapor mass flux in the diverging channels is generally less than in the straight channel. This indicates that the rate of removing energy from the flow in the diverging channels is less than in the straight channel, and there is a corresponding higher quality in the diverging channels. Therefore, the local quality with vapor extraction in the high heat flux cases in diverging channels is greater than in straight channels. Based on this result, it can be implied that the effects of vapor extraction on the reduction of the local quality is less effective in diverging channels compared to straight channels, especially in high heat flux cases.

4.6.2 Global Results

In this section, combined effects of in-situ vapor extraction in diverging channels on the global results of the channel pressure drop, outlet quality, total extracted mass flow rate and proposed stability parameter are presented and discussed. The trends of vapor extraction are similar for all channel geometries studied, first the contrast of global results

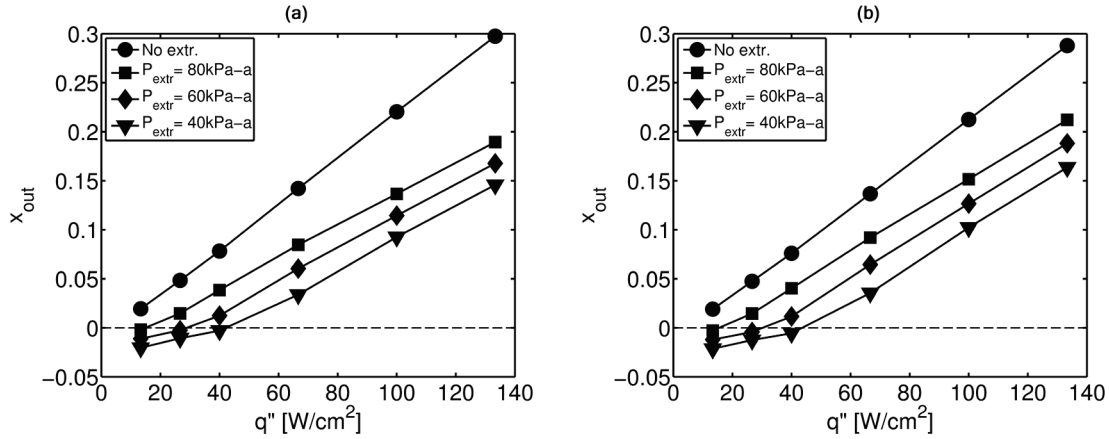

Figure 36. Quality at the outlet versus heat flux for a range of extraction pressures for (a) straight channel (b) channel with 0.23° half-diverging angle.

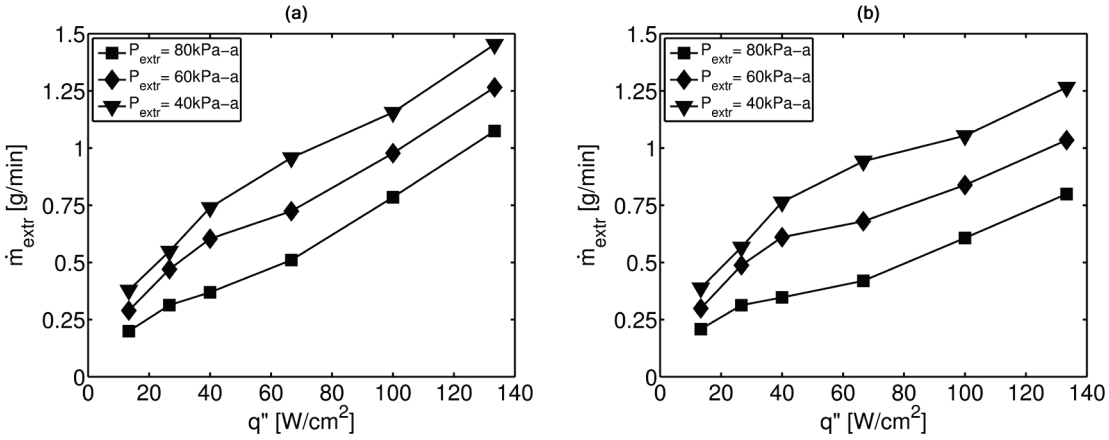

Figure 37. Extracted vapor mass flow rate versus heat flux for a range of extraction pressures for (a) straight channel (b) channel with 0.23° half-diverging angle.

for the straight channel versus the diverging channel with a half-diverging angle of 0.23°, are presented. The outlet quality and the total extracted vapor mass flow rate are plotted as a function of the heat flux in Figures 36 and 37, respectively, for three different extraction pressures, including no extraction. By increasing the heat input rate, the outlet quality increases as expected for all cases. By applying in-situ vapor extraction, the outlet quality significantly decreases with an increased reduction with decreasing extraction pressure (higher extraction pressure differential). Also, the heat rate increases the

extraction rate increases due to the higher average channel pressure, consequently. The effect of diverging channel is small for these cases on the outlet quality, which is due to a reduction of the mass extraction for the diverging channel which is discussed later.

Figure 38 presents the channel pressure drop as a function of heat flux for three different extraction pressures, including no extraction. With lower extraction pressure, the pressure drop decreases, which is a result of the reduction of quality due to higher vapor extraction. While the channel pressure drop can be reduced by decreasing the extraction pressure, there is a limit to the channel pressure drop reduction that vapor extraction can obtain. This occurs when the outlet quality become negative for the low heat flux cases shown in Figure 38, or when only single-phase flow occurs. The channel pressure drop reduction by vapor extraction can be achieved with the limitation that the pressure drop can be reduced to approximately that for single-phase flow. However, when the extraction pressure is lower beyond that required for full vapor extraction, the channel pressure drop slightly increases although this effect is small. This is because, although the evaporative extraction slightly reduces the fluid mass flux, it also extracts energy from fluid resulting in a lower fluid temperature and thereby slightly higher viscosity.

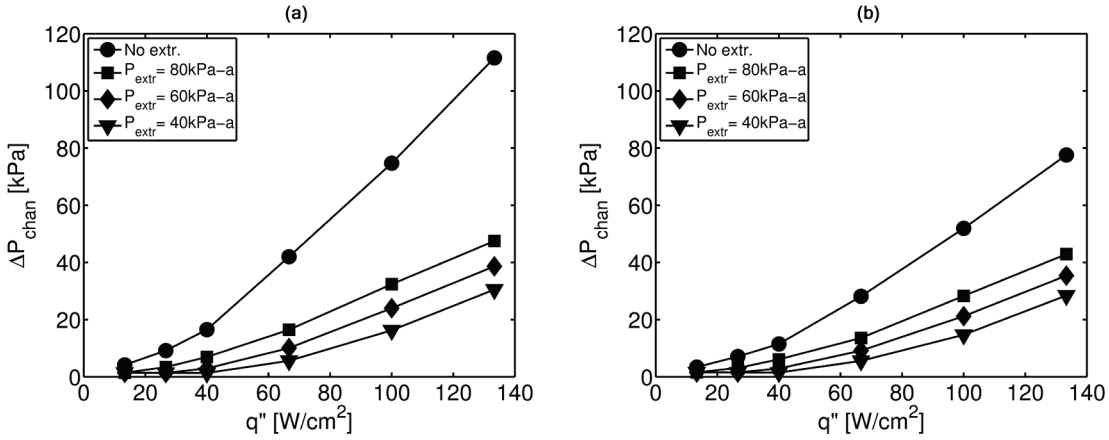

Figure 38. Pressure drop versus heat flux for a range of extraction pressures for (a) straight channel (b) channel with 0.23^{o} half-diverging angle.

The stability parameter *St* versus heat flux for three different extraction pressures including no extraction is presented in Figure 39. The horizontal dashed line represents the predicted stability limit; for *St* less than one, the flow is considered stable. Similar to trends of the pressure drop and quality, the value of the stability parameter increases with increasing heat input rate, and decreases with decreasing extraction pressure. When comparing the allowable heat flux to maintain stable flow, this predictor shows an increase of the heat flux, by applying 40 kPa-a extraction pressure, from approximately 35 to 107 W/cm^2 for a straight channel and from approximately 47 to 122 W/cm^2 for a diverging channel with half-diverging angle of 0.23^o. This is primarily due to the effect of the expansion rate of bubbles, corresponding to a backward expansion force that causes the flow to be unstable, see Eq. (120). The in-situ vapor extraction reduces the expansion rate by directly extracting the generated vapor where it is formed, as well as reduces the energy inside the channel by extracting energy out with the extracted vapor.

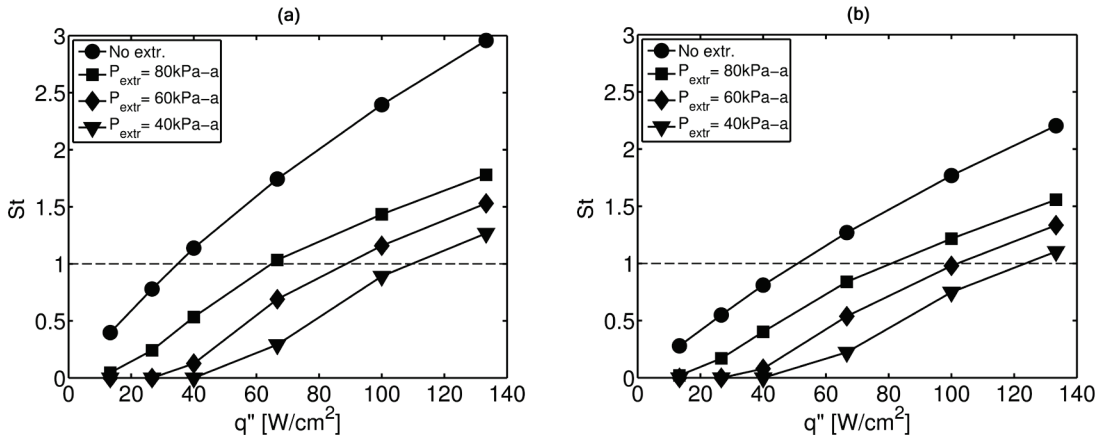

Figure 39. Stability parameter *St* versus heat flux for a range of extraction pressures for (a) straight channel (b) channel with 0.23^o half-diverging angle.

Figure 36, 38 and 39 confirm that the channel pressure drop, outlet quality, and therefore the stability parameter decrease more with vapor extraction as the heat input increases. This trend is more pronounced for the high heat flux cases which require higher channel pressure conditions. The reason for this can be shown from Figure 37

where the extracted mass flow not only increases by decreasing the extraction pressure, but also with increasing heat input rate. For the cases that the flow is entirely single-phase, i.e. $x_{out} < 0$, the extraction driving pressure, based on the vapor pressure, increases with average channel pressure, which increases the bulk temperature which also increases with increasing heat input rate. A consequence of this is that the evaporative extraction rate in the single-phase flow increases with heat input rate. In the two-phase flow regime, the saturation pressure is determined by the channel pressure. Because the two-phase pressure drop is a strong function of vapor quality which increases with increasing heat input rate, the channel pressure also increases with heat input rate, and thereby increases the local extraction driving pressure and vapor extraction rate. Consequently, the vapor extraction rate, in both single-phase and two-phase flows, increases with increasing heat input rate.

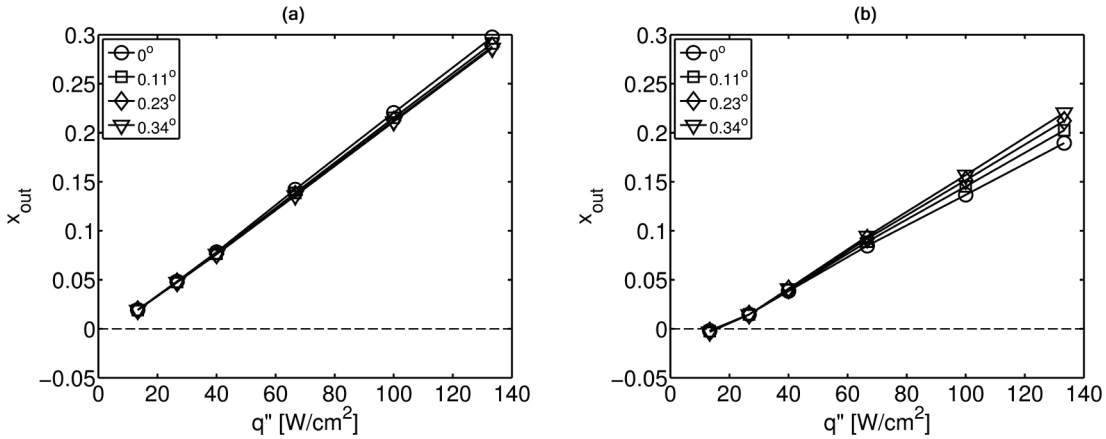

Figure 40. Quality at the outlet versus heat flux for four different diverging angles (a) without vapor extraction (b) with vapor extraction at an extraction pressure of 80 kPa-a.

The effects of increasing channel diverging angle are investigated with the cases with extraction pressure of 80 kPa-a used as representative. The outlet quality versus heat flux is presented in Figure 40 for flow in four different half-diverging angles between 0^o and 0.34^o. The outlet quality for no-extraction cases in Figure 40(a) are almost identical for a given heat flux but show a slight decrease with increasing diverging angle. The minor variations are caused by the small difference in pressure drop that

slightly alters the fluid properties and inlet temperature. The outlet quality during vapor extraction shown in Figure 40(b) is lower compared to no-extraction cases as would be expected. The outlet quality of the channel with the larger diverging angle is generally greater. The differences of outlet qualities with increased divergence during vapor extraction are more significant with high heat flux conditions. These differences are the direct results of changes to the extracted vapor, which is discussed in detail later.

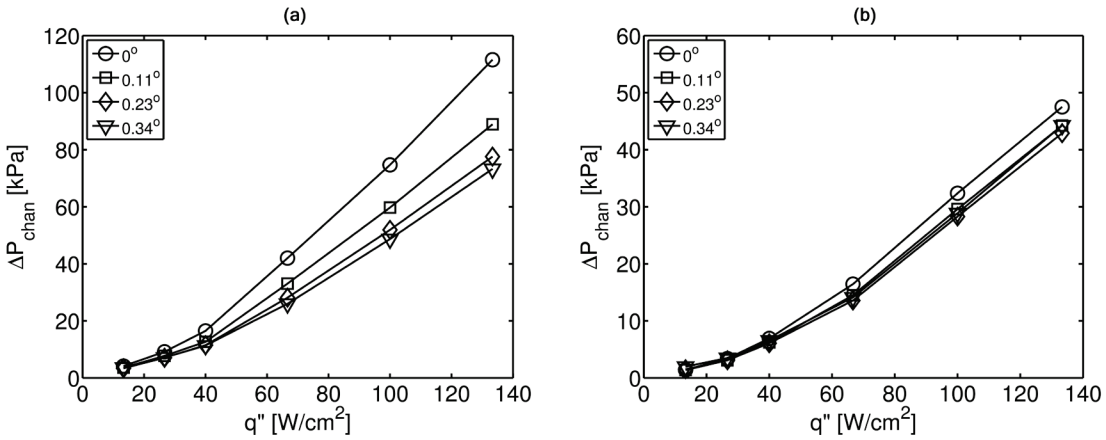

Figure 41. Pressure drop versus heat flux for four different diverging angles (a) without vapor extraction (b) with vapor extraction at an extraction pressure of 80 kPa-a; note the difference in pressure drop scales.

The channel pressure drop shown in Figure 41 in the diverging channels is noticeably less than in the straight channel although the outlet quality is almost identical. It should be noted in Figure 41 that the overall pressure drop with and without extraction have different ranges of pressure drop in order to focus on the effects of geometries on the global results. This is because, for the specific channel configurations and operating conditions used in this study, the effects of diverging channel do not affect the global results as much as the effects of in-situ vapor extraction. As the channel diverging angle increases, the channel pressure drop generally decreases due to local mass flux reduction and flow deceleration. Because the single-phase pressure drop is significantly less than the two-phase pressure drop, the overall channel pressure drop is mostly affected by impact on the two-phase pressure drop. As shown in Figure 32, the local pressure

gradient in the two-phase flow region for the diverging channels is generally less than in the straight channel. The overall pressure drop in the diverging channels is generally less than in the straight channel, and the pressure drop reduction improves with increasing heat flux. This is because the local two-phase pressure gradient is amplified for flows with high quality. Consequently, the no-extraction cases show a greater reduction in pressure drop with increasing channel divergence.

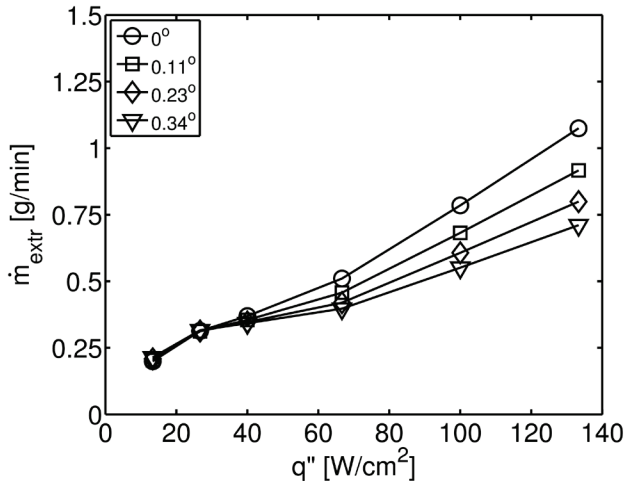

Figure 42. Extracted vapor mass flow rate versus heat flux for four different diverging angles with extraction pressure of 80 kPa-a.

The variation of total extracted vapor mass flow rate as a function of heat flux is given in Figure 42 versus diverging angle. The effect of diverging angle on mass extraction is greater for higher heat input rates. The reason for this greater sensitivity at higher heat flux values is the greater average pressure differential across the membrane. The extraction driving pressures are not significantly different among the different diverging channels for the low heat flux cases, a change from 21.0 to 20.4 kPa between 0^o and 0.34^o divergence for heat flux of 26.7 W/cm^2 versus from 55.4 to 44.4 kPa for heat flux of 133.3 W/cm^2. Because the cross-sectional area in the upstream half of the channel decreases as the channel diverges more, there is a steep two-phase pressure gradient near the beginning of the channel in the high heat flux cases resulting in a reduction in the overall average channel pressure. Therefore, for the same operating conditions, the total

extracted mass flow rate decreases with increasing diverging angle. As previously mention, the differences of extracted vapor directly affect the differences of outlet qualities for the different channels, shown in Figure 40(b). The overall reduction in outlet quality due to extraction also shows the same trend as total vapor extraction rate shown in Figure 42, in that it increases with increasing heat input and decreases with increasing diverging.

It should be noted that although the channel pressure drop may be generally reduced by increasing diverging angle, it is possible to over expand the channel resulting in a greater channel pressure drop. For example, Figure 41(b) shows that the channel with a half-diverging angle of 0.34^o has a larger pressure drop than the 0.23^o channel. This is because the effect of reducing quality due to vapor extraction is less effective as the channel divergence increases. This effect may overcome the deceleration in the diverging channel and result in larger overall channel pressure drop because the quality is higher due to less vapor extraction.

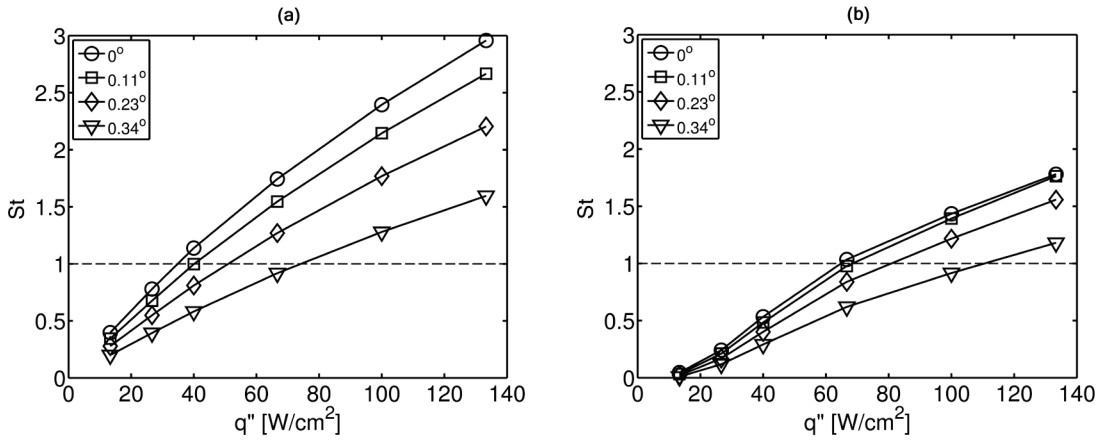

Figure 43. Stability parameter versus heat flux for four different diverging angles (a) without vapor extraction (b) with vapor extraction at an extraction pressure of 80 kPa-a.

The comparison of the stability parameter for the various diverging channels is presented in Figure 43. In all cases both with and without extraction, the stability parameter in the diverging channel is significantly less than in the straight channel. The

explanation for this is the influence of the diverging channel on the forces related to this stability parameter. As a bubble is suppressed by the diverging channel walls, the normal force of the wall acting on the bubble also tends to force the bubble to expand downstream. Moreover, as the size of the cross-sectional area of the diverging channel increases along the flow direction, the greater the upstream expansion force (assuming a nearly uniform bubble pressure). In addition, the forward inertia of the flow in a diverging channel is also greater due to the smaller inlet cross-sectional area of the diverging channel leading to a higher upstream mass flux. Although the surface tension force in a straight channel is greater because of the greater wetted perimeter at the inlet, the larger backward expansion force in the straight channel has a greater effect on the stability parameter, resulting in a reduction of the stability parameter for a diverging channel.

Figure 43(b) shows that by coupling vapor extraction with a diverging channel, the stability parameter is further reduced in all cases studied. This indicates that the flow stability in a diverging channel can be further improved by applying in-situ vapor extraction because the rate of vapor expansion is reduced by vapor extraction, and thereby reducing the backward expansion force. Similar to the pressure drop reduction, the improvement in flow stability in a diverging channel is less than in a straight channel due to the lower vapor extraction rate. That is to say, the fractional reduction of St is less for the diverging channel with extraction compared to a straight channel with extraction.

4.7 CONCLUSIONS

The development of a one-dimensional numerical model and a new stability parameter applicable for flow boiling in straight and diverging channels has been presented and discussed. The one-dimensional model was validated with available experimental data in the literature. The predicted channel pressure drop, outlet quality, extracted vapor rate and stability as well as the local distribution of channel pressure, quality, bulk temperature and extracted mass flux have been presented and discussed. The predicted results confirm the hypothesis that diverging channel helps stabilizing the flow boiling, and that in-situ vapor extraction can be used to improve the channel pressure

drop and flow stability, and regulate the outlet quality because it reduces the rate of net quality inside the channel. The enhancement of flow stability in a diverging channel can be further improved by coupling with in-situ vapor extraction although the effects of vapor extraction on flow boiling in term of pressure drop and quality reduction are less effective in a diverging channel compared to that in a straight channel. Overall, significant improvements to the allowable, stable, heat flux are predicted by coupling a diverging channel with in-situ vapor extraction.

4.8 ACKNOWLEDGEMENTS

The authors acknowledge the financial support from Office of Naval Research (N00014-09-1-1079). The authors would also like to thank Prof. Weilin Qu for providing the experimental data of pressure drop used to validate model in this study.

4.9 NOMENCLATURE

A	Area
c_p	Specific heat
C_{LM}	Phase interaction parameter
D_h	Hydraulic diameter
$f_{loc,lo}$	Local all-liquid phase friction factor
G	Mass flux
h	Heat transfer coefficient
H	Channel depth
i	Enthalpy
i_{lv}	Heat of vaporization
L	Channel length
MAE_A	Mean absolute error between model and experimental results of A
$\dot{m}_{in}$	Inlet mass flow rate
$\dot{m}_{extr}$	Extracted vapor mass flow rate

P_{extr}	Extraction absolute pressure
$\wp_w$	Wetted perimeter
q	Heat input rate
q''	Heat flux
R	Instability parameter proposed in [12] and [76]
R_{extr}	Extraction flow resistant
St	Stability parameter
T	Temperature
v	Specific volume
w	Channel width
x	Thermodynamic equivalent quality
X^2	Lockhart-Martinelli parameter

Greek

α	Void fraction
ΔP_{chan}	Channel pressure drop
$\Delta P_{driv,loc}$	Local extraction driving pressure
δ	Thickness
θ_d	Half-diverging angle
κ	Specific permeability
μ	Dynamic viscosity
ν	Kinematic viscosity
ρ	Density
ϕ_l^2	Two-phase multiplier

Subscripts

1φ	Single-phase
2φ	Two-phase
acc	Acceleration

b	Bulk
back	Backward
bub	Bubble
c	Cross-sectional
exp	Expansion
extr	Extraction
fric	Frictional
heat	Heated
I	Inertia
in	Inlet
l	Liquid phase
orf	Orifice
out	Outlet
S	Surface tension
sat	Saturation
v	Vapor phase
w	Wall

5 GENERAL CONCLUSIONS

The effects of vapor extraction during flow boiling have been discussed. The extraction regimes and the regime transition criteria have been identified and systematically developed from a physical-modeling perspective. These models can be used as a basis of the development of regime-based vapor extraction, and as future design tools. Although the overall transition model was not validated herein, the model components have been validated in part in other system applications, and the proposed validation methodology for the extraction regime transition criteria is suggested.

The hypothesis that in-situ vapor extraction helps reducing system pressure drop, migrating flow instability, and improving heat transfer capabilities have been numerically validated in microscale fractal-like branching network and diverging microchannel geometries. Based on the vapor extraction rate validation, the saturated pressure based on the local average film temperature rather than the bulk channel pressure is the best representative for the channel pressure adjacent to the membrane that drives the vapor through the membrane according to Darcy's law. The results from the predictive model based on conservation of mass and energy, coupled with pressure drop and heat transfer correlations show that the decreased pressure drop and the improvement of flow stability are a consequence of reduced local quality. Vapor extraction also shows the potential to reduce the overall operating temperature of a heat sink due to the evaporative cooling effect that reduces the bulk fluid temperature within the channel. At least 25% reduction in pressure drop by applying vapor extraction is found in the study of flow boiling with vapor extraction in fractal-like branching network. Although the effectiveness of vapor extraction coupling with a diverging channel geometry is reduced compared to that in the straight channel, significant improvements are shown.

BIBLIOGRAPHY

[1] Garimella, S. V., and Sobhan, C. B., 2003, "Transport in Microchannels–a Critical Review," Annual review of heat transfer, 13(13), pp. 1-50.
[2] Bertsch, S. S., Groll, E. A., and Garimella, S. V., 2008, "Review and Comparative Analysis of Studies on Saturated Flow Boiling in Small Channels," Nanoscale & Microscale Thermophysical Engineering, 12(3), pp. 187-227.
[3] Kakac, S., and Bon, B., 2008, "A Review of Two-Phase Flow Dynamic Instabilities in Tube Boiling Systems," International Journal of Heat and Mass Transfer, 51(3-4), pp. 399-433.
[4] Qu, W., and Mudawar, I., 2003, "Measurement and Prediction of Pressure Drop in Two-Phase Micro-Channel Heat Sinks," International Journal of Heat and Mass Transfer, 46(15), pp. 2737-2753.
[5] Kosar, A., Kuo, C.-J., and Peles, Y., 2006, "Suppression of Boiling Flow Oscillations in Parallel Microchannels by Inlet Restrictors," Journal of Heat Transfer, 128(3), pp. 251-260.
[6] Wang, G., Cheng, P., and Bergles, A. E., 2008, "Effects of Inlet/Outlet Configurations on Flow Boiling Instability in Parallel Microchannels," International Journal of Heat and Mass Transfer, 51(9-10), pp. 2267-2281.
[7] Lu, C. T., and Pan, C., 2009, "A Highly Stable Microchannel Heat Sink for Convective Boiling," Journal of Micromechanics and Microengineering, 19(5), p. 055013.
[8] Zhang, L., Wang, E. N., Goodson, K. E., and Kenny, T. W., 2005, "Phase Change Phenomena in Silicon Microchannels," International Journal of Heat and Mass Transfer, 48(8), pp. 1572-1582.
[9] Kuo, C. J., and Peles, Y., 2008, "Flow Boiling Instabilities in Microchannels and Means for Mitigation by Reentrant Cavities," Journal of Heat Transfer, 130(7), pp. 072402-072410.
[10] Lee, P. C., and Pan, C., 2008, "Boiling Heat Transfer and Two-Phase Flow of Water in a Single Shallow Microchannel with a Uniform or Diverging Cross Section," Journal of Micromechanics and microengineering, 18, pp. 1-13.
[11] Lu, C. T., and Pan, C., 2008, "Stabilization of Flow Boiling in Microchannel Heat Sinks with a Diverging Cross-Section Design," Journal of Micromechanics and Microengineering, 18(7), p. 075035.
[12] Lee, H. J., and Yao, S.-C., 2008, "Stability Analysis and Network Design of Evaporative Micro-Channels," Proc. ASME HT2008-56337 pp. 699-707.
[13] Salakij, S., Liburdy, J. A., and Pence, D. V., 2010, "Modeling Extraction Regime Transitions for Microchannel Vapor Extraction Map in Two-Phase Cooling Applications," Proc. ASME IMECE2010-40976 pp. 1375-1386.
[14] Salakij, S., Liburdy, J. A., and Pence, D. V., 2012, "Modeling Convective Boiling in Single Diverging Channel with in-Situ Vapor Extraction," accepted ASME HT2012-58268, Puerto Rico, USA.
[15] Salakij, S., Liburdy, J. A., and Pence, D. V., 2013, "Modeling Convective Boiling in Single Diverging Channel with in-Situ Vapor Extraction," in preparation to submit to Journal of Heat Transfer.

[16] Apreotesi, M. A., Pence, D. V., and Liburdy, J. A., 2007, "Vapor Extraction from Flow Boiling in a Fractal-Like Branching Heat Sink," Proc. ASME InterPACK 2007-33423, pp. 321-328
[17] Apreotesi, M. A., 2007, "Microscale Thermal Management Utilizing Vapor Extraction from a Fractal-Like Branching Heat Sink,"M.S. Thesis, Oregon State University, Corvallis, OR.
[18] Salakij, S., Liburdy, J. A., and Pence, D. V., 2009, "Modeling in-Situ Vapor Extraction During Convective Boiling," Proc. ASME FEDSM 2009-78522, pp. 507-518.
[19] David, M. P., Miler, J., Steinbrenner, J. E., Yang, Y., Touzelbaev, M., and Goodson, K. E., 2011, "Hydraulic and Thermal Characteristics of a Vapor Venting Two-Phase Microchannel Heat Exchanger," International Journal of Heat and Mass Transfer, 54(25-26), pp. 5504-5516.
[20] Fang, C., David, M., Rogacs, A., and Goodson, K., 2010, "Volume of Fluid Simulation of Boiling Two-Phase Flow in a Vapor-Venting Microchannel," Frontiers in Heat and Mass Transfer, 1(1), pp. 1-11.
[21] Salakij, S., Liburdy, J. A., Pence, D. V., and Apreotesi, M., 2013, "Modeling in Situ Vapor Extraction During Convective Boiling in Fractal-Like Branching Microchannel Networks," International Journal of Heat and Mass Transfer, 60, pp. 700-712.
[22] Xu, J., Vaillant, R., and Attinger, D., 2010, "Use of a Porous Membrane for Gas Bubble Removal in Microfluidic Channels: Physical Mechanisms and Design Criteria," Microfluidics and Nanofluidics, 9(4), pp. 765-772.
[23] Cappello, N., Pence, D., and Liburdy, J., 2013, "Mass Transport Limitations through Porous Hydrophobic Membranes," accepted FEDSM2013-16559, Incline village, Nevada, USA.
[24] Alexander, B. R., and Wang, E. N., 2009, "Design of a Microbreather for Two-Phase Microchannel Heat Sinks," Nanoscale and Microscale Thermophysical Engineering, 13(3), pp. 151-164.
[25] Harirchian, T., and Garimella, S. V., 2010, "A Comprehensive Flow Regime Map for Microchannel Flow Boiling with Quantitative Transition Criteria," International Journal of Heat and Mass Transfer, 53(13-14), pp. 2694-2702.
[26] Revellin, R., and Thome, J. R., 2007, "A New Type of Diabatic Flow Pattern Map for Boiling Heat Transfer in Microchannels," Journal of Micromechanics and Microengineering, 17(4), pp. 788-796.
[27] David, M. P., Steinbrenner, J. E., Miler, J., and Goodson, K. E., 2011, "Adiabatic and Diabatic Two-Phase Venting Flow in a Microchannel," International Journal of Multiphase Flow, 37(9), pp. 1135-1146.
[28] Taitel, Y., and Dukler, A. E., 1977, "A Model for Slug Frequency During Gas-Liquid Flow in Horizontal and near Horizontal Pipes," International Journal of Multiphase Flow, 3(6), pp. 585-596.
[29] Barnea, D., Luninski, Y., and Taitel, Y., 1983, "Flow Pattern in Horizontal and Vertical Two Phase Flow in Small Diameter Pipes," The Canadian Journal of Chemical Engineering, 61(5), pp. 617-620.

[30] Sarti, G. C., Gostoli, C., and Bandini, S., 1993, "Extraction of Organic Components from Aqueous Streams by Vacuum Membrane Distillation," Journal of Membrane Science, 80(1), pp. 21-33.
[31] Tomaszewska, M., 1999, "Membrane Distillation," Environment Protection Engineering 25, pp. 37-47.
[32] Lawson, K. M., and Lloyd, D. R., 1997, "Membrane Distillation," Journal of Membrane Science, 124(1), pp. 1-25.
[33] Martinez-Diez, L., and Vazquez-Gonzalez, M. I., 2000, "A Method to Evaluate Coefficients Affecting Flux in Membrane Distillation," Journal of Membrane Science 173, pp. 225-234.
[34] de Gennes, P.-G., Brochard-Wyart, F., and Quéré, D., 2004, Capillarity and Wetting Phenomena: Drops, Bubbles, Pearls, Waves, New York, Springer.
[35] Zivi, S. M., 1964, "Estimation of Steady-State Steam Void-Fraction by Means of the Principle of Minimum Entropy Production," Journal of Heat Transfer, 86, pp. 247-252.
[36] Barnea, D., Shoham, O., and Taitel, Y., 1982, "Flow Pattern Transition for Downward Inclined Two Phase Flow; Horizontal to Vertical," Chemical Engineering Science, 37(5), pp. 735-740.
[37] Hsu, Y. Y., 1962, "On the Size Range of Active Nucleation Cavities on a Heating Surface," Journal of Heat Transfer, 84, pp. 207-216.
[38] Sato, T., and Matsumura, H., 1963, "On the Conditions of Incipient Subcooled-Boiling with Forced Convection," Bulletin of JSME, 7, pp. 365-372.
[39] Ghiaasiaan, S. M., and Chedester, R. C., 2002, "Boiling Incipience in Microchannels," International Journal of Heat and Mass Transfer, 45(23), pp. 4599-4606.
[40] Kandlikar, S. G., 2006, "Nucleation Characteristics and Stability Considerations During Flow Boiling in Microchannels," Experimental Thermal and Fluid Science, 30(5), pp. 441-447.
[41] Ribatski, G., Wojtan, L., and Thome, J. R., 2006, "An Analysis of Experimental Data and Prediction Methods for Two-Phase Frictional Pressure Drop and Flow Boiling Heat Transfer in Micro-Scale Channels," Experimental Thermal and Fluid Science, 31, pp. 1-19.
[42] Brutin, D., and Tadrist, L., 2004, "Pressure Drop and Heat Transfer Analysis of Flow Boiling in a Minichannel: Influence of the Inlet Condition on Two-Phase Flow Stability," International Journal of Heat and Mass Transfer, 47(10-11), pp. 2365-2377.
[43] Tadrist, L., 2007, "Review on Two-Phase Flow Instabilities in Narrow Spaces," International Journal of Heat and Fluid Flow, 28(1), pp. 54-62.
[44] Pence, D. V., 2002, "Reduced Pumping Power and Wall Temperature in Microchannel Heat Sinks with Fractal-Like Branching Channel Networks," Microscale Thermophysical Engineering, 6, pp. 319-330.
[45] Daniels, B. J., 2008, "A Study of Adiabatic and Diabatic Flow Boiling in Parallel Microchannels and Fractal-Like Branching Microchannels,"Ph.D. Dissertation, Oregon State University, Corvallis, OR.
[46] Daniels, B. J., Pence, D. V., and Liburdy, J. A., 2005, "Predictions of Flow Boiling in Fractal-Like Branching Microchannels," Proc. ASME IMECE2005-82484, pp. 359-368

[47] Daniels, B. J., Liburdy, J. A., and Pence, D. V., 2007, "Adiabatic Flow Boiling in Fractal-Like Microchannels," Heat Transfer Engineering, 28, pp. 817-825.
[48] Daniels, B. J., Liburdy, J. A., and Pence, D. V., 2011, "Experimental Studies of Adiabatic Flow Boiling in Fractal-Like Branching Microchannels," Experimental Thermal and Fluid Science, 35(1), pp. 1-10.
[49] Zhang, C., Chen, Y., Wu, R., and Shi, M., 2011, "Flow Boiling in Constructal Tree-Shaped Minichannel Network," International Journal of Heat and Mass Transfer, 54(1-3), pp. 202-209.
[50] Heymann, D., Pence, D., and Narayanan, V., 2010, "Optimization of Fractal-Like Branching Microchannel Heat Sinks for Single-Phase Flows," International Journal of Thermal Sciences, 49(8), pp. 1383-1393.
[51] Heymann, D. B., and Pence, D. V., 2011, "Constrained Optimization of One-Dimensional Two-Phase Flow in Fractal-Like Branching Microchannel Heat Sinks," Proc. AJTEC2011-44353, pp. T10123-T10123-10110.
[52] Lockhart, R. W., and Martinelli, R. C., 1949, "Proposed Correlation of Data for Isothermal Two-Phase, Two-Component Flow in Pipes," Chemical Engineering Progress, 45(1), pp. 39-48.
[53] Mishima, K., and Hibiki, T., 1996, "Some Characteristics of Air-Water Two-Phase Flow in Small Diameter Vertical Tubes," International Journal of Multiphase Flow, 22, pp. 703-712.
[54] Lee, H. J., and Lee, S. Y., 2001, "Pressure Drop Correlations for Two-Phase Flow within Horizontal Rectangular Channels with Small Heights," International Journal of Multiphase Flow, 27, pp. 783-796.
[55] Lee, J., and Mudawar, I., 2005, "Two-Phase Flow in High-Heat-Flux Micro-Channel Heat Sink for Refrigeration Cooling Applications: Part I--Pressure Drop Characteristics," International Journal of Heat & Mass Transfer, 48(5), pp. 928-940.
[56] Hwang, Y. W., and Kim, M. S., 2006, "The Pressure Drop in Microtubes and the Correlation Development," International Journal of Heat and Mass Transfer, 49, pp. 1804-1812.
[57] Tran, T. N., Wambsganss, M. W., and France, D. M., 1996, "Small Circular- and Rectangular-Channel Boiling with Two Refrigerants," International Journal of Multiphase Flow, 22, pp. 485-498.
[58] Yu, W., France, D. M., Wambsganss, M. W., and Hull, J. R., 2002, "Two-Phase Pressure Drop, Boiling Heat Transfer, and Critical Heat Flux to Water in a Small-Diameter Horizontal Tube," International Journal of Multiphase Flow, 28, pp. 927-941.
[59] Kandlikar, S. G., 1990, "A General Correlation for Two-Phase Flow Boiling Heat Transfer Coefficient inside Horizontal and Vertical Tubes," Journal of Heat Transfer, 102, pp. 219-228.
[60] Kandlikar, S. G., and Balasubramanian, P., 2004, "An Extension of the Flow Boiling Correlation to Transition, Laminar, and Deep Laminar Flows in Minichannels and Microchannels," Heat Transfer Engineering, 25(3), pp. 86-93.
[61] Lee, H. J., and Lee, S. Y., 2001, "Heat Transfer Correlation for Boiling Flows in Small Rectangular Horizontal Channels with Low Aspect Ratios," International Journal of Multiphase Flow, 27, pp. 2043-2062.

[62] Warrier, G. R., Dhir, V. K., and Momoda, L. A., 2002, "Heat Transfer and Pressure Drop in Narrow Rectangular Channels," Experimental Thermal and Fluid Science, 26, pp. 53-64.
[63] Yen, T.-H., Kasagi, N., and Suzuki, Y., 2003, "Forced Convective Boiling Heat Transfer in Microtubes at Low Mass and Heat Fluxes," International Journal of Multiphase Flow, 29(12), pp. 1771-1792
[64] Lee, J., and Mudawar, I., 2005, "Two-Phase Flow in High-Heat-Flux Micro-Channel Heat Sink for Refrigeration Cooling Applications: Part II—Heat Transfer Characteristics," International Journal of Heat and Mass Transfer, 48, pp. 941–955.
[65] Pence, D. V., and Enfield, K., 2004, "Inherent Benefits in Microscale Fractal-Like Devices for Enhanced Transport Phenomena," Design and Nature II: Comparing Design in Nature with Science and Engineering, M. Collins, and C. A. Brebbia, eds., WIT Press, Southampton, Boston, pp. 317–328.
[66] Salakij, S., 2009, "Modeling Convective Boiling Flow with in-Situ Local Vapor Extraction,"M.S. Thesis, Oregon State University, Corvallis, OR.
[67] Shah, R. K., and London, A. L., 1978, "Larminar Flow Forced Convection in Ducts," Acadamic Press, New York, Sans Francisco, London, pp. 196-222.
[68] Chisholm, D., 1967, "A Theoretical Basis for the Lockhart–Martinelli Correlation for Two-Phase Flow," International Journal of Heat and Mass Transfer, 10, pp. 1767-1778.
[69] Chisholm, D., and Laird, A. D. K., 1958, "Two-Phase Flow in Rough Tubes," Journal Heat Transfer, 80, pp. 276-283.
[70] Carey, V. P., 2008, "Liquid-Vapor Phase-Change Phenomena," Taylor and Francis, New York, NY, pp. 479-536.
[71] Qu, W., and Mudawar, I., 2004, "Transport Phenomena in Two-Phase Micro-Channel Heat Sinks," Journal of Electronic Packaging, Transactions of the ASME, 126, pp. 213-224.
[72] Lee, H. J., and Yao, S.-c., 2010, "System Instability of Evaporative Micro-Channels," International Journal of Heat and Mass Transfer, 53(9-10), pp. 1731-1739.
[73] Lee, H. J., Liu, D. Y., and Yao, S.-c., 2010, "Flow Instability of Evaporative Micro-Channels," International Journal of Heat and Mass Transfer, 53(9-10), pp. 1740-1749.
[74] Hwang, J. J., Tseng, F. G., and Pan, C., 2005, "Ethanol–Co2 Two-Phase Flow in Diverging and Converging Microchannels," International Journal of Multiphase Flow, 31(5), pp. 548-570.
[75] Kandlikar, S. G., 2004, "Heat Transfer Mechanisms During Flow Boiling in Microchannels," Journal of Heat Transfer, 126(1), pp. 8-16.
[76] Lee, H. J., Liu, D. Y., and Yao, S.-c., 2010, "Flow Instability of Evaporative Micro-Channels," International Journal of Heat & Mass Transfer, 53(9/10), pp. 1740-1749
[77] Heymann, D. B., 2011, "On the Optimization of Performance in Fractal-Like Branching Microchannel Heat Transfer Devices,"Ph.D. Dissertation, Oregon State University, Corvallis, OR.
[78] Collier, J. G., and Thome, J. R., 2004, Convective Boiling and Condensation, Oxford University Press, New York.

[79] McAdams, H. W., Woods, W. K., and Bryan, R. L., 1942, "Vaporization inside Horizontal Tubes—II—Benzene–Oil Mixtures," Transactions of the ASME, 64, pp. 193-200.
[80] Chicchitti, A., Lombardi, C., Silvestri, M., Soldaini, G., and Zavattarelli, R., 1960, "Two-Phase Cooling Experiments-Pressure Drop, Heat Transfer and Burnout Measurements," Energia Nucleare, 7(6), pp. 407-425.
[81] Armand, A. A., 1959, "The Resistance During the Movement of a Two-Phase System in Horizontal Pipes," Atomic Energy Research Establishment (AERE) Libr. Trans., 828.